We thank the reviewers for their comments. We have modified the text in response to these comments below. Specifically, we have clarified the differences in reaction conditions regarding the "RO_2+NO_3 dominant" and "RO_2+RO_2 dominant" reactions, as well as amended the discussion of Fig. 9 in the revised manuscript to better reflect the differences in the two reaction conditions. In the revised manuscript, we also make minor adjustments to our VBS fitting in order to include C* = 0.1 $\mu g/m^3$ and represent these fits on a mass basis for their direct implementation in aerosol models. All changes made are minor and do not affect the conclusions of the manuscript.

Response to Referee 1 (Referees' comments are italicized)

1. First paragraph of intro: suggest a slight rewording - leading with BVOCs being a major source of SOA does not make the observation of "modern" carbon a discrepancy – it resolves it – maybe instead of "However, . . .", "This resolves the apparent contradiction that ambient organic aerosols . . ."?

Author response: As requested, we have changed the sentence in the revised manuscript from:

Page 2681 Line 6: "However, there exists a contradiction that ambient organic aerosol (even in urban areas) is predominately "modern", indicating a biogenic origin (Lewis et al., 2004; Schichtel et al., 2008; Marley et al., 2009) but often correlates with anthropogenic tracers (de Gouw et al., 2005; Weber et al., 2007)."

To:

"While this is supported by the observation that ambient organic aerosol is predominantly "modern" and therefore biogenic in origin (Lewis et al., 2004; Schichtel et al., 2008; Marley et al., 2009), there exists an apparent contradiction because ambient organic aerosol is well-correlated with anthropogenic tracers (de Gouw et al., 2005; Weber et al., 2007)."

2. P. 2686 line 4 & SI material about HCHO required: How well do you know the amount of HCHO present at the beginning of the HO2+RO2 experiments? Are you able to constrain it by any measurement (HCHO, production rate of any products?), or is it determined by the volume of solution injected?

Author response: We estimated the concentration of HCHO in the chamber at the beginning of the "RO_2+HO_2 dominant" experiments from the volume of the HCHO solution injected into the glass bulb and from the assumption that all the HCHO injected into the glass bulb volatilized and is introduced into the chamber. While we did not measure the HCHO to constrain the uncertainty in its concentration, we expect the uncertainty to be small as the loss of HCHO (volatile compound) during the injection process is expected to be small.

3. P. 2686 line 8-9: I suggest modeling the oxidation of β-pinene in both conditions to both demonstrate clearly this dominance of NO3 in the HO2 conditions, and show the difference in rate and how it affects the timing of aerosol yield calculations. I see you have O3 measurements – you could use these to constrain this model experimentally?

Author response: As requested, we have provided the modeled oxidation of β-pinene under "RO_2+NO_3 dominant" conditions in the supplementary material. The kinetic model predicts that > 99 % of the β-pinene reacts with NO_3 instead of ozone. The model for the "RO_2+NO_3 dominant" reaction indicates a rapid reaction time (~1 min) for β-pinene within the chamber.

Similarly, we attempted to model the oxidation of β-pinene under "RO_2+HO_2 dominant" conditions. Unfortunately, the model does not converge with the inclusion of HCHO in the model but does converge when HCHO is not included. When HCHO is not included, the model shows that majority (> 99 %) of the β-pinene reacts with NO_3 rather than ozone. We calculate the ratio of HCHO:β-pinene needed to promote RO_2+HO_2 reaction, details of which are in the SI. The appropriate amount of HCHO (based on the calculated HCHO:β-pinene ratio needed) is injected in the "RO_2+HO_2" dominate experiments. The added HCHO can also react with nitrate radicals. However, since the β-pinene+NO_3 reaction is 13 faster than HCHO+ NO_3 the presence of HCHO does not affect the availability of NO_3 for β-pinene oxidation. Ultimately, most β-pinene (>99%) still reacts with NO_3.

The amount of time to reach peak growth in our experiments is longer than the modeled oxidation of β-pinene under "RO_2+NO_3 dominant" conditions. Although complete β-pinene oxidation is expected to occur within minutes, the amount of time to reach peak growth experimentally (also addressed in comment #7) is 10-15 minutes in all reaction conditions except for the "RO_2+HO_2 dominant" experiments under high humidity (which took 30 min). One possible reason for this discrepancy is that due to the fast reaction rates, most of the β-pinene has reacted before the chamber is well mixed, which will result in a lapse between aerosol formation and its measurement by the HR-ToF-AMS and SMPS. The timescales at which products condense onto seed particles are also not known. Due to these experimental constraints, we are unable to directly correlate the rates in our kinetic model to our measured rates of aerosol growth and the time it takes to reach aerosol peak growth.

We change Figure 9 to show the dominance of the BVOC+NO_3 reaction and amend the caption to:

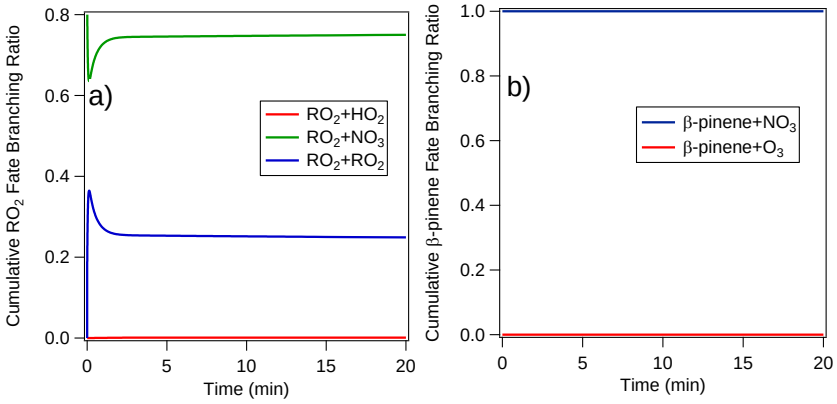

Figure S9: a) The RO_2 branching ratio and b) β-pinene fate for a typical "RO_2+NO_3" dominant experiment (Experiment 5 in Table 1 of the main text). The branching ratios are determined from the reactions in the Master Chemical Mechanism (MCM v 3.2). The plots show the cumulative amount of products formed from each possible reaction.

4. p. 2687 line 15-16: Can you put an uncertainty estimate on the initial [HC] based on the volume measurement accuracy?

Author response: Table 1 shows the uncertainties of the initial [HC] based on the volume measurement accuracy.

5. P. 2690 line 21-22: The reference for wall losses refers to measurements made in a different chamber. If such data are already published for this chamber, could refer to that, else perhaps include the size-dependent wall loss rates measured for this chamber in the supplemental?

Author response: The original text referenced Keywood et al. (2004) only for the methodology for correcting for particle wall loss. To clarify any confusion regarding the size-dependence wall loss rates used for our experiments, we have changed the text from:

Page 2690 Line 21: "All SOA growth data are corrected for particle wall loss by applying size-dependent wall loss coefficients determined from wall loss experiments (Keywood et al., 2004)."

To:

"All SOA growth data are corrected for particle wall loss by applying size-dependent wall loss coefficients determined from wall loss experiments at GTEC following the methodology described in Keywood et al. (2004)."

The wall-loss coefficients for this chamber have not been published. As requested, we have added a figure showing the size-dependent wall loss rates measured in this chamber to the supplementary information:

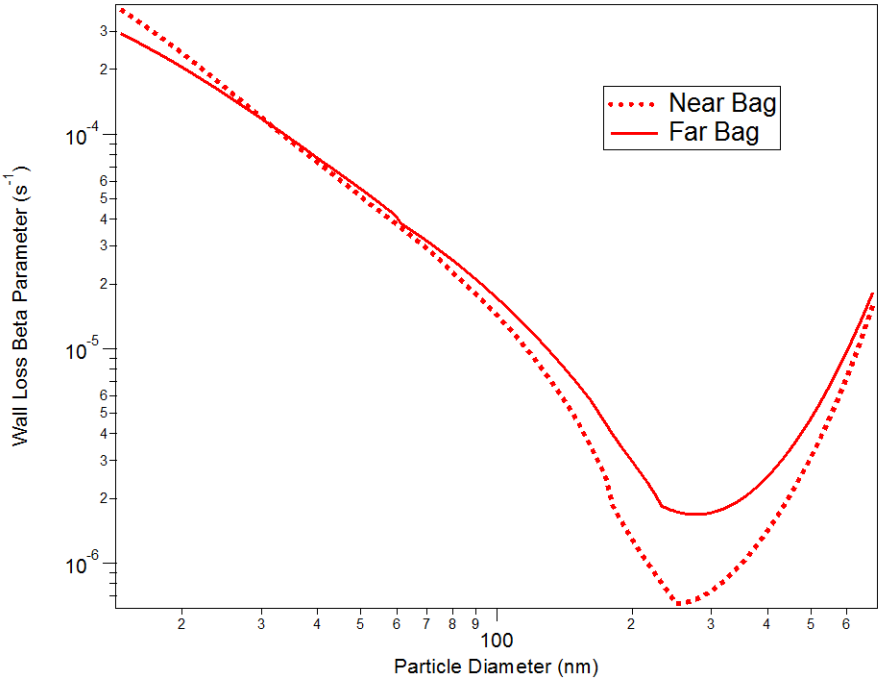

"Figure S10: Size-dependent particle wall loss rates, β, calculated for both chambers at GTEC. Wall loss rates are determined by wall loss experiments performed using ammonium sulfate seed particles atomized from an 8 mM solution and measuring their decays over time. The first-order decay coefficients were measured for each particle size bin over the course of the wall-loss experiment."

6. Ibid line 26: suggest "aerosol mass concentration produced (deltaMo)"

Author response: We have made the suggested modification.

7. Ibid line 29: Can you add some text about at what time the SMPS aerosol volume was taken for the mass yields – fixed time after injection? Or peak in volume? If the latter, how different was the lag time between starting reactions & aerosol peak for each type of experiment? Perhaps label the time of delta(Mo) on Figure 2.

Author response: The SMPS aerosol volume used to calculate the aerosol mass yields in each experiment is the peak SMPS aerosol volume (averaged over 30 min). We have stated on page 2689, lines 24-26 that "Peak aerosol growth is typically observed within 10-15 minutes for all reaction conditions except in humid (RH= 50%, 70%) "RO_2+HO_2 dominant" experiments, where aerosol reaches peak growth in about 30 minutes." As Fig. 2 already contains a huge amount of information, we feel that adding the time of delta(Mo) will make the figure harder to understand.

To clarify this, we have changed the sentence:

Page 2690 Line 28: "For all experiments, aerosol mass concentration is obtained from the SMPS aerosol volume concentration and the calculated aerosol density."

To:

"For all experiments, aerosol mass concentration is obtained from the SMPS aerosol volume concentration (averaged over 30 min at peak growth) and the calculated aerosol density."

8. P. 2691 line 5: Is it your view that these dry/humid conditions numbers are significantly different from one another?

Author response: We think that the densities from the dry and humid experiments are not significantly different from one another (within 5% of each other). Prior to the experiments, we did not know how similar/different they would be. Thus we performed nucleation experiments under different conditions to determine the density at those specific conditions.

9. P. 2692 line 5: "which make up about 11% of the total organics signal" – wording is slightly confusing – are NO+ and NO2+ part of the organics signal (sounds like it with this phrasing) or is their magnitude equal to 11% of the organics signal (what I think you mean)

Author response: To clarify this, we have changed the sentence

Page 2692, Line 3: "A key feature of the mass spectrum is the high intensity of the nitrate ions at NO^+ and NO_2^+, which make up about 11% of the total organics signal."

To:

"A key feature of the mass spectrum is the high intensity of the nitrate ions at NO^+ and NO_2^+, which make up about 11% of the combined organic and nitrate signals."

10. Ibid around line 10: General question: why would the NO+:NO2+ ratio be different for different oxidant regimes if the apparent product composition is largely identical? Or are these not really significantly different?

Author response: At this time, it is not clear what causes the difference in the NO^+:NO_2^+ ratio in the different oxidation regimes (on average, 6.5 for "RO_2+NO_3 dominant" experiments and 8.6 for "RO_2+HO_2 dominant" experiments). It is possible that while the aerosol yields and product composition are similar in the different oxidation regimes, the relative concentrations of the particle phase organic nitrates may be different, resulting in the difference in the NO^+:NO_2^+ ratios. For example, the *m/z* 358 is higher in the "RO_2+HO_2 dominant" experiments, which we believe may be due to increased production of ROOH in the "RO_2+HO_2 dominant" experiments. It is also possible that the functional groups surrounding the nitrate group may affect the NO^+:NO_2^+ ratio. Additionally, it is possible that the products formed in the two reaction conditions are different but having similar volatility, thus resulting in similar mass yields but different NO^+:NO_2^+ ratios for the two oxidant regimes.

11. Ibid line 19-21: I don't think this generalization really follows from the previous sentence, since these are 2 specific terpenes, and these fragments could be highly structure dependent.

Author response: We agree that with the reviewer that the abundance of the $C_5H_7^+$ and $C_7H_7^+$ fragments may be highly dependent on the structure of the SOA components. However, as stated in the original text, the AMS mass spectra of the SOA formed form the oxidation (photooxidation, nitrate radical oxidation, ozonolysis) of BVOCs such as isoprene and α-pinene, does not exhibit large intensities at$C_5H_7^+$ and $C_7H_7^+$ (Ng et al., 2008; Chhabra et al., 2010). We suggest that these fragments may be important for monoterpene chemistry based on our observations but more study on the AMS fragmentation pattern for SOA formed by a larger suite of terpenes is needed. As such, we have revised the manuscript to be more circumspect in our explanation on the use of $C_5H_7^+$ and $C_7H_7^+$ fragments as indicators for monoterpene SOA oxidation, and have changed the sentence:

Page 2692, Line 17: "These ions have also been observed in SOA formed from the ozonolysis of β-caryophyllene (Chen et al., 2014). Therefore, *m/z* 67 ($C_5H_7^+$) and *m/z* 91 ($C_7H_7^+$) could potentially serve as useful indicators for SOA formed from monoterpene/sesquiterpene oxidations in ambient aerosol mass spectra."

To:

"These ions make up a larger fraction of the HR-ToF-AMS signal for SOA formed from the ozonolysis of β-caryophyllene (Chen et al., 2014) when compared to other biogenic SOA. Therefore, *m/z* 67 ($C_5H_7^+$) and *m/z* 91 ($C_7H_7^+$) could potentially serve as useful indicators for SOA formed from monoterpene/sesquiterpene oxidations in ambient aerosol mass spectra. However, more studies of SOA formed from the oxidation of biogenic VOCs are necessary to apportion ambient OA based on these fragments."

12. P. 2694, line 24-25: the product of reaction 9 in the scheme shown is not a dihydroxynitrate.

Author response: The reviewer is correct. The product should be "cyclic ether hydroxynitrate" instead. This has been corrected.

13. P. 2695 line 22: "1.5h shift" should read "1,5-H shift"

Author response: This has been corrected.

14. P. 2699 2nd paragraph: general question about yield fitting: How do you interpret that the coefficient at 10 ug/m3 is exactly zero? Did you do any sensitivity tests e.g. with a bigger basis set, or removing a point, to check how robust this fit is?

Author response: The coefficients for the VBS represent the best mathematical fit to all of our data. The coefficient at 10 μg m^{-3} is representative of that fit. The point we would like to emphasize in this discussion is not the exact coefficients used but rather the overall trend of the volatility fit. Specifically, the VBS fit to our data indicates that the β-pinene+NO_3 SOA system is composed of both low-volatility and high-volatility products.

As suggested by the reviewer, we checked the robustness of the fit by removing a data point. By removing the second lowest point in the yield curve on Fig. 3 and re-fitting the data, the new yield curve shown below is very similar to our original yield curve, with a difference only about 10% at the lowest mass loading. Therefore, the original yield curve is robust and is not biased by the second lowest point during fitting.

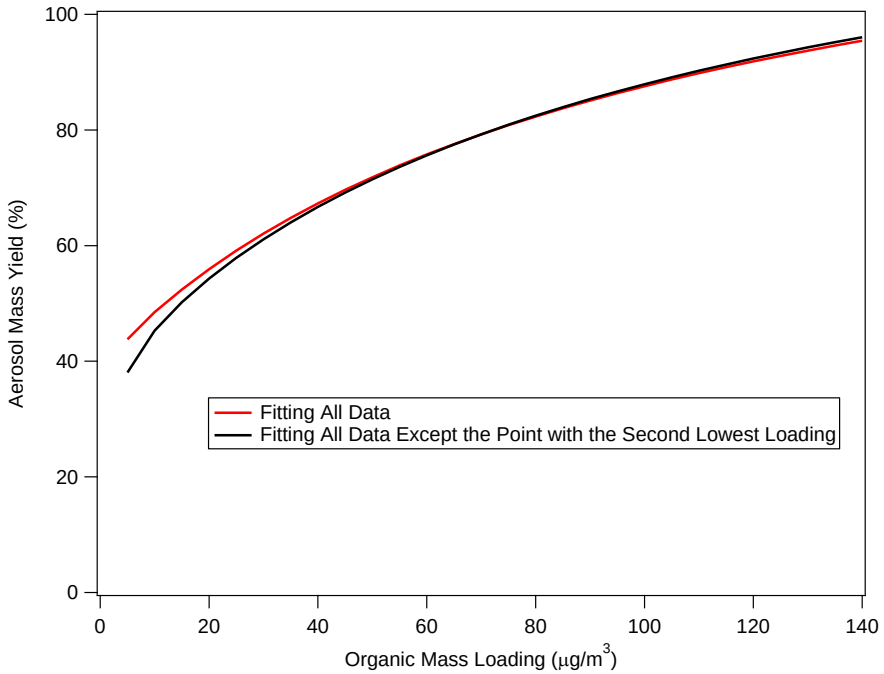

We would like to make some revisions to the VBS fits presented in the original text. In the original manuscript, a molar basis was used for the VBS fitting using an average molecular weight of 230 amu but this was not specifically stated in the original text. In the revised manuscript, we change the fits to a mass basis. In addition, we would also like to correct the data in Griffin et al. (1999) to adjust for the deviations in temperature from 25 °C and change the basis set from C* = {1,10,100,1000} to C* = {0.1, 1, 10, 100}. This will allow for a direct comparison of our VBS fits with the fit parameters currently used in aerosol models (e.g. Pye et. al (2010)). This adjustment will be clearly stated in the revised manuscript. After making these adjustments, Table 3 has been changed from:

	Saturation Vapor Pressure, C* (μg/m^3)			
	1	10	100	1000
β-pinene+NO_3 (this study)	0.272	0.000	0.437	0.291
Griffin et al. (1999)	0.000	0.117	0.785	0

To:

	Saturation Vapor Pressure, C* (μg/m^3)			
	0.1	**1**	**10**	**100**
β-pinene+NO_3 (this study)	**0.373**	**0.033**	**0.000**	**0.941**
Griffin et al. (1999)	**0.000**	**0.000**	**0.301**	**1.204**

We have also changed:

Page 2699, Line 8: "The fit coefficients for the volatility basis set are shown in Table 3 for the aerosol yields of β-pinene+NO_3 from this study and that of Griffin et al. (1999)"

To:

"The fit coefficients for the volatility basis set are shown in Table 3 for the aerosol yields of β-pinene+NO_3 from this study and that of Griffin et al. (1999). It is noted that the data from Griffin et al. (1999) have been adjusted to a temperature of 25 °C and a density of 1.41 g cm^{-3}"

To further test the robustness of our fit and confirm that the fit is not biased due to the basis set chosen, we can also expand the basis set to C* = {0.1,1,10,100,1000}. Expanding the basis set to C* = {0.1,1,10,100,1000} gives a different set of parameters with a fit shown in the figure below. The curves deviate by a maximum of 4% in the range of the mass loadings measured in all experiments. While the fitting parameters have changed, the overall fit is robust.

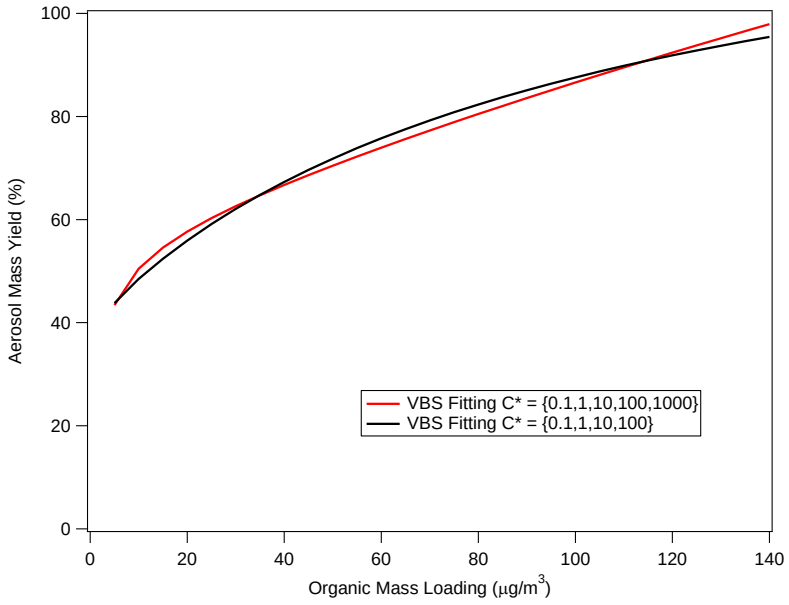

15. P. 2702 line 18-19, refers to SI figure S9: my reading of figure S9 is not that RO2+RO2 reaction "are not significant" – in fact a substantial fraction appears to go via these cross-reactions

Author response: While the reviewer is correct in pointing out that there are some RO_2+RO_2 cross reactions, the majority (~70%) of the RO_2 radicals react with the NO_3 radical based on our modeling results. While it is impossible to completely eliminate RO_2 cross reactions, the experimental conditions were designed to minimize the RO_2+RO_2 reaction pathway and ensure that majority of the RO_2 radicals react with NO_3 radicals in the "RO_2+NO_3 dominant" experiments. We determine that the "RO_2+HO_2 dominant" experiments also minimize the RO_2+RO_2 pathway based on the concentrations of HCHO injected as discussed in the SI.

16. P. 2704 line 3: what does "relative reactivity for both reaction channels" mean? In general, this figure (Fig. 9) and its interpretation were confusing. You seem to be asserting that the trend is the same across both oxidant conditions, but if the bars are correctly labeled (on the righthand panel the dry and humid are switched), the similarity in trend is not apparent.

Author response: In our discussion of Fig. 9, the comparison we are referring to is only between the two bars for RO_2+NO_3 and between the two bars for RO_2+HO_2, and not between the NO_3 panel and the HO_2 panel. To clarify this, we have added the following discussion before the sentence:

Page 2704 Line 4: "The relative reactivity for both reaction channels is similar within one standard deviation for all humidity conditions studied, indicating that each condition may have a similar product distribution."

"By comparing the amounts (areas) of the 235 and 270 nm absorbing species, the effect of humidity on the two branching pathways (RO_2+HO_2 and RO_2+NO_3) can be assessed. How much -ONO_2, -C=O, ROOR and ROOH is produced under each humidity level determines the relative reactivity between the humid vs. dry conditions of each branching pathway."

Additionally we have added the following after the sentence:

Page 2704 Line 4: "The relative reactivity for both reaction channels is similar within one standard deviation for all humidity conditions studied, indicating that each condition may have a similar product distribution."

"A comparison between the RO_2 + HO_2 and RO_2 + NO_3 pathways cannot be made in this manner because the NO_3 concentrations were different. The seemingly smaller areas for species produced in the HO_2 panel could simply be due to a larger amount of non-nitrated organic matter being produced that absorbs at the normalization wavelength."

17. Furthermore, line 6: this molecular assignment is wrong/inconsistent. The formula you have listed would have m/z =245, not 244, and the reaction you refer to (R22) you have elsewhere (bottom of 2695) described as producing a carboxylic acid, not a hydroperoxide. This should be clarified in the figure as well, by making the functional group unambiguous. This UHPLC portion of the evidence is most difficult to understand and I suggest reworking the discussion of this data. If you stick with the reasoning about R22 being an alternate pathway to a different, high-NO3 product, it would be useful to have that competing pathway also indicated on the mechanism scheme.

Author response: The MW and m/z are correct as written and have not been changed. Reaction R22 does form a carboxylic acid. The product (MW = 245 amu) formed form the R21 and R22 reactions can also be formed from R19 and R20. The reaction combination R19 and R20 can occur in both the "RO_2+NO_3 dominant" and "RO_2+HO_2 dominant" experiments while the reaction combination of R21 and R22 is expected to be prevalent in "RO_2+HO_2 dominant" experiments. We therefore expect an enhancement of the product with MW = 245 amu in the "RO_2+HO_2 dominant" experiments.

To clarify this, we have changed the text:

Page 2704 Line 5: "One slight difference is the enhancement in the production of $C_{10}H_{15}NO_6$ (*m/z* 244, an ROOH species) in the "RO_2+HO_2 dominant" experiments, which increases by 2 and 7 times under dry and humid conditions, respectively, relative to the "RO_2+NO_3 dominant" experiments."

To:

"One slight difference is the enhancement in the production of $C_{10}H_{15}NO_6$ (*m/z* 244, a RCOOH species) in the "RO_2+HO_2 dominant" experiments, which increases by 2 and 7 times under dry and humid conditions, respectively, relative to the "RO_2+NO_3 dominant" experiments."

We have also changed the sentence:

Page 2704 Line 10: "This can be explained by an increase in reaction R22 in Fig. 8."

To:

"This can be explained by an enhancement of the reaction sequence R21 + R22 in Fig. 8, which is enhanced at high HO_2 radical concentrations."

18. P. 2706 line 10 "carbons, the upper-bound molar organic nitrate"

Author response: This has been corrected.

19. P. 2707 lines 17-19: Could there not be some RO2+NO3 vs RO2+HO2 difference in organic nitrate hydrolysis rate because subsequent reactions render some products more likely to "keep" the nitrate moiety intact where others might jettison the NO2? Did you compare different oxidant fates and see no difference?

Author response: As suggested by the reviewer, we compared the nitrate hydrolysis rates in the "RO_2+HO_2 dominant" and "RO_2+NO_3 dominant" reaction conditions. We compare the experiments where $(NH_4)_2SO_4$ + H_2SO_4 seed were used, since we only run the "RO_2+HO_2 dominant" experiments with this type of seed. When using $(NH_4)_2SO_4$ + H_2SO_4 seed, we expect the rates of hydrolysis to be faster than those experiments using $(NH_4)_2SO_4$ seed (Rindelaub et

al., 2015). It is therefore difficult to determine the extent of hydrolysis for experiments with $(NH_4)_2SO_4$ + H_2SO_4 seed because the hydrolysis of tertiary organic nitrates may occur so quickly that a portion of the organic nitrates hydrolyze before peak aerosol growth. Even though much of the tertiary organic nitrates could hydrolyze quickly, tt is still clear from the graph that under all conditions, a small fraction of the organic nitrate species hydrolyze over the span of several hours. We do note that one of the experiments (12.2 ppb, "RO_2+HO_2 dominant") may have a slightly slower rate of hydrolysis. In this case, the hydrolysis may have been slow enough that the organic nitrates do not hydrolyze appreciably prior to peak growth. Therefore, the peak value that we normalize the data by may have been higher for this experiment compared to other conditions.

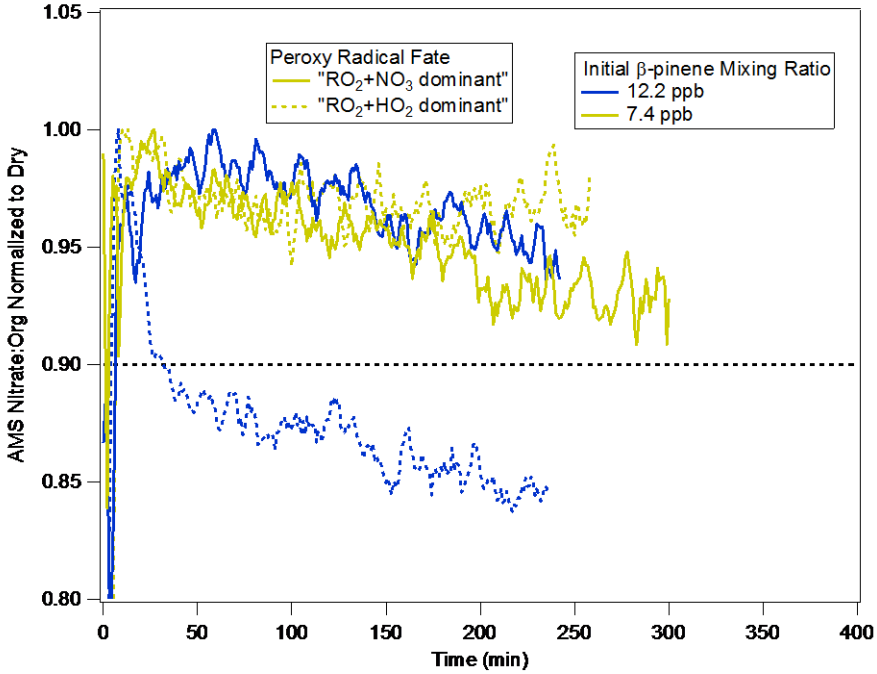

In order to emphasize that the fraction of tertiary nitrates to total nitrates may have some variation in each experiment, we change:

Page 2707, Line 12: "As the oxidation products typically contain only one nitrate group (Fig. 8), we infer that 90% of the organic nitrates formed from the β-pinene+NO_3 reaction are primary nitrates."

To:

"As the oxidation products typically contain only one nitrate group (Fig. 8), we infer that, within experimental error, approximately 90% of the organic nitrates formed from the β-pinene+NO_3 reaction are primary nitrates."

20. Ibid line 28: Suggest to replace "nitrate radical chemistry" with "nitrate + β-pinene" because many terpenes have internal double bonds, this feature of producing few tertiary nitrates is unique to β-pinene and shouldn't overgeneralized

Author response: We expect the majority of terpenes to produce primary or secondary organic nitrates from nitrate radical oxidation. The list of terpenes commonly emitted by vegetation shown by Guenther et al. (2012), while not an exhaustive list, demonstrates that the commonly emitted terpenes typically have at least one double bond containing either a primary or secondary carbon; the exception is tricyclene which does not have a double bond. Upon reaction of the nitrate radical with the least substituted carbon (Wayne et al., 1991), these terpenes will form organic nitrates with nitrate functional groups present on either the primary or secondary carbon. Darer et al. (2011) have shown that primary and secondary organic nitrates have slow hydrolysis rates.

While the reviewer is correct in pointing out that many terpenes have internal double bonds, these terpenes typically have internal double bonds that contain a tertiary and secondary carbon. We still expect such terpenes to produce mainly secondary organic nitrates since the nitrate radical will add predominantly to the secondary carbon (to produce a secondary organic nitrate) because it is the least substituted carbon (Wayne et al., 1991).

To clarify this point in the revised manuscript, we have changed:

Page 2708 Line 1: "As primary and tertiary organic nitrates have drastically different hydrolysis rates, it is imperative that their relative contribution be accurately represented in models when determining the fate of ambient organic nitrates."

To:

"While we directly demonstrate this to be true in the case of β-pinene+NO_3 system, this can also be applied to commonly emitted terpenes, including those with internal double bonds. From the list of terpenes in Guenther et al. (2012), all unsaturated terpenes have at least one double bond with a secondary or primary carbon. For example, α-pinene contains an internal double bond connecting a tertiary carbon to a secondary carbon. The nitrate radical is more likely to attack the less substituted carbon (i.e., the secondary carbon) and form a secondary organic nitrate. As primary/secondary and tertiary organic nitrates have drastically different hydrolysis rates, it is imperative that their relative contribution be accurately represented in models when determining the fate of ambient organic nitrates."

21. Same comment @ p. 2708 lines 16-19: this is only true where terminal double bonds dominate – so, where dominated by β-pinene.

Author response: We refer the reviewer to the response to comment #20. As explained above, most commonly emitted terpenes with internal double bonds have one secondary carbon and one tertiary carbon. In the nitrate radical reaction of such terpenes, the nitrate radical will add predominantly to the less substituted carbon of the internal double bond (Wayne et al., 1991),

which in this case is the secondary carbon, to form a secondary organic nitrate. The resulting secondary organic nitrate will have slow hydrolysis lifetimes (Darer et al., 2011).

22. *P. 2711 line 6: inversely? Does this mean this partitioning coefficient is wall/gas, not gas/wall? Clarify.*

Author response: The partitioning coefficient we refer to in the original text is to the gas-wall partitioning coefficient. The original text meant to explain that if a particular compound (Compound A) has a lower vapor pressure than another (Compound B), it is expected that Compound A is more likely to partition to the chamber walls than compound B.

To clarify this, we have changed the sentence:

Page 2711 Line 6: "Additionally, the gas-wall partitioning coefficient has also been shown to correlate inversely with the vapor pressure for each compound (Yeh and Ziemann, 2014), where highly oxidized species typically have lower vapor pressures (Pankow and Asher, 2008)."

To:

"Additionally, the gas-wall partitioning coefficient for a specific compound has also been shown to increase with decreasing vapor pressure (Yeh and Ziemann, 2014), with highly oxidized species typically having lower vapor pressures than less oxidized species (Pankow and Asher, 2008)."

23. *Ibid, line 10: this phrase is unclear: "causing these compounds to re-partition back to the gas phase to re-establish equilibrium." The oxidized molecules partition to the walls more quickly, only to partition back faster?*

Author response: The original text meant to explain that compounds that are lost quickly to the walls are also expected to evaporate quickly from the particle phase in order to maintain particle-gas equilibrium.

To clarify this, we have changed the text from:

Page 2711 Line 8: "If vapor-phase wall loss is the driving factor for the decrease in organics in this study, it would be expected that oxidized compounds would decrease more rapidly, causing these compounds to re-partition back to the gas phase to re-establish equilibrium"

To:

"If vapor-phase wall loss is the driving factor for the decrease of organics in this study, it would be expected that oxidized compounds would be lost to the walls more rapidly. Subsequently, these highly oxidized compounds would re-partition back to the gas phase in order to re-establish particle-gas equilibrium."

491*24. Table 1: the range of delta(HC) here doesn't seem to match Fig. 7, where the range of initial b-*
492 *pinene concentrations is 9-21 ppb, which would be 50-117 ug m-3. Also, I suggest using the*
493 *same units throughout. If the times after chemistry initiation at which yields were evaluated is*
494 *vastly different for different conditions, maybe include that time in this table?*
495
496 **Author response:** The concentrations listed in Table 1 of the original manuscript are the
497 nominal β-pinene concentrations based on a 10 m^3 chamber used for the experiments presented
498 in this paper and so the concentrations are different from those presented in Table 1. These
499 numbers were therefore inaccurate and have been corrected for a chamber volume of 12 m^3.
500
501 We also agree with the reviewer that the same units should have been used throughout the
502 manuscript. As requested by the reviewer, in order to stay consistent with the values shown in
503 Table 1, we have added a column in Table 1 to report the mixing ratio of β-pinene in ppb to be
504 consistent with Figure 7. The updated figure and table are shown below:

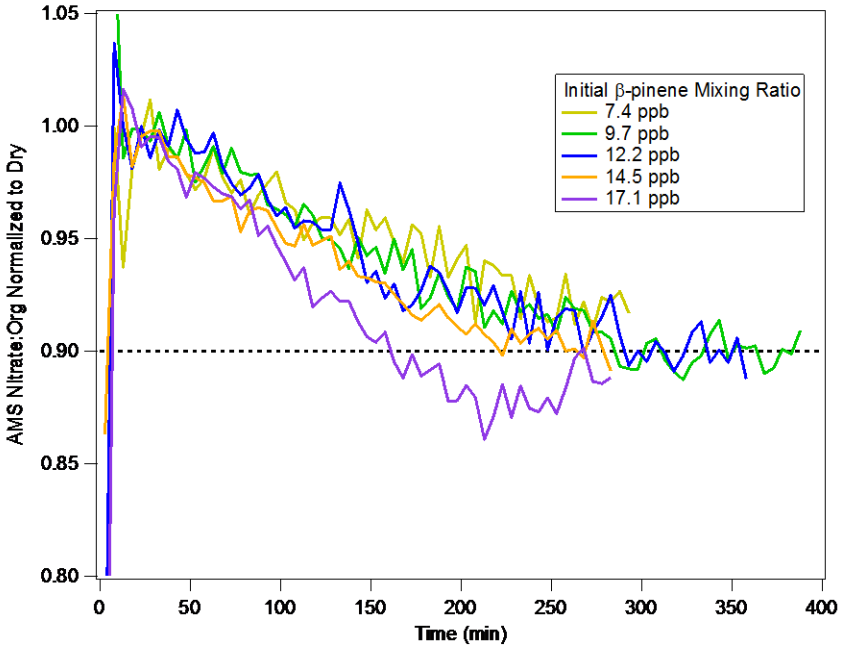

505
506

Experiment	RH (%)	Condition	Seed	ΔHC[c] (ppb)	ΔHC[c] (μg/m^3)	ΔM_o[d] (μg/m^3)	Mass Yield (%)
1	< 2	RO_2+NO_3	AS[a]	2.5±0.2	13.8±1.3	5.3±0.41	38.3±5.5
2	< 2	RO_2+NO_3	AS	2.5±0.2	13.8±1.3	5.4±0.15	38.7±4.0
3	< 2	RO_2+NO_3	AS	7.4±0.7	41.5±3.9	25.3±0.54	61.0±6.0
4	< 2	RO_2+NO_3	AS	9.9±0.9	55.4±5.2	--[e]	--
5	< 2	RO_2+NO_3	AS	12.4±1.2	69.2±6.5	--	--
6	< 2	RO_2+NO_3	AS	12.4±1.2	69.2±6.5	44.9±0.73	64.9±6.3
7	< 2	RO_2+NO_3	AS	14.9±1.4	83.0±7.8	--	--
8	< 2	RO_2+NO_3	AS	17.4±1.6	96.9±9.1	--	--
9	< 2	RO_2+NO_3	AS	24.8±2.4	138.4±13.1	134.6±1.51	97.2±9.3
10	< 2	RO_2+NO_3	AS	24.8±2.4	138.4±13.1	114.7±2.51	82.9±8.2
11	51	RO_2+NO_3	AS	2.4±0.2	13.2±1.2	7.3±0.57	55.4±8.2

12	50	RO_2+NO_3	AS	2.4±0.2	13.2±1.2	6.8±0.36	51.7±6.3
13	49	RO_2+NO_3	AS	7.1±0.7	39.6±3.7	23.0±0.65	57.9±6.0
14	49	RO_2+NO_3	AS	9.5±0.9	52.8±5.0	34.2±0.89	64.8±6.6
15	51	RO_2+NO_3	AS	9.5±0.9	52.8±5.0	33.1±0.56	62.5±6.1
16	50	RO_2+NO_3	AS	11.9±1.1	66.1±6.2	43.5±0.60	65.9±6.4
17	50	RO_2+NO_3	AS	11.9±1.1	66.1±6.2	42.2±0.98	63.9±6.4
18	51	RO_2+NO_3	AS	14.2±1.3	79.3±7.5	60.7±0.83	76.6±7.4
19	51	RO_2+NO_3	AS	16.6±1.6	92.5±8.7	68.4±1.26	73.9±7.2
20	71	RO_2+NO_3	AS	11.9±1.1	66.1±6.2	50.5±1.32	76.4±7.8
21	70	RO_2+NO_3	AS	11.9±1.1	66.1±6.2	50.0±0.44	75.7±7.2
22	72	RO_2+NO_3	AS	23.7±2.2	132.1±12.5	125.5±1.35	95.0±9.0
23	68	RO_2+NO_3	AS	23.7±2.2	132.1±12.5	132.9±1.33	100.6±9.5
24	51	RO_2+NO_3	AS+SA[b]	7.1±0.7	39.6±3.7	25.5±0.69	64.4±6.6
25	50	RO_2+NO_3	AS+SA	11.9±1.1	66.1±6.2	46.4±1.10	70.4±6.8
26	51	RO_2+NO_3	AS+SA	16.6±1.6	92.5±8.7	74.4±1.23	80.5±7.7
27	< 3	RO_2+HO_2	AS	7.4±0.7	41.5±3.9	27.0 ±0.54	64.9±6.4
28	< 3	RO_2+HO_2	AS	7.4±0.7	41.5±3.9	22.9±0.71	55.0±5.8
29	< 3	RO_2+HO_2	AS	12.4±1.2	69.2±6.5	49.3±0.97	71.2±7.1
30	< 3	RO_2+HO_2	AS	12.4±1.2	69.2±6.5	36.1±1.17	52.2±5.6
31	< 2	RO_2+HO_2	AS	17.4±1.6	96.9±9.1	71.2±2.32	73.4±7.8
32	< 3	RO_2+HO_2	AS	37.3±3.5	207.6±19.6	216.1±1.96	104.1±9.9
33	49	RO_2+HO_2	AS	35.6±3.4	198.2±18.7	147.8±1.42	74.6±7.1
34	69	RO_2+HO_2	AS+SA	2.4±0.2	13.2±1.2	5.1±0.59	38.5±8.1
35	69	RO_2+HO_2	AS+SA	4.7±0.4	26.4±2.5	16.1±1.14	61.0±9.0
36	66	RO_2+HO_2	AS+SA	7.1±0.7	39.6±3.7	30.3±0.71	76.4±7.8
37	66	RO_2+HO_2	AS+SA	11.9±1.1	66.1±6.2	47.7±1.77	72.1±8.1
38	< 1	RO_2+NO_3	None	12.4±1.2	69.2±6.5	42.3±0.46	61.1±5.8
39	50	RO_2+NO_3	None	11.9±1.1	66.1±6.2	44.3±0.34	67.0±6.4
40	<2	RO_2+HO_2	None	12.4±1.2	69.2±6.5	18.7±0.51	27.0±2.8
41	66	RO_2+HO_2	None	11.9±1.1	66.1±6.2	28.5±0.60	43.1±4.2
42	50	RO_2+HO_2	None	11.9±1.1	66.1±6.2	18.4±0.34	27.8±2.7
43	<2	RO_2+HO_2	AS*	12.4±1.2	69.2±6.5	33.6±0.79	48.5±4.9
44	68	RO_2+HO_2	AS+SA*	11.9±1.1	66.1±6.2	46.6±0.86	70.6±7.0
45	66	RO_2+HO_2	AS+SA*	11.9±1.1	66.1±6.2	44.5±0.87	67.3±6.7

25. *Fig. 3: Looks to me like the second-lowest point drives the shape of the yield curve – maybe check fit parameters without that point to see if robust. Also, you refer to x axis error bars which are not present in the plot.*

Author response: The x-axis error bars for these experiments are included in the graph in the original manuscript. The size of each individual data point is larger than the stated uncertainties for the x-axis and cannot be seen in the closed triangles.

In terms of fitting the data without the second lowest mass loading, as we discussed in response to comment #14, this does not affect yield curve and thus our fitting is robust.

26. Fig. 4 same missing x axis error bars. Why not include the unseeded yields on here too (currently in Figure S8)? This would make the comparison easier, rather than eyeballing data vs. the seeded fit line in the supplemental. If this makes the plot too busy, I retract the comment, just thought it would ease comparison.

Author response: We refer the reviewer to the response to comment #25 regarding the x-axis error bars in Figure 4.

In the original manuscript, the unseeded yields for all experimental conditions are shown on Fig. S8. Moving the unseeded yields for the "RO_2+NO_3 dominant" and "RO_2+HO_2 dominant" from Fig. S8 to Fig. 3 and Fig. 4, respectively, puts too much information on the figures that we think would be distracting to the reader.

27. Fig. 7: add into the caption that these data are all for the RO2+NO3 experiments.

Author response: As requested, we have revised the caption of Fig. 7 from:

"Figure 7: The AMS Nitrate:Org ratio of humid (RH = 50%) experiments normalized to the corresponding dry experiments with same initial β-pinene mixing ratio, five-minute averaged. This ratio is referred to as $(Nitrate:Org)_{norm}$ in the main text. For comparison purpose, all data are normalized to the highest $(Nitrate:Org)_{norm}$ ratio."

To:

"Figure 7: The AMS Nitrate:Org ratio of humid (RH = 50%) experiments normalized to the corresponding dry experiments with same initial β-pinene mixing ratio, five-minute averaged, for "RO_2+NO_3 dominant" experiments. This ratio is referred to as $(Nitrate:Org)_{norm}$ in the main text. For comparison purpose, all data are normalized to the highest $(Nitrate:Org)_{norm}$ ratio."

28. See comment 16 above about Figure 9 confusion. If you keep this plot, I suggest adding to the caption to state that 235 nm corresponds to ROOR & ROOH and 270 nm to C=O and nitrate functional groups.

Author response: To clarify this, we have changed the caption of Fig. 9 from:

"Figure 9: Ratio of the total areas integrated under UV-visible chromatograms collected at (gray bars) 235nm and (teal bars) 270nm relative to 205nm for experiments dominated by (left-hand side panel) RO_2+NO_3 reaction and (right-hand side panel) RO_2+HO_2 reaction under both humid and dry conditions."

To:

"Figure 9: Ratio of the total areas integrated under UV-visible chromatograms collected at 235 nm (gray bars, ROOR and ROOH) and 270 nm (teal bars, -C=O and -ONO_2) relative to 205 nm for experiments dominated by RO_2+NO_3 reaction (left-hand side panel) and RO_2+HO_2 reaction (right-hand side panel) under both humid and dry conditions."

29. Figure 10: Was this spectrum selected because agreement was better than RO2+NO3 conditions? Or because more likely to be atmospherically relevant? Would it look any different? I suggest omitting "Fraction of" in the annotation. "Signal x3" is clear.

Author response: The mass spectrum shown in Fig. 10 was chosen because it is more likely to be atmospherically relevant, specifically for the SOAS campaign where the RO_2+HO_2 reaction pathways are believed to be dominant under high humidity and the aerosol are highly acidic. This is explained in the original manuscript, which stated that at SOAS, the predicted liquid water content is high while the predicted aerosol pH is in the acidic region. (Cerully et al., 2014;Guo et al., 2014).

As requested, we have removed the words "Fraction of" in the annotation.

SI: Suggest modeling the HO2+RO2 experiments as well as RO2+NO3 – since you are producing HO2 simultaneous to NO3+VOC reactions this is slightly more complex – so it would be better to model these conditions using MCM rather than just determining the ratio of HCHO to bpin. I suggest creating an analogous plot to S9 showing dominant fate for both RO2 fate cases.

Author response: As we discussed in our response to comment #3, our model did not converge when we included HCHO in the simulations. Although it is possible that some HO_2 radicals could be produced from the NO_3+VOC reactions, Fig. S9 does show that these reactions do not produce an appreciable concentration of HO_2 radicals under "RO_2+NO_3 dominant" experiments as evidenced by the low RO_2+HO_2 reaction modeled in this scenario. Furthermore, HO_2 radicals produced by the NO_3+VOC reaction would only increase the RO_2+HO_2 reactions in "RO_2+HO_2 dominant" results, but we already suggest this to be the major pathway without this additional HO_2.

<u>Response to Referee 2-Major Comments (Referees' comments are italicized)</u>

1. The authors present significant detail in terms of the identification of gas-phase organic nitrates in the system and some information on particle-phase composition such as the fact that 45-74% of the aerosol is likely organic nitrates. The information provided in the form of an Odum 2-product or VBS fit allows for an easy, but incremental, update to existing monoterpene+NO3 SOA pathways in models. As organic nitrates are being increasingly recognized for their importance in recycling or removing NOx from the atmosphere, contributing to nitrogen deposition in sensitive ecosystems, etc. they are being included in greater detail in models. Given the significant contribution of organic nitrates to aerosol, can modeling of monoterpene+NO3 aerosol be further advanced to allow for a greater consistency between gas and aerosol-phase mechanisms? With aerosol yields on the order of 27 to 104%, adding an Odum 2-product SOA

yield on top of a gas-phase mechanism could lead to substantial double counting. Is there a later generation product (such as an organic nitrate) or rate limiting step beyond the initial monoterpene+NO3 that models could base SOA formation on?

Author response: We agree that coupling the gas-phase mechanism with the Odum's two product model can lead to double counting and both methods should not be used simultaneously. However, the Odum's two product yield can provide a needed restraint for gas-phase mechanisms that predict aerosol yield based on the partitioning of products from each generation. Partitioning and abundance of each generation product can be adjusted to match the yield curve, so it is imperative that the yield curve accurately predict SOA yield at all atmospherically relevant aerosol concentrations.

If there are later generation products, Fig. 2 shows that the particle volume, HR-ToF-AMS organics, and several gas phase species measured by CIMS reach a maximum at around 15 minutes into the onset of reaction. As this is on a time scale similar to that of the mixing time of the chamber, determination of any intermediate compounds that are formed after initial β-pinene reaction and before the final products is difficult. There is evidence of later-generation products through hydrolysis. Our study showed that only a minority (10%) of the particulate organic nitrates hydrolyze (Fig. 7).

The hydrolysis of organic nitrates formed by most BVOC+NO_3 reactions are likely primary/secondary nitrates (see our response to comment #20 by Reviewer 1). Organic nitrates formed by the photooxidation of terpenes under high NO_x conditions, however, are more likely to form tertiary nitrates that hydrolyze in the span of hours (Darer et al. 2011). To accurately model the ambient hydrolysis of organic nitrates, it is important to consider the relative contributions of organic nitrates formed from nitrate radical chemistry and photooxidation. The hydrolysis of organic nitrates can produce HNO_3. On the other hand, organic nitrates that do not hydrolyze, can potentially be photolyzed or oxidized by OH radicals to release NO_x back into the atmosphere (Suarez-Bertoa et al., 2012) or lost by dry or wet deposition. Therefore, it is essential to determine the appropriate branching ratio of primary/secondary vs tertiary organic nitrates in order to accurately model global and regional NO_x cycles.

2. Can the laboratory AMS spectra be tied more quantitatively to the field LO-OOA? The critical link seems to focus on m/z 67 and 91. Given that those peaks are only a portion of the spectrum, how to you attribute the majority of the spectrum to monoterpene+NO3 reactions?

Author response: We believe that the LO-OOA factor identified from the SOAS AMS data has a large contribution from monoterpene+NO_3 chemistry, specifically β-pinene+NO_3, based on the following three pieces of evidence. First, Xu et al. (2015) showed that the LO-OOA factor peaks at night, which indicates that LO-OOA is primarily formed by nighttime chemistry, where nitrate radical oxidation is likely dominant. Second, LO-OOA has a strong correlation with the estimated organic nitrate concentration, which makes up a significant fraction of SOA formed by monoterpene+NO_3 chemistry (Spittler et al., 2006; Fry et al., 2009; Perring et al., 2009; Rollins et al., 2009; Kwan et al., 2012; Fry et al., 2014). Third, Xu et al. (2015) showed high nocturnal monoterpene emissions at SOAS, a substantial fraction of which is made up of β-pinene. This

suggests that the particle phase products formed from the β-pinene+NO_3 reaction contribute a significant fraction to the nighttime SOA at SOAS.

While we cannot exclusively rule out the contributions of various chemical reactions (BVOCs, oxidants), the above evidences suggested that LO-OOA has significant contributions from the β-pinene+NO_3 reaction. This is subsequently validated by similarities in the LO-OOA factor and the mass spectrum β-pinene+NO_3 via the $C_5H_7^+$ (m/z 67) and $C_7H_7^+$ (m/z 91) fragments. The similarities in AMS mass spectra are often not determined by the absolute abundance of each peaks, but the overall mass spectra signature (the relative intensities of the peaks).

Response to Referee 2-Minor Comments (Referees' comments are italicized)

1. Is beta-pinene likely a good surrogate for all monoterpene+NO3 SOA formation behavior in the southeast US? How likely is the abundance of species like alpha-pinene likely to bring down the overall monoterpene+NO3 effective yield?

Author response: We believe that the β-pinene+NO_3 chemistry produces a large portion of the SOA formed by the monoterpene+NO_3 chemistry. Xu et al. (2015) previously reported that the α-pinene and β-pinene concentrations are higher than those of other monoterpenes by a factor of 5. In addition, Fry et al. (2014) and Spittler et al. (2006) have previously shown that the SOA mass yield from the α-pinene+NO_3 reaction is very low and does not contribute much to the SOA in the Southeast US. Therefore, we propose that the majority of the SOA produced by monoterpene+NO_3 chemistry could be attributed to the β-pinene+NO_3 reaction.

The abundance of species like α-pinene likely lowers the overall monoterpene+NO_3 effective yield, and models may over-predict aerosol yields from monoterpene+NO_3 chemistry if only the β-pinene+NO_3 reaction is considered. Therefore, we recommend that aerosol models implement subgroups for monoterpene+NO_3 aerosol mass yields instead of lumping all monoterpene+NO_3 yields into a single category.

2. Page 2691, in adjusting the yield curve for density other than 1, both the yield and loading should be multiplied by the density shifting the entire curve up and to the right. It's not clear if both the loading and Y values were adjusted or just the Y.

Author response: The reviewer is correct, only the yields were shifted by the density in the original manuscript. We have corrected this error in the revised manuscript and the density is now accounted for in both the yields and mass loadings in the revised figure. In addition to correcting the mass loading by density, we also corrected the data presented by Griffin et al. (1999) to account for the different temperatures used in their experiments. Using an enthalpy of vaporization of 42 kJ/mol and an average temperature of 306K used in Griffin et al. (1999), we adjusted the one-product fit parameter, K, for 298K using the Clausius-Claperyon equation (Chung and Seinfeld, 2002). After correcting for the density and temperature, the yield curve from Griffin et al. (1999) compares to our data as shown in the figure below.

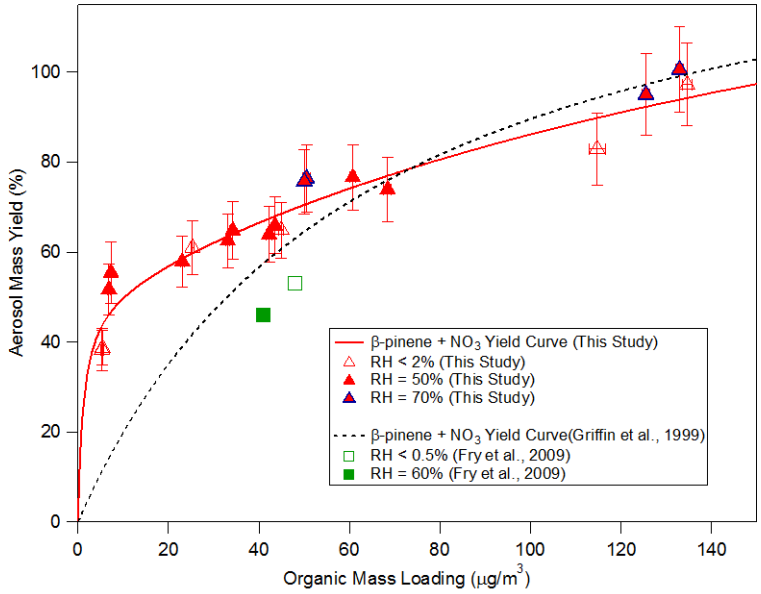

In addition, Table 2 in the original manuscript showed data previously presented by Griffin et al. (1999) without density or temperature corrections. In the revised manuscript, we have changed the parameters in Table 2 to reflect the adjustments based on density and temperature.

Table 2: Fit parameters for two-product model proposed by Odum et al. (1996)

	α_1	K_1	α_2	K_2
β-pinene+NO_3 (this study)	**1.187**	**0.004546**	**0.496**	**0.880**
Griffin et al. (1999)	**1.464**	**0.0158**		

Due to these changes, the following modifications have been made to the text:

Page 2691 Line 22**:** "As Griffin et al. (1999) assumed an aerosol density of 1.0 g cm^{-3}, the yield curve from Griffin et al. (1999) shown in Fig. 3 has been multiplied by the density calculated in this study for "RO_2+NO_3 dominant" experiments under dry conditions (i.e. 1.41 g cm^{-3})."

To:

As Griffin et al. (1999) assumed an aerosol density of 1.0 g cm^{-3}, the experimental data from Griffin et al. (1999) shown in Fig. 3 have been multiplied by the density calculated in this study for "RO2+NO3 dominant" experiments under dry conditions (i.e. 1.41 g cm^{-3}).

After this sentence:

Page 2691 Line 25: "The data shown in Fig. 3 from Fry et al. (2009) have also incorporated a particle density of 1.6 g cm^{-3} calculated in their study."

We add:

"In addition to correcting for density, the yield curve partitioning coefficient, K, from Griffin et al. (1999) has been adjusted from 306K to 298K using an enthalpy of vaporization of 42 kJ mol^{-1} (Chung and Seinfeld, 2002)."

We also change:

Page 2698 Line 12: "The two-product yield curve in Griffin et al. (1999) was generated from chamber experiments with $\Delta M_o > 30$ μg m^{-3} (range of ΔM_o =30–470 μg m^{-3}) and extrapolated down to lower loadings."

To:

"The yield curve in Griffin et al. (1999) was generated from chamber experiments with $\Delta M_o > 45$ μg m^{-3} (range of ΔM_o =45–660 μg m^{-3}) and extrapolated down to lower loadings."

We also add the following reference to the list of references:

Chung, S. H., and Seinfeld, J. H.: Global distribution and climate forcing of carbonaceous aerosols, Journal of Geophysical Research: Atmospheres, 107, 4407, 10.1029/2001JD001397, 2002.

3. Figure 8: The description of "RO2+HO2" and "RO2+NO3" dominant regimes is used throughout the text. Is there a way to highlight how Figure 8 is different under those two regimes in a simple way? In terms of relative abundance of species or major reaction pathways?

Author response: As requested, we have highlighted the reactions that are enhanced in the RO_2+HO_2 dominant pathway in Figure 8 (highlighted in purple). We believe that all the other reaction pathways shown in Figure 8 are possible under both the "RO_2+NO_3 dominant" and "RO_2+HO_2 dominant" pathways.

The Figure 8 caption is changed to read:

"Figure 8: Generation of gas-phase species with molecular weights (MW) of 215, 229, and 231 amu detected by CIMS (red font), aerosol species with MW=245 amu in filters analyzed by UHPLC-MS (blue font). Reaction numbers are given in green font and reaction with generic radical Q$^{\cdot}$ (e.g. NO_3, RO_2, etc.) is used to symbolize any species abstracting hydrogen atoms. Reactions which can be accomplished by any of the radicals present (RO_2, HO_2, NO_3 etc.) are symbolized by reaction with generic radical L$^{\cdot}$. Reactions enhanced in the RO_2+HO_2 dominant pathway are highlighted in purple."

The updated figure is shown below.

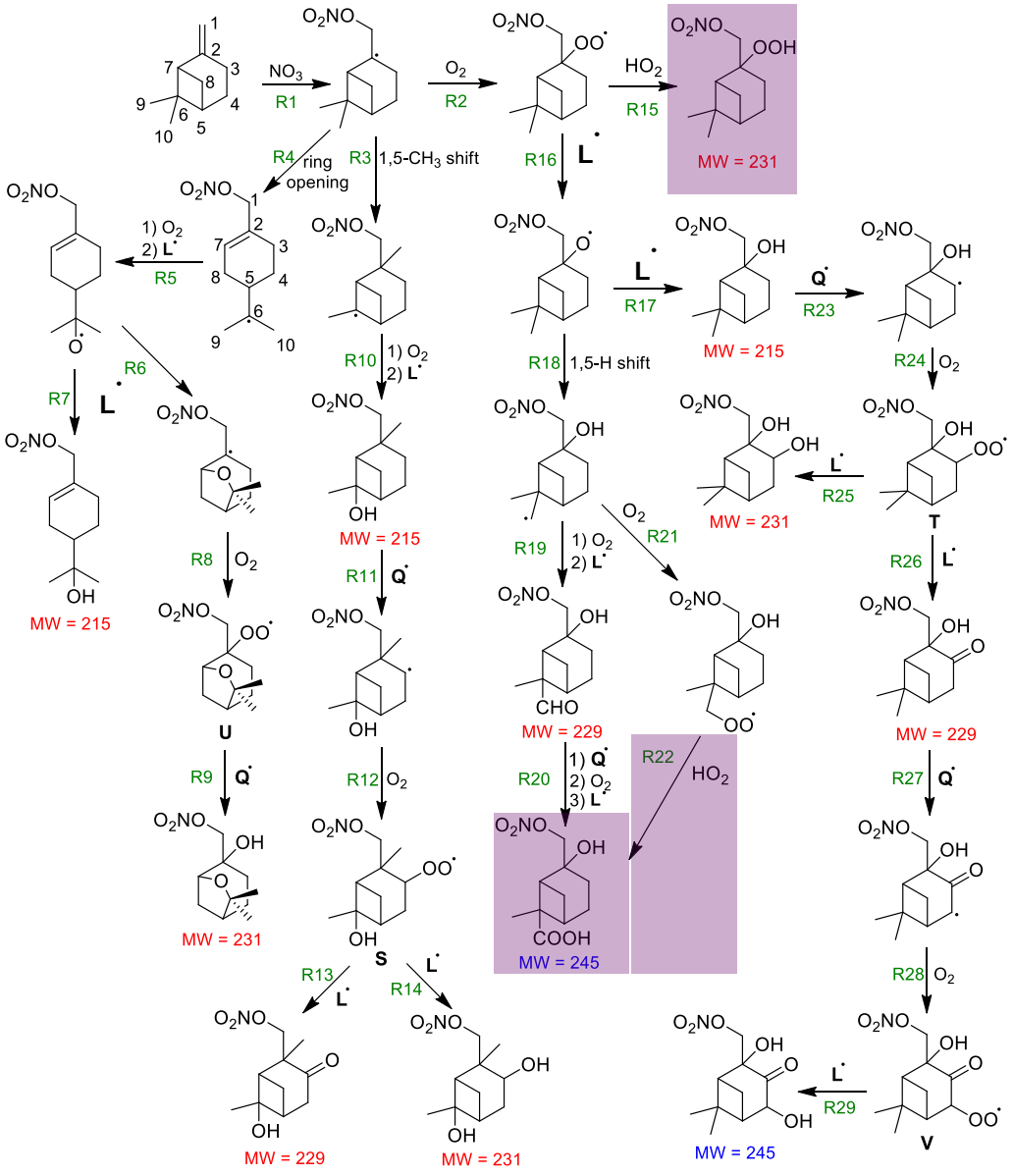

765
766
767
768 *4. Page 2698 line 20-29, page 2699: Is all the data from Griffin et al. 1999 shown in figure 3*
769 *(just 2 points)? Discussing the mass loadings of those points more clearly demonstrates the*
770 *shortcomings of previous work than discussing the previous Odum fit. Also note that on line 12*
771 *on page 2698, the Griffin fit is referred to as an Odum 2-product, while only one product was*
772 *successfully fit in Table 2.*
773
774 **Author response:** There are four data points presented in the study by Griffin et al. (1999).
775 However only two of these data points have a mass loading below 216 μg m^{-3}, the highest mass
776 loading recorded in our study. These are the two data points shown in the original manuscript.
777 After correcting the yield curve produced using Griffin et al. (1999) for temperature, only the
778 yield curve will be shown because the Clausius-Clayperyon equation cannot be used to correct
779 individual data points. The high mass loadings in the study by Griffin et al. (1999) lead to an

under prediction of aerosol yield at low loadings and we believe that these high mass loadings and the pervious Odum fit are intertwined.

The reviewer is correct in pointing out that the Griffin fit should not be referred to as an Odum two-product fit since only one product was successfully fit in Table 2.

Therefore we have changed:

Page 2698 Line 12: "The two-product yield curve in Griffin et al. (1999) was generated from chamber experiments with $\Delta M_o > 30$ μg m^{-3} (range of ΔM_o =30–470 μg m^{-3}) and extrapolated down to lower loadings."

To:

"The yield curve in Griffin et al. (1999) was generated from chamber experiments with $\Delta M_o > 45$ μg m^{-3} (range of ΔM_o =45–660 μg m^{-3}) and extrapolated down to lower loadings."

<u>The following are additional minor changes the authors would like to make to the text:</u>

1) In the original manuscript, the ratio for NO^+:NO_2^+ was based on where the majority of the data clustered. We feel that it is more appropriate to report the full range and add to the discussion of the NO^+:NO_2^+ ratio in the revised manuscript

Page 2680 Line 9: "The ions at *m/z* 30 (NO^+) and *m/z* 46 (NO_2^+) contribute about 11% to the total organics signal in the typical aerosol mass spectrum, with NO^+:NO_2^+ ratio ranging from 6 to 9 in all experiments conducted."

To:

The ions at *m/z* 30 (NO^+) and *m/z* 46 (NO_2^+) contribute about 11% to the total organics signal in the typical aerosol mass spectrum, with NO^+:NO_2^+ ratio ranging from 4.8 to 10.2 in all experiments conducted.

We also changed

Page 2692 Line 7: "The mass spectrum for the aerosol generated in the "RO_2+HO_2 dominant" and "RO_2+NO_3 dominant" experiments are similar, one notable difference being the NO^+:NO_2^+ ratio. While the NO^+:NO_2^+ ratio is typically 6-7.5 for "RO_2+NO_3 dominant" experiments, it is typically 8-9 for "RO_2+HO_2 dominant" experiments."

To:

"The mass spectrum for the aerosol generated in the "RO_2+HO_2 dominant" and "RO_2+NO_3 dominant" experiments are similar. One notable difference between the "RO_2+HO_2 dominant" and "RO_2+NO_3 dominant" experiments is the NO^+:NO_2^+ ratio for

the organic nitrates (R-ON), which ranges from 4.8-10.2 for all experiments. While the NO^+:NO_2^+ ratio averages 6.5 for "RO_2+NO_3 dominant" experiments, it averages 8.6 for "RO_2+HO_2 dominant" experiments. Since the R-ON may depend on the instrument, we normalize the R-ON to the NO^+:NO_2^+ of ammonium nitrate (R-AN), which is expected to be a better metric (Farmer et al., 2010). In our study, multiple measurements of R-AN are obtained from the ionization efficiency (IE) calibrations and the average value is about 1.8 (range of 1.2-2.7). We calculate the average R-ON:R-AN ratio to be 3.2 for "RO_2+NO_3 dominant" experiments and 4.8 for "RO_2+HO_2 dominant" experiments.

Additionally, after the sentence:

Page 2705 Line 14: Previous studies (Fry et al., 2009;Bruns et al., 2010) on the β-pinene+NO_3 reaction suggested that the NO^+:NO_2^+ ratio for β-pinene+NO_3 SOA is on the order of 10:1, higher that the values determined in this study.

We add:

One explanation for the difference in R-ON between this study and previous literature is instrument bias. Different instruments may have different R-ON values. One way to circumvent this bias is to compare the R-ON:R-AN ratio. The averaged R-ON:R-AN for all experiments is 3.9, which is in agreement with values calculated by Fry et al. (2009) and Bruns et al. (2010) (range 3.7-4.2).

2) We change:

Page 2681 Line 21: "Results from previous field studies provided evidence of aerosol formation from nitrate radical oxidation of BVOCs during both daytime and nighttime (McLaren et al., 2004; Iinuma et al., 2007; Fuentes et al., 2007; Brown et al., 2009; Rastogi et al., 2011; Rollins et al., 2012; Brown et al., 2013; Rollins et al., 2013).

To:

"Results from previous field studies provided evidence of aerosol formation from nitrate radical oxidation of BVOCs during both daytime and nighttime (McLaren et al., 2004; Iinuma et al., 2007; Fuentes et al., 2007; Brown et al., 2009; Rastogi et al., 2011; Rollins et al., 2012; Brown et al., 2013; Rollins et al., 2013). Monoterpenes have also been found to make up as much as 28% non-methane organic carbon emissions from biomass burning in both field and laboratory studies (Akagi et al., 2013; Hatch et al., 2015; Stockwell et al., 2015). Fires from biomass burning are more likely to smolder at night and are therefore more likely to emit monoterpenes (Akagi et al., 2013)."

3) We find that we were using older rate constants to model the equilibrium partitioning of the N_2O_5 with NO_2 and NO_3 instead of the constants reported in Table S1. We have updated our model to include the rate constants from Saunders et al. (2003), as reported in Table S1. With this, the ratio of the amount of N2O5 injected to hydrocarbon injected is 6:1 (instead of 4:1) in the RO_2+NO_3 experiments. The change in the rate constants only slightly changes the branching

ratios of RO_2+NO_3, RO_2+RO_2, and RO_2+HO_2 and do not affect the dominant branching ratio in either the "RO_2+NO_3 dominant" or "RO_2+HO_2 dominant" experiments. The RO_2+NO_3 reaction still dominates the "RO_2+NO_3 dominant" experiments and the RO_2+HO_2 reaction still dominates the RO_2+HO_2 dominant" experiments as stated in the text.

We change

Page 2687 Line 2: We aim for an initial N_2O_5:β-pinene ratio of ~4:1.

To:

We aim for an initial N_2O_5:β-pinene ratio of ~6:1.

4) In the study done by Hallquist et al. (1999), we refer to an experiment conducted at low mass loading. In the study by Hallquist et al. (1999), the experiment was performed at 7 ppb of β-pinene but, in error, this was reported as 7 μg m^{-3}. To correct this, we change

Page 2699, Line 26: "There is a substantial difference between our β-pinene+NO3 SOA yield and that from Hallquist et al. (1999), which reported an aerosol mass yield of 10% for a mass loading of 7 μg m^{-3}".

To:

"There is a substantial difference between our β-pinene+NO3 SOA yield and that from Hallquist et al. (1999), which reported an aerosol mass yield of 10% for a mass loading of 4 μg m^{-3}".

5) In error, the sentences below reference the wrong reaction. Therefore, we change:

Page 2702 Line 22: "The reaction of RO_2+NO_3 produces an RO radical (Fig. 8, Reaction R2) which can undergo decomposition or isomerization (Orlando and Tyndall, 2012; Ziemann and Atkinson, 2012)."

To:

"The reaction of RO_2+NO_3 produces an RO radical (Fig. 8, Reaction R16) which can undergo decomposition or isomerization (Orlando and Tyndall, 2012; Ziemann and Atkinson, 2012)."

6) We change

Page 2710 Line 1: "Since the Org:Sulfate ratio decreases after SOA reaches peak growth (Fig. 6), it is likely that aerosol fragmentation is the dominant aging pathway of SOA."

To:

"The use of Org:sulfate is a good proxy for aerosol aging when the organics only condense onto existing ammonium sulfate particles. A study by Loza et al. (2012) has demonstrated that in the case of rapid condensation of organic species, the time scale of condensation is less than the time scale of diffusion to existing seed particle. When in this "diffusion-limited growth" regime, the organic mass partially nucleates to form new particles. Since the nucleated particles are smaller than those particles in which ammonium sulfate acted as a seed for condensation, organics contained in these nucleated particles will be lost to the chamber walls more rapidly than the existing seed particles (Fig. S10). This could lead to in an overall decrease in the Org:sulfate ratio. In our study, the Org:Sulfate ratio decreases after SOA reaches peak growth (Fig. 6). It is possible that this decrease is caused by wall loss of organic particles formed in the diffusion-limited growth regime. It is also possible that fragmentation of aerosol components is the dominant aging pathway, resulting in a decrease in the Org:Sulfate ratio."

7) We change

Page 2710 Line 4: "Fragmentation of SOA alone would cause all AMS organic families to either decrease or remain constant relative to sulfate."

To:

"Rapid loss of organics due to particle wall loss or fragmentation of SOA would cause all AMS organic families to either decrease or remain constant relative to sulfate."

8) Table 1: The experiments are renumbered to correct for the omission of the number "44"

9) In order to correct the absence of the CO^+ fragment in the mass spectra in Fig. 2 and Fig. 10, we change these figures to include the CO^+ fragment:

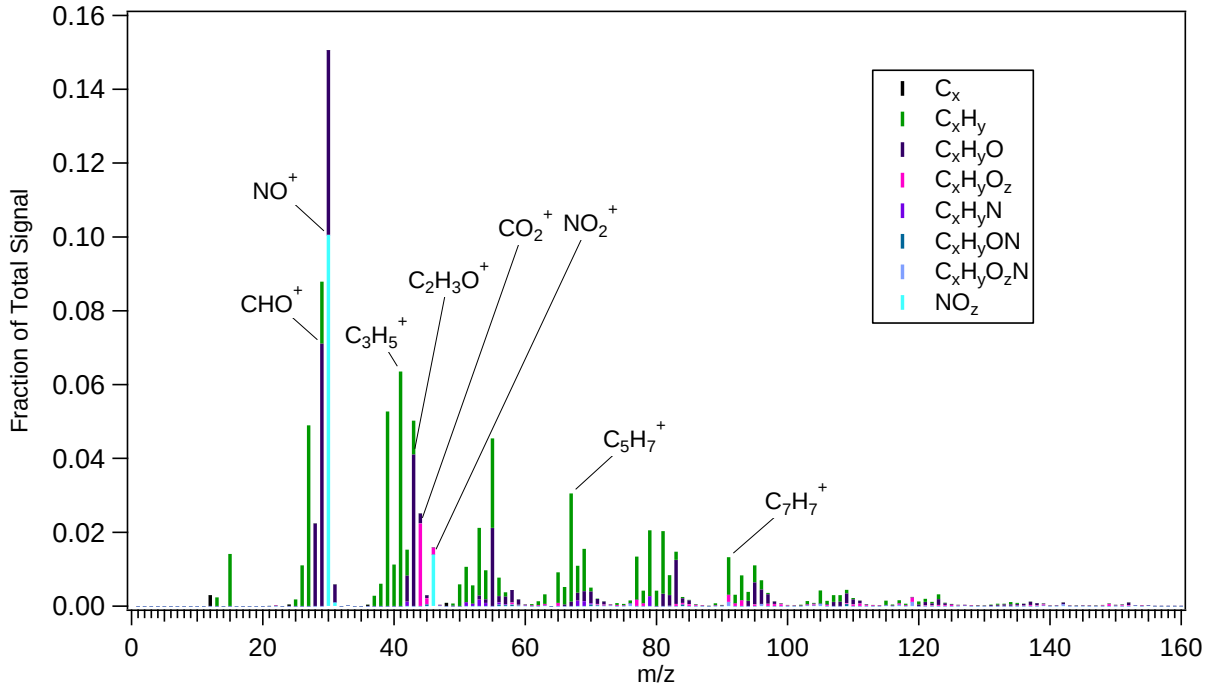
Fraction of Total Signal
0.16
0.14
0.12
0.10
0.08
0.06
0.04
0.02
0.00
0
20
40
60
80
100
120
140
160
m/z
NO+
CHO+
C3H5+
C2H3O+
CO2+
NO2+
C5H7+
C7H7+
Cx
CxHy
CxHyO
CxHyOz
CxHyN
CxHyON
CxHyOzN
NOz

949
950

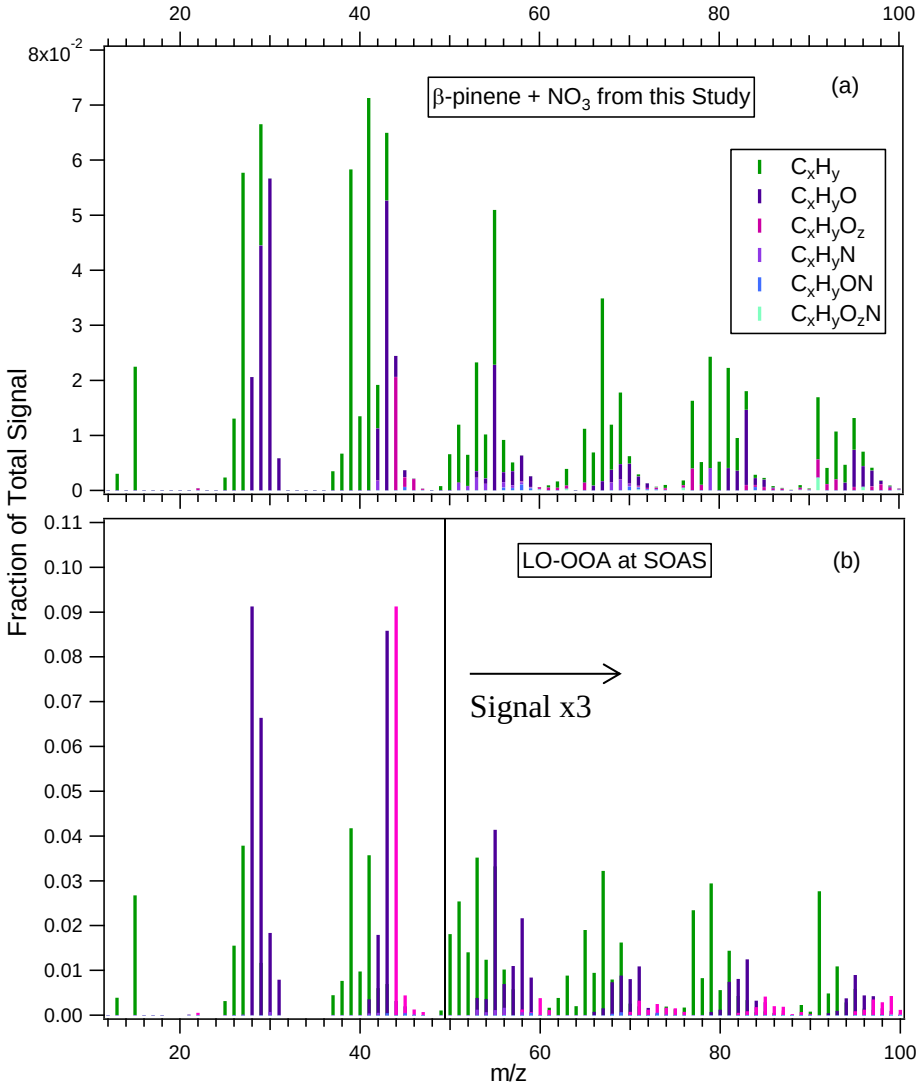

This resulted in some changes in the calculation of some of our numbers, specifically the ratio of the NO^+ + CH_2O^+ / (NO_2^+ + $CH_2O_2^+$) ratio and $C_5H_7^+/C_7H_7^+$ ratios. We change

Page 2705 Line 18: Specifically, if we were to include the contribution of the organic CH_2O^+ fragment at *m/z* 30 (in addition to contribution from NO^+ and NO_2^+), the corresponding NO^+:NO_2^+ ratios would be higher, i.e., 10:1 for "RO_2+NO_3 dominant" experiments and 13:1 for "RO_2+HO_2 dominant" experiments.

To:

Specifically, if we were to include the contribution of the organic CH_2O^+ and $CH_2O_2^+$ fragments at *m/z* 30 and *m/z* 46 (in addition to contribution from NO^+ and NO_2^+), the corresponding NO^+:NO_2^+ ratios would be higher, i.e., 9:1 for "RO_2+NO_3 dominant" experiments and 11:1 for "RO_2+HO_2 dominant" experiments.

We also change:

Page 2713, Line 5: Most noticeable of these are *m/z* 67 ($C_5H_7^+$) and *m/z* 91 ($C_7H_7^+$) with a ratio of these two ions ($C_5H_7^+$: $C_7H_7^+$) of about 2.9 (ranging from 2.5-3.5 in other experiments).

To:

Most noticeable of these are *m/z* 67 ($C_5H_7^+$) and *m/z* 91 ($C_7H_7^+$) with a ratio of these two ions ($C_5H_7^+$: $C_7H_7^+$) of about 2.9 (ranging from 2.5-3.6 in other experiments).

<u>The following references have also been added in the revised manuscript:</u>

Akagi, S. K., Yokelson, R. J., Burling, I. R., Meinardi, S., Simpson, I., Blake, D. R., McMeeking, G. R., Sullivan, A., Lee, T., Kreidenweis, S., Urbanski, S., Reardon, J., Griffith, D. W. T., Johnson, T. J., and Weise, D. R.: Measurements of reactive trace gases and variable O3 formation rates in some South Carolina biomass burning plumes, Atmos. Chem. Phys., 13, 1141-1165, doi:10.5194/acp-13-1141-2013, 2013.

Hatch, L. E., Luo, W., Pankow, J. F., Yokelson, R. J., Stockwell, C. E., and Barsanti, K. C.: Identification and quantification of gaseous organic compounds emitted from biomass burning using two-dimensional gas chromatography-time-of-flight mass spectrometry, Atmos. Chem. Phys., 15, 1865-1899, doi:10.5194/acp-15-1865-2015, 2015.

Loza, C. L., Chhabra, P. S., Yee, L. D., Craven, J. S., Flagan, R. C., and Seinfeld, J. H.: Chemical aging of m-xylene secondary organic aerosol: laboratory chamber study, Atmos. Chem. Phys., 12, 151-167, doi:10.5194/acp-12-151-2012, 2012.

Stockwell, C. E., Veres, P. R., Williams, J., and Yokelson, R. J.: Characterization of biomass burning emissions from cooking fires, peat, crop residue, and other fuels with high-resolution proton-transfer-reaction time-of-flight mass spectrometry, Atmos. Chem. Phys., 15, 845-865, doi:10.5194/acp-15-845-2015, 2015.

Xu, L., Suresh, S., Guo, H., Weber, R. J., and Ng, N. L.: Aerosol characterization over the southeastern United States using high resolution aerosol mass spectrometry: spatial and seasonal variation of aerosol composition, sources, and organic nitrates, Atmos. Chem. Phys. Discuss., 15, 10479-10552, doi:10.5194/acpd-15-10479-2015, 2015a.

Secondary Organic Aerosol (SOA) Formation from the β-pinene+NO_3 System: Effect of Humidity and Peroxy Radical Fate

C. M. Boyd[1]; J. Sanchez[1]; L. Xu[1]; A. J. Eugene[2]; T. Nah[1]; W. Y. Tuet[1]; M. I. Guzman[2]; N. L. Ng[1,3*]

[1]School of Chemical and Biomolecular Engineering, Georgia Institute of Technology, Atlanta, GA 30332, USA

[2]Department of Chemistry, University of Kentucky, Lexington, KY 40506, USA

[3]School of Earth and Atmospheric Sciences, Georgia Institute of Technology, Atlanta, GA 30332, USA

[*]Correspondence to: Nga Lee Ng (ng@chbe.gatech.edu)

Abstract

The formation of secondary organic aerosol (SOA) from the oxidation of β-pinene via nitrate radicals is investigated in the Georgia Tech Environmental Chamber facility (GTEC). Aerosol yields are determined for experiments performed under both dry (RH < 2%) and humid (RH = 50% and RH = 70%) conditions. To probe the effects of peroxy radical (RO_2) fate on aerosol formation, "RO_2+NO_3 dominant" and "RO_2+HO_2 dominant" experiments are performed. Gas-phase organic nitrate species (with molecular weights of 215 amu, 229 amu, 231 amu, and 245 amu) are detected by chemical ionization mass spectrometry and their formation mechanisms are proposed. The ~~ions at *m/z* 30 (~~NO^+~~)~~ (at *m/z* 30) and ~~*m/z* 46 (~~NO_2^+~~)~~ (at *m/z* 46) ions contribute about 11% to the combined ~~total~~ organics and nitrate signals in the typical aerosol mass spectrum, with NO^+:NO_2^+ ratio ranging from ~~6 to 9~~4.8 to 10.2 in all experiments conducted. The SOA yields in the "RO_2+NO_3 dominant" and "RO_2+HO_2 dominant" experiments are comparable. For a wide range of organic mass loadings (5.1-216.1 μg/m^3), the aerosol mass yield is calculated to be 27.0-104.1%. Although humidity does not appear to affect SOA yields, there is evidence of particle-phase hydrolysis of organic nitrates, which are estimated to compose 45-74% of the organic aerosol. The extent of organic nitrate hydrolysis is significantly lower than that observed in previous studies on photooxidation of volatile organic compounds in the presence of NO_x. It is estimated that about 90 and 10% of the organic nitrates formed from the β-pinene+NO_3 reaction are primary organic nitrates and tertiary organic nitrates, respectively. While the primary organic nitrates do not appear to hydrolyze, the tertiary organic nitrates undergo hydrolysis with a lifetime of 3-4.5 hours. Results from this laboratory chamber study provide the fundamental data to evaluate the contributions of monoterpene+NO_3 reaction to ambient organic aerosol measured in the southeastern United States, including the Southern Oxidant and Aerosol Study (SOAS) and the Southeastern Center for Air Pollution and Epidemiology (SCAPE) study.

1) Introduction

Owing to their high emissions and high reactivity with the major atmospheric oxidants (O_3, OH, NO_3), the oxidation of biogenic volatile organic compounds (BVOCs) emitted by vegetation, such as isoprene (C_5H_8), monoterpenes ($C_{10}H_{16}$), and sesquiterpenes ($C_{15}H_{24}$), is believed to be the dominant contributor to global secondary organic aerosol (SOA) formation (e.g., ~~(~~Kanakidou et al., 2005). While this is supported by the observation that ambient organic aerosol is predominantly "modern" and therefore biogenic in origin ~~However, there exists a contradiction that ambient organic aerosol (even in urban areas) is predominately "modern", indicating a biogenic origin~~ (Lewis et al., 2004; Schichtel et al., 2008; Marley et al., 2009), there exists an apparent contradiction because ambient organic aerosol is well-correlated with anthropogenic tracers ~~but often correlates with anthropogenic tracers~~ (de Gouw et al., 2005; Weber et al., 2007). This apparent discrepancy could be reconciled if anthropogenic pollution influences the atmospheric oxidation of BVOCs and their aerosol formation pathways. The oxidation of BVOCs by nitrate radicals (NO_3), formed from the reaction of ozone with NO_2, provides a direct link between anthropogenic pollution and the abundance of biogenic carbon in atmospheric aerosol.

Biogenic hydrocarbons react rapidly with nitrate radicals (Atkinson and Arey, 2003a) and the secondary organic aerosol (SOA) yields are generally higher than in photooxidation and ozonolysis (e.g., ~~(~~Griffin et al., 1999; Hallquist et al., 1999; Spittler et al., 2006; Ng et al., 2008; Fry et al., 2009; Rollins et al., 2009; Fry et al., 2011; Fry et al., 2014). As monoterpene emissions are not entirely light-dependent, they are emitted during the day and at night (Fuentes et al., 2000; Guenther et al., 2012) and can contribute substantially to ambient organic aerosol. Monoterpenes have also been found to make up as much as 28% of non-methane organic carbon emissions from biomass burning in both field and laboratory studies (Akagi et al., 2013; Hatch et al., 2015; Stockwell et al., 2015). Fires from biomass burning are more likely to smolder at night and are therefore more likely to emit monoterpenes, which can then react with nitrate radicals (Akagi et al., 2013). Results from previous field studies provided evidence of aerosol formation from nitrate radical oxidation of BVOCs during both daytime and nighttime (McLaren et al.,

2004; Iinuma et al., 2007; Fuentes et al., 2007; Brown et al., 2009; Rastogi et al., 2011; Rollins et al., 2012; Brown et al., 2013; Rollins et al., 2013). Specifically, many of these studies found a significant increase in the amount of monoterpene organic aerosol and oxidation products at night, which could be attributed to nighttime monoterpene oxidation by nitrate radicals (McLaren et al., 2004; Iinuma et al., 2007; Rastogi et al., 2011). Results from recent flight measurements in ~~the~~ Houston, TX also showed that organic aerosol was enhanced in the nocturnal boundary layer at levels in excess of those attributable to primary emissions, implying a source of SOA from the BVOCs+NO_3 reaction (Brown et al., 2013).

Global modeling studies showed large variations in the total SOA burden that can be attributed to the oxidation of BVOCs by nitrate radicals, ranging from ~5 to 21% (Hoyle et al., 2007; Pye et al., 2010). Specifically, Pye et al. (2010) showed that the inclusion of nitrate radical oxidation reaction doubled the total amount of terpene (monoterpenes and sesquiterpenes) aerosol, pointing to the significant contribution of this chemistry to total organic aerosol burden. In these modeling studies, all aerosol formation from the nitrate radical oxidation of terpenes was calculated based on the β-pinene+NO_3 SOA yields obtained in Griffin et al. (1999). A recent modeling study by Russell and Allen (2005) determined that as much as 20% of all nighttime SOA is from the reaction of β-pinene+NO_3. Due to the significance of nitrate radical oxidation pathway in SOA formation, it is important that the SOA yields for BVOCs+NO_3, and especially that of β-pinene+NO_3, are well-constrained from fundamental laboratory studies and accurately represented in models.

The majority of the previous laboratory studies of the BVOCs+NO_3 chemistry were performed under dry conditions (Berndt and Boge, 1997b, a; Wängberg et al., 1997; Griffin et al., 1999; Hallquist et al., 1999; Bonn and Moorgat, 2002; Spittler et al., 2006; Ng et al., 2008; Rollins et al., 2009; Fry et al., 2009; Perraud et al., 2010; Fry et al., 2011; Kwan et al., 2012; Jaoui et al., 2013; Fry et al., 2014). The effect of relative humidity on SOA formation, however, could potentially be important for nighttime (where NO_3 radicals dominate) and early morning chemistry as the ambient RH is typically higher at these times. Several recent studies have investigated the effect of water on SOA formation from the nitrate radical oxidation pathway but the results are inconclusive. For instance, Spittler et al. (2006) found that the SOA yield is lower

at 20% RH compared to dry conditions, suggesting that water vapor may alter the gas-phase oxidation mechanism and/or partitioning into the particle phase, thus shifting the equilibrium partitioning of organic compounds. However, other studies showed that the presence of water vapor did not affect particle size distributions and SOA formation (Bonn and Moorgat, 2002; Fry et al., 2009). Thus, the role of water in SOA formation from nitrate radical oxidation of BVOCs is still unclear.

Another important parameter in SOA formation from BVOCs+NO_3 is the fate of peroxy radicals, which directly determines the oxidation products, SOA yields, and aerosol chemical and physical properties (Kroll and Seinfeld, 2008; Orlando and Tyndall, 2012; Ziemann and Atkinson, 2012). Previous studies regarding the effects of peroxy radical fates on SOA formation from BVOCs typically focused on photooxidation and ozonolysis systems (e.g., ~~(~~Presto et al., 2005; Kroll et al., 2006; Ng et al., 2007a; Eddingsaas et al., 2012; Xu et al., 2014) and isoprene+NO_3 chemistry (Kwan et al., 2012; Ng et al., 2008; Nguyen et al., 2014). To our knowledge, the effects of differing peroxy radical branching on SOA formation from nitrate radical oxidation of monoterpenes have not been investigated. The relative importance of different peroxy radical reaction channels concerning BVOCs+NO_3 chemistry in the atmosphere is not well established (Brown and Stutz, 2012). While earlier studies by Kirchner and Stockwell (1996) suggested that RO_2+NO_3 is more important in the nighttime atmosphere, a recent study by Mao et al. (2012) showed that the HO_2 mixing ratios are often on the order of 10 ppt at night. It is therefore possible that RO_2+HO_2 pathway could be an important pathway in nighttime oxidation of BVOCs.

Nitrate radical chemistry is expected to produce a substantial amount of organic nitrate compounds, owing to direct addition of nitrate radical via reaction with a double bond. Organic nitrates have been observed to form a substantial portion of atmospheric aerosol in field studies (Brown et al., 2009; Day et al., 2010; Zaveri et al., 2010; Beaver et al., 2012; Rollins et al., 2012; Fry et al., 2013; Rollins et al., 2013; Brown et al., 2013; Xu et al., 2015a). Organic nitrate formation has a significant impact on total NO_x lifetime, especially in NO_x-limited regions where NO_x lifetime is sensitive to the formation rates of organic nitrates (Browne and Cohen, 2012). Ambient organic nitrates can be formed through photooxidation of VOCs in the presence of NO_x

(Chen et al., 1998; Arey et al., 2001; Yu et al., 2008) and through nitrate radical addition (Spittler et al., 2006; Perring et al., 2009; Rollins et al., 2009; Kwan et al., 2012). One removal mechanism for atmospheric organic nitrates is hydrolysis in the particle phase (e.g., (Sato, 2008; Szmigielski et al., 2010; Darer et al., 2011; Hu et al., 2011; Liu et al., 2012; Rindelaub et al., 2015). Modeling studies have assumed that the majority (75%) of the organic nitrates formed in the day are composed of tertiary nitrates based on results from the photooxidation of α-pinene and β-pinene in the presence of NO_x (Browne et al., 2013). However, the organic nitrates formed from photooxidation and nitrate radical oxidation could have different chemical structures (primary, secondary, and tertiary) and need to be investigated to better constrain the fates of organic nitrates (e.g., hydrolysis lifetime) in the atmosphere over their entire life cycle (both day and night).

The goal of this study is to determine the aerosol yields and characterize the mechanisms and chemical composition of SOA formation from the β-pinene+NO_3 system. Laboratory chamber experiments are performed in the dark under dry and humid conditions. To investigate the effects of peroxy radical fates on SOA yields and chemical composition, the experiments are designed to probe the "RO_2+NO_3" vs. "RO_2+HO_2" reaction pathways. Aerosol yields are obtained over a wide range of initial β-pinene mixing ratios. Based on the measured gas-phase and particle-phase oxidation products, mechanisms for SOA formation from β-pinene+NO_3 are proposed. Results from this study are used to evaluate the contributions of nitrate radical oxidation of monoterpenes to ambient organic aerosol measured in the southeastern United States (US), including the Southern Oxidant and Aerosol Study (SOAS) and the Southeastern Center for Air Pollution and Epidemiology (SCAPE) study.

2) Experimental

2.1) Laboratory Chamber Experiments

All experiments are performed in the Georgia Tech Environmental Chamber facility (GTEC), which consists of two 12 m^3 flexible Teflon (FEP 2 mil) chambers suspended in a 21 ft. x 12 ft. temperature-controlled enclosure. The full operational temperature range of the facility is 4–40 ±0.5 ^oC. A schematic of the chamber facility is shown in Fig. 1. Each of the chambers has three

Teflon manifolds with multiple sampling ports. Ports allow for the introduction of clean air, gas-phase reagents, seed aerosol, and for measurements of RH, temperature, gas-phase composition, and particle-phase composition. The chambers are surrounded by blacklights (Sylvania, 24922) with output predominately in the ultraviolet region between 300 nm and 400 nm, with a maximum at 354 nm. The blacklights are supplemented by natural sunshine fluorescent lights (Sylvania, 24477), which have wavelengths between 300 nm to 900 nm. The j_{NO2} of the chamber facility is 0.28 min^{-1} when all of the blacklights are turned on.

Experimental conditions are summarized in Table 1. Prior to each experiment, the chambers are cleaned by flowing pure air (generated from AADCO, 747-14) for at least 24 hours at a rate of 40 LPM, or equivalent to 0.2 chamber volumes per hour. This ensures that the ozone, NO, and NO_2 concentrations are less than 1 ppb and the particle concentration is lower than 10 cm^{-3}. Experiments are performed in the dark under either dry (RH < 2%) or humid (RH = 50%, 70%) conditions. The air is humidified by passing pure air through bubblers prior to introduction into the chamber. The temperature and humidity inside each Teflon chamber are measured using a hygrothermometer (Vaisala, HMP110). Seed aerosol is generated by atomizing an ammonium sulfate solution (8 mM) or an ammonium sulfate/sulfuric acid mixture ($[(NH_4)_2SO_4]$:$[H_2SO_4]$ = 3:5, molar ratio) into the chamber. The seed number and mass concentration prior to typical experiments are approximately 2.0×10^4 cm^{-3} and 30 $\mu g/m^3$. The pH of the $(NH_4)_2SO_4$ seed and $(NH_4)_2SO_4$+H_2SO_4 seed at RH = 50% is about 4.6 and 2.4, respectively, based on calculations from prior studies (Gao et al., 2004). Nucleation experiments are performed under both dry and humid (RH = 50%, 70%) conditions to determine organic aerosol density and characterize vapor wall loss effects on SOA yields. All experiments are performed at 298K.

Experiments are designed to probe the effects of peroxy radical chemistry (RO_2+HO_2 vs. RO_2+NO_3) on SOA formation from the reaction of β-pinene with nitrate radicals. The procedure for chemical injection depends on the desired fate of the peroxy radicals in the experiments. To enhance the branching ratio of RO_2+HO_2 in the chamber experiments, formaldehyde is first added to the chamber (Nguyen et al., 2014). Formalin solution (Sigma-Aldrich, 37% HCHO) is injected into a glass bulb and clean air is passed over the solution until it evaporates. After this, seed aerosol, NO_2 (Matheson, 500 ppm), and ozone (generated by passing zero air through a UV

radiation cell, Jelight 610) are injected into the chamber. NO_2 and O_3 concentrations are chosen ($[NO_2]$:$[O_3]$ ≈ 4:3) to ensure that 99% of the β-pinene reacts with nitrate radicals instead of ozone. The NO_2 and O_3 react to form nitrate radicals and subsequently N_2O_5 through the following reactions:

$$NO_2 + O_3 \rightarrow NO_3 + O_2 \quad \text{(R1)}$$

$$NO_3 + NO_2 \leftrightarrow N_2O_5 \quad \text{(R2)}$$

Formaldehyde then reacts with nitrate radicals to form HO_2 radicals via the following reaction:

$$HCHO + NO_3 + O_2 \rightarrow HNO_3 + CO + HO_2 \quad \text{(R3)}$$

Enough formaldehyde (3-22 ppm) is added to the chamber to ensure that the RO_2+HO_2 radical branching ratio is an order of magnitude higher than the RO_2+RO_2 and RO_2+NO_3 pathways (Supplement). The chamber content is allowed to mix for ~30 minutes, after which a desired amount of β-pinene is injected into a glass bulb, where it is introduced into the chamber by passing clean air through the glass bulb. Introduction of β-pinene into the chamber marks the beginning of the experiment. We refer to this set of experiments as "RO_2+HO_2 dominant" experiments.

For "RO_2+NO_3 dominant" experiments, seed aerosol is first introduced into the chamber, followed by β-pinene injection. After allowing ~30 minutes for the β-pinene concentration to stabilize, N_2O_5 is injected into the chamber. To generate N_2O_5, a mixture of NO_2 and O_3 is pre-reacted in a flow tube (flow rate = 1.3 LPM, residence time = 71 sec) before entering the chamber. The N_2O_5 concentration is estimated by modeling the reaction of NO_2 and O_3 in the flow tube. For this set of experiments, the introduction of N_2O_5 marks the beginning of the experiment. We aim for an initial N_2O_5:β-pinene ratio of ~~4~~6:1. It is noted that the ozone concentration in the chamber is sufficiently low that at least 99% of β-pinene reacts with nitrate radicals. N_2O_5 continuously dissociates to form NO_2 and nitrate radicals during the experiment to reestablish equilibrium as the nitrate radicals react with β-pinene. The high initial N_2O_5 and nitrate radical concentrations relative to β-pinene favor the RO_2+NO_3 pathway.

For all experiments except "RO_2+HO_2 dominant" experiments conducted under humid conditions (RH = 50%, 70%), a Gas Chromatograph-Flame Ionization Detector (GC-FID, Agilent 6780A) measures a β-pinene concentration of zero (below detection limit) within the first scan (scan time = 11.7 min) after the experiment begins. This suggests that β-pinene is completely consumed within 11.7 minutes of N_2O_5 injection for the "RO_2+NO_3 dominant" experiments and that β-pinene is fully reacted away before being detected by the GC-FID in the "RO_2+HO_2 dominant" experiments under dry conditions. The concentration of β-pinene is calculated from the mass of the hydrocarbon injected and the volume of the chamber. The chamber volume is determined to be approximately 12 m^3 by injecting a known volume of NO_2 standard (Matheson, 500 ppm) into the chamber and measuring the resulting NO_2 concentration inside the chamber.

Ozone and NO_x concentrations are monitored with an O_3 Analyzer (Teledyne ~~200EU~~T400) and an ultrasensitive chemiluminescence NO_x monitor (Teledyne 200EU~~T200~~), respectively. Total aerosol volume and size distributions are measured with a Scanning Mobility Particle Sizer (SMPS, TSI). The SMPS consists of a differential mobility analyzer (DMA) (TSI 3040) and Condensation Particle Counter (CPC) (TSI 3775). Bulk particle chemical composition is measured with an Aerodyne High Resolution Time-of-Flight Aerosol Mass Spectrometer (HR-ToF-AMS). The working principle and operation of the HR-ToF-AMS are described in detail elsewhere (DeCarlo et al., 2006). The HR-ToF-AMS provides quantitative measurements of organics, nitrate, sulfate, ammonium, and chloride. Elemental analysis are performed on the data to determine elemental composition (e.g., O:C, N:C ratios) of the bulk aerosol (Canagaratna et al., 2015).

A suite of gas-phase oxidation products and N_2O_5 are measured using a Quadrupole Chemical Ionization Mass Spectrometer (CIMS) with I^- as the reagent ion, which has high selectivity towards reactive nitrogen species, peroxides, and carboxylic acids (Huey, 2007; McNeill et al., 2007; Zhao et al., 2012). The CIMS uses methyl iodide to produce I^- ions that ionize gas-phase products through association (Slusher et al., 2004; Zheng et al., 2011). It has been shown that I^- addition to gas-phase molecules provides a molecule-iodide adduct that preserves the original

species of the compounds being sampled. The gas-phase species are detected as *m/z* = MW+127. Masses with specific *m/z* are selected for detection using a quadrupole mass filter. These species are then detected by an electron multiplier which amplifies incident charge through secondary electron emission to produce a measurable current that scales with gas-phase concentration. Due to unavailability of standards for the oxidation products, the instrument is not calibrated for these compounds and concentrations are not reported. However, the CIMS data allow for identification and comparison of the abundance of specific gas-phase oxidation products formed in different experimental conditions.

2.2) Analysis of Particle-Phase Products

Aerosol samples are collected on Teflon filters (Pall Corp. R2PL047, 1-μm pore size and 47-mm diameter) during the SOA experiments (Experiments 9, 10, 22, 23, 32, 33 in Table 1) and for a series of blank/control experiments. These blank experiments are 1) clean chamber (no aerosol) at RH < 2%, 2) clean chamber (no aerosol) at RH = 50%, 3) clean chamber at RH =50% with only N_2O_5 injected, and 4) clean chamber at RH < 2% with only β-pinene injected. All filters collected during the chamber experiments and controls are stored at a temperature below −20°C before sample extraction and preparation for chromatographic analysis.

Each filter is extracted twice by sonication (Branson 3510) for 15 min in 2.50 mL acetonitrile (Fisher Optima, LC-MS grade). After combining both aliquots, each extracted sample is blown dry under a gentle stream of nitrogen (Scott-Gross, UHP), reconstituted with 1000 μL acetonitrile, and transferred to a chromatographic vial. Samples are analyzed with an Accela (Thermo Fisher Scientific) ultra-high-performance liquid chromatographer (UHPLC) equipped with a 1250 quaternary delivery pump, a photodiode array detector (PDA) with a 5-cm LightPipe flow cell, and a mass spectrometry (MS) detector (Thermo MSQ Plus). Samples are injected (50 μL) with an Accela autosampler into the reversed-phase chromatographic column (Hypersil gold C18, 50 × 2.1 mm, 1.9 μm particle size, Thermo Scientific). Excalibur software is used to control the UHPLC-PDA-MS system. Chromatographic separation at a constant flow rate of 800 μL min^{-1} from 0 to 1 min is isocratic with 90% (A) 0.10 mM formic acid (Fisher Optima, LC-MS grade) in ultrapure water (18.2 MΩ cm Purelab Flex, Veolia) and 10% (B) 0.10 mM formic acid

in acetonitrile. Gradient elution from 1 to 8 min reaches a 10:90 ratio of solvents A:B and remain isocratic from 8 to 10 min. Selected chromatograms utilize 0.4-1.0 mM acetic acid (Acros, glacial ACS, 100.0% by assay) instead of 0.1 mM formic acid in the mobile phase. After the PDA registered the UV–visible spectra from 190 to 700 nm, the flow is interfaced with an electrospray ionization (ESI) probe (1.9 kV needle voltage, 350°C probe temperature, and 70 psi N_2 nebulizing gas) to the MS detector set to detect negative ions in the range of *m/z* 50 to 650 amu. Selected samples are analyzed under variable cone voltage (10-100 V) to register the fragmentation pattern of the peaks and gain structural information of the products. The extraction method shows an efficient 98.8% recovery, when 98.6 μg of 4-nitrophenol (Acros, 98.0%) are spiked onto a blank filter.

3) Results

Gas-phase oxidation and aerosol growth is observed to be a rapid process in the β-pinene+NO_3 reaction. Peak aerosol growth is typically observed within 10-15 minutes for all reaction conditions except in humid (RH= 50%, 70%) "RO_2+HO_2 dominant" experiments, where aerosol reaches peak growth in about 30 minutes. Figure S1 shows a typical mass spectrum for the CIMS data. Specifically, the major gas-phase products are detected at *m/z* 342, 356, 358, and 372 (which correspond to MW = 215 amu, 229 amu, 231 amu, 245 amu, respectively). These compounds likely correspond to organic nitrate species. Figure 2 shows the time series of these species and the aerosol growth over the course of a typical "RO_2+HO_2 dominant" experiment in dry conditions. The products at *m/z* 356 and 358 (MW = 229 amu and 231 amu) decrease over the course of the experiment. While this can be attributed to vapor phase wall loss, it is also possible that these gas-phase compounds undergo further reaction. This is further supported by the increase in the species at *m/z* 372 (MW = 245 amu). The proposed gas-phase oxidation mechanism and formation of compounds at *m/z* 372 from compounds at *m/z* 356 will be discussed further in Section 4.1.

Although all the above gas-phase species are observed under all reaction conditions, *m/z* 358 (MW = 231 amu) is significantly higher in the "RO_2+HO_2 dominant" experiments than in the "RO_2+NO_3 dominant" experiments (Fig. S2), which is indicative of differences in the gas-phase

chemistry depending on the RO_2 fate. Under both "RO_2+HO_2 dominant" and "RO_2+NO_3 dominant" conditions, experiments conducted under dry conditions have significantly higher N_2O_5 concentrations than humid conditions (by at least a factor of 2) as measured by CIMS. This is likely due to N_2O_5 uptake (loss) on the wet chamber surfaces and/or seed aerosol. The relative abundance of N_2O_5 under different experimental conditions is important in terms of β-pinene reaction rate and aging of aerosol, which are discussed in Sections 4.2.2 and 4.4, respectively.

All SOA growth data are corrected for particle wall loss by applying size-dependent wall loss coefficients determined from wall loss experiments at GTEC following the methodology described in ~~All SOA growth data are corrected for particle wall loss by applying size-dependent wall loss coefficients determined from wall loss experiments~~ Keywood et al. (2004). The size-dependent particle wall loss rates calculated for both chambers at GTEC are shown in Fig. S3. Figures 3 and 4 show the SOA yields for "RO_2+NO_3 dominant" and "RO_2+HO_2 dominant" experiments over a wide range of aerosol mass loadings (ΔM_o = 5.1-216.1 μg/m^3). The SOA yields lie in the range of 27.0-104.1% over the conditions studied. Aerosol mass yield (Y) is defined as the aerosol mass concentration produced (ΔM_o) divided by the mass concentration of hydrocarbon reacted (ΔHC), Y= $\Delta M_o/\Delta HC$ (Odum et al., 1996; Bowman et al., 1997; Odum et al., 1997b; Odum et al., 1997a). For all experiments, aerosol mass concentration is obtained from the SMPS aerosol volume concentration (averaged over 30 min at peak growth) and the calculated aerosol density. The aerosol density is calculated from the SMPS volume distribution and the HR-ToF-AMS mass distribution in the nucleation experiments (Bahreini et al., 2005). The densities of the organic aerosol generated in nucleation experiments under dry and humid (RH = 50%, 70%) conditions are determined to be 1.41 g cm^{-3}~~g/cm^3~~ and 1.45 g cm^{-3}~~g/cm^3~~ for the "RO_2+NO_3 dominant" experiments and 1.54 g cm^{-3}~~g/cm^3~~ and 1.61 g cm^{-3}~~g/cm^3~~ for the "RO_2+HO_2 dominant" experiments.

It can be seen from Fig. 3 that the aerosol yields in the "RO_2+NO_3 dominant" experiments under dry vs. humid conditions in the presence of $(NH_4)_2SO_4$ seed are similar. The presence of the more acidic $(NH_4)_2SO_4$+H_2SO_4 seed does not appear to enhance SOA production in the "RO_2+NO_3 dominant" experiments (Fig. S4~~3~~). Therefore, we fit the Odum two-product model (Odum et al., 1996; Odum et al., 1997a) to all of our experimental data shown in Fig. 3 to obtain

a single yield curve. The SOA yield parameters are given in Table 2. Shown in Fig. 4 are the aerosol yields from "RO_2+HO_2 dominant" experiments under dry vs. humid (RH = 70%) conditions. The SOA yield curve (solid red line) for the "RO_2+NO_3 dominant" experiments is also shown for comparison.

For comparison, SOA yields from previous β-pinene+NO_3 laboratory chamber studies (Griffin et al., 1999; Fry et al., 2009) are also shown in Fig. 3. Without adding HCHO as an additional HO_2 source, it is likely that the experiments in Griffin et al. (1999) and Fry et al. (2009) are more similar to our "RO_2+NO_3 dominant" experiments. Specifically, Fry et al. (2009) noted that the β-pinene+NO_3 reaction likely does not produce significant concentrations of HO_2 radicals and therefore have a low HO_2/RO_2 ratio. As Griffin et al. (1999) assumed an aerosol density of 1.0 g cm^{-3}~~g/cm^3~~, the ~~yield curve~~experimental data from Griffin et al. (1999) shown in Fig. 3 has been multiplied by the density calculated in ~~this~~ our study for "RO_2+NO_3 dominant" experiments under dry conditions (i.e., 1.41 g cm^{-3}~~g/cm^3~~). The data shown in Fig. 3 from Fry et al. (2009) have also incorporated a particle density of 1.6 ~~g/cm^3~~g cm^{-3} calculated in their study. In addition to correcting for density, the yield curve partitioning coefficient, K, from Griffin et al. (1999) has been adjusted from 306K to 298K using an enthalpy of vaporization of 42 kJ mol^{-1} for comparison to results from our study (Chung and Seinfeld, 2002). It is noted that the SOA yields obtained in the current study are higher than those in Griffin et al. (1999) and Fry et al. (2009), particularly at lower aerosol mass loadings that are more relevant to ambient environments. These results are discussed in more detail in Section 4.2.

Bulk aerosol composition from the experiments is characterized by the HR-ToF-AMS. A typical high-resolution mass spectrum for aerosol formed under dry conditions where the RO_2+NO_3 pathway is dominant (Experiment 5 in Table 1) is shown in Fig. 5. A key feature of the mass spectrum is the high intensity of the nitrate ions at NO^+ and NO_2^+, which make up about 11% of the combined organics and nitrate signals~~about 11% of the total organics signal~~. The majority (> 90%) of the nitrogen atoms is detected at these two ions with the remaining nitrogen-containing ions detected at higher masses as $C_xH_yO_zN$. The mass ~~spectrum~~ spectra for the aerosol generated in the "RO_2+HO_2 dominant" and "RO_2+NO_3 dominant" experiments are similar.~~,~~ O~~o~~ne notable difference between the "RO_2+HO_2 dominant" and "RO_2+NO_3 dominant" experiments is ~~being~~

the NO^+:NO_2^+ ratio for the organic nitrates (R-ON), which ranges from 4.8-10.2 in all experiments. While the NO^+:NO_2^+ ratio ~~is typically 6-7.5~~averages 6.5 for "RO_2+NO_3 dominant" experiments, it ~~is typically 8-9~~averages 8.6 for "RO_2+HO_2 dominant" experiments. Since the values of R-ON may depend on the instrument, we normalize the R-ON to the NO^+:NO_2^+ of ammonium nitrate (R-AN), which is expected to be a better metric (Farmer et al., 2010). In our study, multiple measurements of R-AN are obtained from the ionization efficiency (IE) calibrations and the average value is about 1.8 (range of 1.2-2.7). We calculate the average R-ON:R-AN ratio to be 3.2 for "RO_2+NO_3 dominant" experiments and 4.8 for "RO_2+HO_2 dominant" experiments.

For both types of experiments, there is a negligible difference in the mass spectrum of the aerosol produced in dry or high humidity (RH = 50%, 70%) conditions. In Fig. 5, nitrate and organic ions are each assigned a different color to indicate an individual AMS HR ion family. There are a few notable ions in the aerosol mass spectrum. The signals at *m/z* 67 ($C_5H_7^+$) and *m/z* 91 ($C_7H_7^+$), while not significant in the high resolution mass spectra of several biogenic SOA systems (Ng et al., 2008; Chhabra et al., 2010), are relatively large for β-pinene+NO_3 SOA. These ions also make up a larger fraction of the HR-ToF-AMS signal for SOA formed from the ozonolysis of β-caryophyllene~~These ions have also been observed in SOA formed from the ozonolysis of β-caryophyllene~~ (Chen et al., 2015) when compared to other biogenic SOA. Therefore, *m/z* 67 ($C_5H_7^+$) and *m/z* 91 ($C_7H_7^+$) could potentially serve as useful indicators for SOA formed from monoterpene/sesquiterpene oxidation in ambient aerosol mass spectra. However, more studies of SOA formed from the oxidation of biogenic VOCs are necessary to apportion ambient OA based on these fragments."~~Therefore, *m/z* 67 ($C_5H_7^+$) and *m/z* 91 ($C_7H_7^+$) could potentially serve as useful indicators for SOA formed from monoterpene/sesquiterpene oxidations in ambient aerosol mass spectra.~~

Figure 6 shows the time evolution of the major organic families relative to sulfate measured by the HR-ToF-AMS for a typical dry "RO_2+NO_3 dominant" experiment (Experiment 5 in Table 1). Sulfate is used to normalize the decay of the organic families because it is non-volatile and any decrease in sulfate is reflective of particle wall loss and changes in aerosol collection efficiency (CE) in the HR-ToF-AMS (Henry and Donahue, 2012). Any change of each organic family

relative to sulfate is therefore interpreted as a change in organic mass unrelated to particle wall loss or CE. Non-oxidized fragments (CH family in green) decrease more rapidly relative to sulfate than the more oxidized fragments (CHO1 family in purple, CHOgt1 "fragments with greater than 1 oxygen atom" family in pink). The change in mass for each organic family is determined over a 2.5 hour period following peak aerosol growth (at t ~ 15 min) in each "RO_2+NO_3 dominant" experiment (dry and humid). We find that the CHOgt1 family increases by 4% in dry experiments and remains relatively constant in humid experiments. This is consistent with a larger extent of aerosol aging in the dry experiments and is further discussed in Section 4.4.

Figure 7 shows the time evolution of HR-ToF-AMS nitrate-to-organics ratio in the "RO_2+NO_3 dominant" experiments at RH = 50% normalized by that in the corresponding dry experiments with the same initial hydrocarbon concentration. For simplicity, we refer to this ratio as $(Nitrate:Org)_{norm}$. Normalizing the nitrate-to-organics ratio obtained from the humid experiments to the dry experiments allow for determining the extent of possible organic nitrate hydrolysis under humid conditions. Since only the relative change in the $(Nitrate:Org)_{norm}$ ratio is important for comparison purposes, the maximum $(Nitrate:Org)_{norm}$ measurement for each experiment is set to be unity. Nitrate mass is defined here as the sum of the mass of the NO^+ and NO_2^+ ions. This does not account for the $C_xH_yO_zN$ fragments, but these fragments only account for less than 10% (by mass) of the nitrate functional groups detected by HR-ToF-AMS. As the experiment progresses, the $(Nitrate:Org)_{norm}$ ratio decreases and stabilizes at a value of about 0.9, indicating that there is no further decrease in the mass of nitrate relative to the mass of organics beyond this point. From our particle wall loss experiments, we establish that the particles are lost to the chamber wall with comparable rates under dry and humid conditions, suggesting that the observed decrease in the $(Nitrate:Org)_{norm}$ ratio is not a result of differing particle wall loss in dry and humid experiments. Instead, the decrease under humid conditions is attributed to hydrolysis of organic nitrate compounds in the particle phase. This is further discussed in Section 4.3.2.

4) Discussion

4.1) Proposed Mechanisms

Figure 8 shows the proposed scheme for the generation of species observed by CIMS and UHPLC-PDA-MS analyses from the oxidation of β-pinene with nitrate radicals. The oxidation process starts with Reaction (R1) for the sterically preferred addition of nitrate radical to the primary carbon (C_1) in the double bond of β-pinene (Wayne et al., 1991). The tertiary alkyl radical formed on C_2 can undergo 1) addition of O_2 to form a peroxy radical via Reaction (R2) (Atkinson and Arey, 2003b), 2) a 1,5-CH_3 shift indicated by Reaction (R3) (Miller, 2003) and, 3) rearrangement via Reaction (R4) (Stolle et al., 2009; Schröder et al., 2010). Reaction (R4) is thought to be a favorable pathway because it relieves the ring strain from the cyclobutane while generating a tertiary alkyl radical with a new reactive double bond. In the presence of oxygen, O_2 combines with the alkyl radical to make a peroxy radical, which is then converted to an alkoxy radical via Reaction (R5) (denoted as R^5O here) (Atkinson and Arey, 2003b; Vereecken and Peeters, 2012). Reactions which can be accomplished by any of the radicals present (RO_2, HO_2, NO_3, etc) are symbolized by reaction with generic radical $\mathbf{L}^{\bullet}$, while hydrogen abstractions are symbolized by reaction with generic radical $\mathbf{Q}^{\bullet}$ (e.g., NO_3, RO_2, etc.). R^5O can undergo intramolecular addition to the less substituted C_7 of the newly formed double bond via Reaction (R6), generating a cyclic ether alkyl radical (Vereecken and Peeters, 2004~~;~~, ~~Vereecken and Peeters,~~ 2012). Alternatively, R^5O can undergo hydrogen abstraction from another species via Reaction (R7) to form a hydroxynitrate of MW = 215 amu (R^7OH), a gas-phase species detected by CIMS. The cyclic ether alkyl radical generated by Reaction (R6) combines with O_2 to make peroxy radical **U** by Reaction (R8). The fate of radical **U** is to produce a cyclic ether hydroxynitrate~~dihydroxynitrate~~ with MW = 231 amu via Reaction (R9) (Russell, 1957; Atkinson and Arey, 2003b). A compound with the same molecular weight as ~~the dihydroxynitrate~~ this species is detected by CIMS.

The alkyl radical formed in Reaction (R1) can also undergo a 1,5-CH_3 shift as indicated by Reaction (R3), which forms a tertiary alkyl radical that then combines with O_2 by Reaction (R10). Reaction (R10) produces a hydroxynitrate ($R^{10}OH$) with MW = 215 amu, an isomer that could also correspond to the species observed by CIMS. Further functionalization of $R^{10}OH$

continues after hydrogen abstraction by Reaction (R11), which bond strength calculations predict occur preferentially at the C_3 position (Vereecken and Peeters, 2012). The resulting secondary alkyl radical from Reaction (R11) reacts with O_2 to form peroxy radical **S** via Reaction (R12). The reaction **S** + **L**$^{\bullet}$ forms either a hydroxycarbonyl nitrate with MW = 229 amu by Reaction (R13), or a dihydroxynitrate with MW = 231 amu by Reaction (R14) (Russell, 1957; Atkinson and Arey, 2003b). Both are gas-phase species detected by CIMS.

The peroxy radical formed in Reaction (R2) can be converted to a hydroperoxide with MW = 231 amu (observed in CIMS) by reaction with an HO_2 radical (R15). Since Reaction (R15) is only associated with the RO_2+HO_2 channel, the signal corresponding to the species with MW = 231 amu is expected be higher in the "RO_2+HO_2 dominant" experiments. Figure S2 shows the CIMS signal at m/z = 358 (MW = 231 amu) normalized to Br_2 sensitivity for each type of experiment ("RO_2+NO_3 dominant" and "RO_2+HO_2 dominant", dry and humid conditions). The higher signal in the "RO_2+HO_2 dominant" experiments supports the formation of more ROOH species in the gas phase under this reaction condition.

The peroxy radical formed from Reaction (R2) can also be converted into an alkoxy radical, $R^{16}O$, via Reaction (R16). Hydrogen abstraction by the alkoxy radical $R^{16}O$ can form a third hydroxynitrate isomer with MW = 215 amu by Reaction (R17). Alternatively, $R^{16}O$ can undergo a 1,5-H shift from a $–CH_3$ group by Reaction (R18) to form an alkyl radical at one of the terminal carbons (Carter et al., 1976; Eberhard et al., 1995; Atkinson, 1997; Dibble, 2001). The alkyl radical then reacts with O_2 to form a peroxy radical and subsequently forms an aldehyde with MW = 229 by the overall Reaction (R19) (Russell, 1957; Atkinson and Arey, 2003b). The aldehydic hydrogen is especially susceptible to undergoing hydrogen abstraction (Miller, 1999), followed by O_2 addition to form a peroxy acid radical, and final conversion to a carboxylic acid (Russell, 1957; Atkinson and Arey, 2003b). $R^{20}COOH$ with MW = 245 amu is produced by Reaction (R20), a species registered as an anion by UHPLC-MS at *m/z* 244 (MW = 245 amu) (Fig. S5~~4~~). CIMS data also support the pathways via Reaction (R20) (Fig. 2). The Br_2-normalized CIMS signal for species at *m/z* 356 (MW = 229 amu) decreases with a subsequent increase in species at *m/z* 372 (MW = 245 amu) in the gas phase over the course of the experiment. Due to the lower vapor pressure of carboxylic acid species compared to carbonyl

species (Pankow and Asher, 2008), the majority of carboxylic acid formed from this channel is expected to partition into the particle phase. In addition to Reaction (R20), $R^{20}COOH$ can also be formed through a more direct route by addition of O_2 to the alkyl radical product and then subsequent reaction of the peroxy radical with HO_2 via the sequence of Reactions (R18) + (R21) + (R22) (Ziemann and Atkinson, 2012).

The hydroxynitrate formed by Reaction (R17) can also undergo hydrogen abstraction at the C_3 position, as indicated by Reaction (R23). (Vereecken and Peeters, 2012). Reaction (R24) shows how O_2 addition to the resulting secondary alkyl radical gives peroxy radical **T**, which can either react with **L**$^{\bullet}$ to form a dihydroxynitrate with MW = 231 amu via Reaction (R25) or form a hydroxycarbonyl nitrate with MW = 229 amu via Reaction (R26) (Russell, 1957; Atkinson and Arey, 2003b). In the absence of hydrogen atoms in the C_3 position, hydrogen abstraction occurs from C_4 of the hydroxycarbonyl nitrate species via Reaction (R27) (Vereecken and Peeters, 2012), which then forms a peroxy radical **V** by Reaction (R28) (Atkinson and Arey, 2003b). Reaction (R29), **V** + **L**$^{\bullet}$, yields a dihydroxycarbonyl nitrate with MW = 245 amu (Russell, 1957; Atkinson and Arey, 2003b). This dihydroxycarbonyl nitrate is not expected to be the species appearing in the UHPLC-MS chromatogram (Fig. S54) at *m/z* 244 (MW = 245 amu) because it lacks a –COOH group and likely has a higher vapor pressure than the carboxylic acid species with MW = 245 amu. Instead, it is likely that the dihydroxycarbonyl nitrate is the species observed by CIMS at *m/z* 372 (MW = 245 amu). A third possible isomer (not shown in Fig. 8) with MW = 245 amu and containing a non-carboxylic C=O group, could be similarly formed from the product of Reaction (R13). Likewise, other isomers to those generated after Reaction (R26) can be formed from each possible structure with MW = 229 amu, providing a wide array of precursors to form heavier MW products. The confirmation that several isomers with MW = 245 amu are present in the filter extracts is revealed from the extracted ion chromatogram, EIC, which shows closely eluting peaks at *m/z* 244 (MW = 245 amu) when substituting formic acid for acetic acid (Li et al., 2011) as the modifier in the mobile phase (Fig. S54).

4.2) Aerosol Yields

4.2.1) SOA Yields Over a Wide Range of Organic Mass Loadings

The SOA yields obtained from this study are shown in Fig. 3 and Fig. 4. In recent years, it has been suggested that the loss of organic vapors to the chamber wall could affect SOA yields (Matsunaga and Ziemann, 2010; Loza et al., 2010; Yeh and Ziemann, 2014; Zhang et al., 2014; Zhang et al., 2015). Specifically, Zhang et al. (2014) demonstrated that vapor wall loss could lead to an underestimation of SOA yields by as much as a factor of 4. To evaluate the potential effect of organic vapor wall loss on SOA yields in our study, experiments without seed are carried out at different conditions (dry and humid (RH = 50, 70%); "RO_2+NO_3 dominant" and "RO_2+HO_2 dominant" conditions). The yields from the nucleation experiments are reported in Fig. S9~~8~~ along with the yield curve obtained from seeded experiments. The similar yields for nucleation/seeded "RO_2+NO_3 dominant" experiments (dry and humid) in our study suggest that vapor wall loss has a negligible effect on aerosol yields in these experiments. It is likely that rapid reaction of β-pinene with nitrate radicals in this study mitigate the effect of organic vapor wall loss on SOA yields. Based on the rapid SOA growth (peak growth typically achieved within 10-15 minutes) for these experiments, it is estimated that the effective reaction rate of β-pinene in our experiments is an order of magnitude higher than the rates reported in Zhang et al. (2014). Although the aerosol mass yields for the "RO_2+HO_2 dominant" ~~experiments in~~ nucleation experiments are lower than the corresponding seeded experiments, further increase in the seed concentration does not have a significant effect on yield. Zhang et al. (2014) determined that if vapor phase wall loss is significant in chamber experiments, the addition of more seed particles will lead to an increase in SOA yield. Therefore, it is likely vapor phase wall loss is also negligible in our seeded "RO_2+HO_2 dominant" experiments. It is unclear at this time why nucleation experiments have lower SOA yield only for the "RO_2+HO_2 dominant" experiments. One possibility is that the chamber-wall uptake of ROOH species (which is likely higher in "RO_2+HO_2 dominant" experiments as measured by CIMS (Fig. 2)) is more rapid than other gas-phase species.

A comparison of aerosol yields obtained for the oxidation of β-pinene with nitrate radicals is also shown in Fig. 3. Griffin et al. (1999) performed the first comprehensive study of SOA formation from nitrate radical oxidation of BVOCs. The aerosol yield curve reported for β-pinene+NO_3 by Griffin et al. (1999) is shown next to our yield curve in Fig. 3. The ~~two-product~~ yield curve in Griffin et al. (1999) was generated from chamber experiments with ΔM_o > ~~30~~ 45 μg m^{-3} ~~μg/m^3~~ (range of ΔM_o = ~~30~~45 – ~~470~~ 660 μg m^{-3} ~~μg/ m^{-3}~~) and extrapolated down to lower loadings. The yield curve generated in the current study, however, includes measurements at mass loadings < 10 μg m^{-3} ~~μg/m^3~~ and does not require any extrapolation beyond the bounds of the data to include lower, atmospherically relevant aerosol loadings. As shown in Fig. 3, while the SOA yields from this study are consistent with Griffin et al. (1999) for ΔM_o > 45 μg m^{-3} ~~μg/m^3~~, the yields from this study are as much as a factor of 4 higher than those reported by Griffin et al. (1999) at lower mass loadings.

Instances where the measured yields at low mass loading do not match those extrapolated from higher loadings have been observed for α-pinene ozonolysis (Presto and Donahue, 2006). We attribute this result to limitations of the two-product model, which bins all compounds into only two semi-volatile products of differing vapor pressures, to cover the entire spectrum of volatilities for all chemical products. At higher mass loadings, semi-volatile and volatile compounds can condense onto the particle phase and can potentially make up the majority of the aerosol. When a two-product yield curve is fit to high mass loadings only, the parameters are likely to be biased by the semi-volatile and high volatility products. Therefore, a yield curve fit using data from only high mass loadings will not account for the low-volatility products, which might be the minority products at high organic mass loadings. The two-product fit using high mass loadings therefore cannot be used to predict yields at low mass loadings, where the SOA is mostly comprised of low-volatility products. Since the yield curve generated as part of this study spans a wide range of organic mass loadings, the fitting parameters account for both the low-volatility products and the higher volatility products.

Fitting yield data to the volatility basis set described in Donahue et al. (2006) illustrates how higher volatility bins (products) are favored at higher aerosol mass loadings. The fit coefficients for the volatility basis set are shown in Table 3 for the aerosol yields of β-pinene+NO_3 from this

study and that of Griffin et al. (1999). It is noted that the data from Griffin et al. (1999) have been adjusted to a temperature of 298K and density of 1.41 g cm^{-3} for comparison to results from our study. ~~The~~ As seen in Table 3, the stoichiometric coefficients for the fit of Griffin et al. (1999) are weighted towards higher volatility products while the coefficients fit to the data collected in this study are distributed among lower and higher volatility products.

Fry et al. (2009) conducted a pair of β-pinene+NO_3 chamber experiments under dry and humid (RH = 60%) conditions. Their results are also shown in Fig. 3. The yields from Fry et al. (2009) are about 20% lower than the current study. A more recent study by Fry et al. (2014) reported aerosol mass yields in the range of 33-44% for the β-pinene+NO_3 system at an organic mass loading of 10 μg m^{-3}~~μg/m^3~~ in a continuous flow chamber under dry conditions. This is approximately 10-30% lower than the yield reported at a similar mass loading in this study. While various experimental conditions can contribute to the difference in aerosol mass yields, we note that the aerosol formation rate in both Fry et al. (2009) and Fry et al. (2014) is slower than this study, which is likely caused by lower oxidant concentrations in Fry et al. (2009) and Fry et al. (2014) compared to this study. Slower reaction times could allow more time for the gas-phase species to partition onto the chamber walls and reduce the amount that partitions onto aerosol (Ng et al., 2007b; Zhang et al., 2014). Thus, organic vapor wall loss might play a role in the lower yields observed in Fry et al. (2009) and Fry et al. (2014). There is a substantial difference between our β-pinene+NO_3 SOA yield and that from Hallquist et al. (1999), which reported an aerosol mass yield of 10% for a mass loading of ~~7~~ 4 μg m^{-3}~~μg/m^3~~. A possible explanation for this is that the mass of β-pinene reacted was not directly measured in Hallquist et al. (1999), instead, it was assumed that the concentration of β-pinene reacted was equivalent to the concentration of N_2O_5 reacted. If there were other loss processes for N_2O_5 in the experiments conducted by Hallquist et al. (1999), the yield reported in their study could be substantially lower than the actual aerosol yield.

4.2.2) Effects of RH and Acidity on SOA Yields

For the "RO_2+NO_3 dominant" experiments, the yields between experiments conducted at dry conditions with ammonium sulfate seed are similar to experiments conducted under high

humidity (RH = 50% and RH = 70%) (Fig. 3). Our results indicate that the relative humidity does not have appreciable effects on the aerosol mass yield. These results are consistent with previous humidity effects studies on photooxidation (Nguyen et al., 2011) and nitrate radical chemistry (Bonn and Moorgat, 2002; Fry et al., 2009). However, these results are inconsistent to the study performed by Spittler et al. (2006), where lower SOA yields were obtained for the α-pinene+NO_3 system under humid conditions (RH = 20%). Spittler et al. (2006) proposed that either the presence of water vapor altered the gas-phase chemistry or that the aerosol water on seed particles prevented gas-phase partitioning. These do not seem to be the case in our study. Similar gas-phase oxidation products are detected by CIMS under both dry and humid conditions and the organics size distribution measured by HR-ToF-AMS overlaps that of the seed aerosol, indicating that the oxidation products are condensing onto the seed particles.

The presence of aerosol water can potentially affect SOA formation through hydrolysis of organic nitrates. It has been observed in previous studies that organic nitrates in aqueous filter extract can undergo hydrolysis to form alcohols and nitric acid (Sato, 2008). The change from nitrate to hydroxyl functional groups could affect gas-particle partitioning and aerosol yields if the organic nitrates and alcohols have different vapor pressures. However, previous studies have shown that hydroxyl groups lower the vapor pressure of an organic compound to the same extent as organic nitrate groups (Pankow and Asher, 2008). In this study, hydrolysis does not appear to be a major reaction pathway for β-pinene+NO_3 SOA under humid conditions. As shown in Section 4.4, only < 10% of OA undergoes hydrolysis. Thus, even if there is a difference in the vapor pressures between organic nitrates and their hydrolysis products, it is unlikely that this would affect aerosol yields in our case.

Aerosol water can also enhance SOA yields by providing a medium for water-soluble species (e.g., glyoxal) to dissolve into the particulate aqueous phase ~~(~~(Ervens et al., 2011). Nitrate radical addition is predicted to add predominantly to a double bond instead of cleaving carbon to carbon bonds (Wayne et al., 1991) and hence fragmentation to small carbon compounds is unlikely. As shown in Fig. 8, the proposed mechanism does not involve carbon cleaving reactions which could result in small, water-soluble compounds. This is further supported by the similarities in SOA yields between dry and humid conditions. If these carbon cleaving reactions dominate and

form small, water-soluble species, the yields should be much higher for the humid conditions than the dry conditions.

We find that aerosol acidity has a negligible effect on the SOA yield for the β-pinene+NO_3 system (Fig. S43). This is opposite to some previous studies where increases in aerosol yields have been found under acidic conditions for other SOA systems (using the same seeds as in our study), such as ozonolysis of α-pinene and photooxidation of isoprene (e.g., (Gao et al., 2004; Surratt et al., 2007). Acid-catalyzed particle-phase reaction such as oligomerization has been proposed for such "acid effects". Although aerosol produced by the β-pinene+NO_3 reaction can potentially undergo oligomerization as well, it appears that the aerosol products are of low enough volatility that further particle-phase reactions (if any) do not enhance SOA yields. This indicates that the "acid effect" is likely different for different SOA systems, which would depend on the parent hydrocarbon, oxidant (ozone, OH, nitrate radicals), and other reaction conditions. In general, the SOA yields for nitrate radical oxidation of BVOCs are higher than corresponding yields in ozonolysis or OH radical oxidation (e.g., Griffin et al., 1999), suggesting that no further particle-phase reaction is needed to make the oxidation products more non-volatile and the "acid effect" could be limited.

4.2.3) Effects of RO_2+NO_3 vs. RO_2+HO_2 Chemistry on SOA Yields

Previous studies have shown that the fate of peroxy radicals can have a substantial effect on SOA formation (Kroll and Seinfeld, 2008; Ziemann and Atkinson, 2012). For instance, it has been shown in laboratory chamber studies that the aerosol yields can differ by a factor of 2 depending on the RO_2 fate for the isoprene+NO_3 system (Ng et al., 2008). Although studies have proposed that RO_2+NO_3 is the major nighttime RO_2 fate in the ambient environments (Kirchner and Stockwell, 1996), results from recent field studies suggested that HO_2 radicals are abundant at night (Mao et al., 2012). The high HO_2 radical concentration could result in the RO_2+HO_2 reaction becoming the dominant RO_2 radical fate in the nighttime atmosphere. In our study, the experimental protocols are designed to promote the "RO_2+NO_3" or "RO_2+HO_2" reaction channel. These two scenarios would be representative of nitrate radical oxidation in environments with varying levels of NO_x. To our knowledge, this is the first study in which the

fate of peroxy radicals is considered in SOA formation from nitrate radical oxidation of monoterpenes. A simple kinetic model based on MCMv3.2 (Saunders et al., 2003) is developed to simulate the gas-phase chemistry for the β-pinene+NO_3 reaction. The simulation results suggest that in both "RO_2+NO_3 dominant" and "RO_2+HO_2 dominant" experiments, the cross-reactions of RO_2 radicals are not a significant reaction pathway (Fig. S10~~9~~). Figure 4 shows that the SOA yields from the "RO_2+HO_2 dominant" experiments are similar to the "RO_2+NO_3 dominant" experiments. The similar yields under these different reaction conditions could arise from a comparable suite of reaction products between the two reaction pathways. The reaction of RO_2+NO_3 produces an RO radical (Fig. 8, Reaction R16~~2~~) which can undergo decomposition or isomerization (Orlando and Tyndall, 2012; Ziemann and Atkinson, 2012). Typically, it is expected that the RO_2+HO_2 reaction will lead to the formation of peroxides (Orlando and Tyndall, 2012; Ziemann and Atkinson, 2012). However, a recent study by Hasson et al. (2012)~~)~~ showed that for highly substituted peroxy radicals, the RO_2+HO_2 reaction favors the formation of RO radicals. Additionally, several previous studies showed that as carbon chain length increases (C2-C4), the RO_2+HO_2 reaction becomes less likely to form the ROOH product and more likely to form the RO product (Jenkin et al., 2007; Dillon and Crowley, 2008; Hasson et al., 2012). In the case of β-pinene+NO_3, RO_2 radicals are expected to form on the tertiary carbon as the nitrate radicals tend to attack the least substituted carbon of a double bond, leading to the formation of tertiary peroxy radicals (Wayne et al., 1991) (Fig. 8). Given β-pinene is a C10 compound and forms a highly substituted peroxy radical, we hypothesize that the RO_2+HO_2 reaction pathway in our study forms RO radicals as suggested by Hasson et al. (2012), leading to a similar peroxy radical fate as in the "RO_2+NO_3 dominant" experiments. We note that the RO_2+HO_2 reaction still leads to formation of ROOH as measured by CIMS (Fig. S2). Thus it appears that the RO_2+HO_2 channel does not exclusively produce RO radicals in our case. Nevertheless, based on the similar SOA yields in the " RO_2+NO_3 dominant" and "RO_2+HO_2 dominant" experiments, we propose that either the RO radical is the dominant product of the RO_2+HO_2 reaction pathway, or that ROOH has a similar volatility to the products formed from the RO radicals in the "RO_2+NO_3 dominant" experiments.

SOA is collected on filters for several experiments and analyzed using UHPLC in order to characterize the particle composition. Figure 9 shows the ratios of the total areas under the UV-

visible chromatograms for "RO_2+HO_2 dominant" and "RO_2+NO_3 dominant" experiments, under both humid and dry conditions. Chromatograms collected at 205, 235, and 270 nm are integrated to get the total area at each wavelength and the standard deviation from two measurements. Total areas are normalized by the estimated organic mass loading on the corresponding filters. The wavelengths chosen represent a good proxy for certain functional groups that absorb in these regions. More specifically, λ = 235 nm corresponds to a region of strong absorption by ROOR and ROOH (Farmer et al., 1943; Turrà et al., 2010; Ouchi et al., 2013), while λ = 270 nm is a compromise wavelength that represents both carbonyl and alkyl nitrate functional groups (Xu et al., 1993; Pavia et al., 2008). Finally, λ = 205 nm is chosen as the normalization wavelength because practically all organic matter present in the sample absorbs in this UV region. Figure 9 shows the ratio of total areas at 235 nm and 270 nm relative to the value at 205 nm, which provides a qualitative comparison of the samples. By comparing the amounts (areas) of the 235 and 270 nm absorbing species, the effect of humidity on each branching pathway (RO_2+HO_2 or RO_2+NO_3) can be assessed. How much -ONO_2, -C=O, ROOR and ROOH is produced under each humidity level determines the relative reactivity between the humid vs. dry conditions of each branching pathway. The relative reactivity for both reaction channels is similar within one standard deviation for all humidity conditions studied, indicating that each condition may have a similar product distribution. A comparison between the RO_2 + HO_2 and RO_2 + NO_3 pathways cannot be made in this manner because NO_3 concentrations were different. The seemingly smaller areas for species produced in the HO_2 panel could simply be due to a larger amount of non-nitrated organic matter being produced that absorbs at the normalization wavelength. However, ~~O~~one slight difference is the enhancement in the production of $C_{10}H_{15}NO_6$ (*m/z* 244, an ~~ROOH~~ RCOOH species) in the "RO_2+HO_2 dominant" experiments, which increases by 2 and 7 times under dry and humid conditions, respectively, relative to the "RO_2+NO_3 dominant" experiments. This observation indicates that in the presence of additional HO_2, the oxidation is directed toward the synthesis of $C_{10}H_{15}NO_6$ (*m/z* 244) more efficiently. This can be explained by an enhancement of the reaction sequence R21 + R22 in Fig. 8, which is enhanced at high HO_2 radical concentrations.~~This can be explained by an increase in reaction R22 in Fig. 8.~~

4.3) Particulate Organic Nitrate Formation and Hydrolysis

4.3.1) Organic Nitrate Formation

The mass spectrum in Fig. 5 indicates the presence of a large fraction (11%) of nitrate in the aerosol formed from the β-pinene+NO_3 reaction. Approximately 90% of the N atoms in the spectrum are found on the NO^+ and NO_2^+ fragments. Most of the nitrate signal is assumed to be from organic species (i.e., organic nitrates) as N_2O_5 uptake to the particles is negligible and the NO^+:NO_2^+ ratio is high. In humid experiments, the heterogeneous hydrolysis of N_2O_5 could lead to the formation of inorganic nitrates (e.g., HNO_3). To evaluate the contribution of inorganic nitrates to the total NO^+ and NO_2^+ ions measured by the HR-ToF-AMS, we perform two characterization experiments (RH = 50%) in which only N_2O_5 (the maximum amount of N_2O_5 used in our aerosol experiments) and seed aerosol ($(NH_4)_2SO_4$ seed or $(NH_4)_2SO_4$+H_2SO_4 seed) are injected into the chambers. In both cases, using a relative ionization efficiency (RIE) of 1.1 for nitrate results in a nitrate growth of less than 0.1 μg m^{-3}~~μg/m^3~~ detected by the HR-ToF-AMS (Rollins et al., 2009). The uptake of N_2O_5 is even less likely in the SOA yield experiments. It has been shown that when comparing to inorganic seed only, the presence of organic matter decreased N_2O_5 uptake by 80% (Gaston et al., 2014). Therefore, the contribution of inorganic nitrates to the total nitrate signals measured by the HR-ToF-AMS in our experiments is negligible.

It has been shown previously that the NO^+:NO_2^+ ratio in the HR-ToF-AMS mass spectrum can be used to infer the presence of particle-phase organic nitrates (Farmer et al., 2010). Specifically, Farmer et al. (2010) suggested that the NO^+:NO_2^+ ratio is much higher for organic nitrates (ratio = 5-15) than inorganic nitrates (ratio ~2.7) and therefore, aerosol with a high NO^+:NO_2^+ ratio likely also has a high concentration of organic nitrates. Figure 5 shows that approximately only two-thirds of the signal at *m/z* 30 is from NO^+, while the remaining signal is from organic CH_2O^+ fragment. At peak aerosol growth under dry and humid conditions, we determine from the high-resolution AMS data that the ~~NO^+:NO_2^+ ratio~~average R--ON value for β-pinene+NO_3 aerosol is ~~typically 6-7.5~~6.5 in "RO_2+NO_3 dominant" experiments and ~~8-9~~an average of 8.6 in "RO_2+HO_2

dominant" experiments. Previous studies (Fry et al., 2009; Bruns et al., 2010) on the β-pinene+NO_3 reaction suggested that the ~~NO^+:NO_2^+ ratio~~ R-ON for β-pinene+NO_3 SOA is on the order of 10:1, higher that the values determined in this study. One possible explanation for the difference in R-ON between this study and previous literature is instrument bias. Different instruments may have different R-ON values. One way to circumvent this bias is to compare the R-ON:R-AN ratio. The R-ON:R-AN for all experiments is 3.9, which is in agreement with values calculated by Fry et al. (2009) and Bruns et al. (2010) (range 3.7-4.2).~~One~~ Another explanation for this difference is the close proximity of the CH_2O^+ ion to the NO^+ ion in the aerosol mass spectrum, which may result in a small bias in the calculated ~~NO^+/NO_2^+ ratio~~R-ON. Specifically, if we were to include the contribution of the organic CH_2O^+ and $CH_2O_2^+$ fragments at *m/z* 30 and *m/z* 46 (in addition to contribution from NO^+ and NO_2^+), respectively, the corresponding NO^+:NO_2^+ ratios would be higher, i.e., ~~10~~9:1 for "RO_2+NO_3 dominant" experiments and ~~13~~11:1 for "RO_2+HO_2 dominant" experiments. Therefore, when using the NO^+:NO_2^+ ratio to estimate organic nitrate contribution in ambient OA, it is imperative that one excludes the organic contribution (if any) at *m/z* 30 when calculating the ratio.

One possible way to estimate the molar fraction of organic nitrates in the aerosol from the HR-ToF-AMS data is to use the N:C ratio of the aerosol formed in the experiments. Since β-pinene is a monoterpene, we assume its oxidation products have approximately 10 carbon atoms. This is a reasonable assumption based on the gas-phase oxidation products detected by CIMS (Fig. 8). The dominant reaction pathway of nitrate radicals is addition via attack of the double bond, adding one nitrate group to the primary carbon and forming a peroxy radical. With one nitrate group and 10 carbons from the β-pinene precursor, the organic nitrate products are expected to have a N:C ratio of about 1:10. If 100% of the SOA formed is composed of organic nitrates, the HR-ToF-AMS data should have a N:C ratio of 0.1. The average N:C ratio for all experiments measured by the HR-ToF-AMS is approximately 0.074 for SOA formed from β-pinene+NO_3 at peak growth. Thus, as an upper bound, it is approximated that the molar fraction of organic nitrates in the aerosol is 74%. Even if there is fragmentation, the organic nitrate fraction in the aerosol would remain fairly high. For instance, if the organic nitrate species only has 9 carbons, the upper-bound molar organic nitrate fraction is approximately 67%. If we assume the organic nitrate and non-organic nitrate species have the same molecular weight, the molar organic nitrate

fraction in the aerosol is equal to the fraction of aerosol mass composed of organic nitrates. In addition to N:C, the HR-ToF-AMS Nitrate:Org mass ratio can also be used to estimate the particle organic nitrate fraction. The average Nitrate:Org mass ratio measured by the HR-ToF-AMS for all experiments is about 0.16. We assume the organic nitrate compound has an average molecular weight between 200 and 300 amu based on the predicted products (Fig. 8), where 62 amu is attributed to the nitrate group ~~with~~ while the remaining mass is from the organic mass. Using both the Nitrate:Org mass ratio and the assumed range of molecular weights for the organic nitrate species, the fraction of aerosol mass composed of organic nitrates is estimated to be 45-68%. We estimate that the fraction of aerosol mass composed of organic nitrates is 60%, based on the average value of the extremes of the two estimates. This is comparable to the fraction of aerosol mass composed of organic nitrates estimated by Fry et al. (2014) (56%) but higher than that reported by Fry et al. (2009) (30-40%). The different experimental conditions in our study vs. those in Fry et al. (2009) may have contributed to the difference in the fraction of aerosol mass composed of organic nitrates. For example, the ratio of NO_2 to O_3 used to make NO_3 radicals in Fry et al. (2009) is lower than this study, which may have led to differing branching ratios of β-pinene+NO_3 vs. β-pinene+O_3.

4.3.2) Hydrolysis and Organic Nitrate Fate

As shown in Fig. 7, for experiments with the same initial hydrocarbon concentration~~s~~, the AMS nitrate-to-organics ratio of the humid experiments normalized by the dry experiments stabilize at a ratio of about 0.9. The nitrate radical addition at the double bond of β-pinene can lead to the formation of either primary or tertiary nitrates. Previous studies of organic nitrate hydrolysis in bulk solutions showed that while saturated primary nitrates hydrolyze on the order of months, tertiary nitrates hydrolyze on the order of hours (Darer et al., 2011). Primary organic nitrates with double bonds can hydrolyze on the order of minutes (Jacobs et al., 2014), but oxidation products from the β-pinene+NO_3 reaction are likely saturated compounds due to the lone double bond of β-pinene (Fig. 8). Therefore, the point at which nitrate mass stops decreasing is interpreted as when all tertiary nitrates have hydrolyzed. As the oxidation products typically contain only one nitrate group (Fig. 8), we infer that, within experimental error, approximately 90% of the organic

nitrates formed from the β-pinene+NO_3 reaction are primary nitrates. These results are consistent with findings that nitrate radical is more likely to attack the less substituted carbon, which, in the case for β-pinene, is the terminal carbon (Wayne et al., 1991). Since the nitrate addition is the first reaction step, any subsequent differences in peroxy radical fate (e.g., RO_2+NO_3 vs. RO_2+HO_2) will not affect the relative amount of primary vs. tertiary nitrates in our systems.

Based on the decay rate of $(Nitrate:Org)_{norm}$, the hydrolysis lifetime of the tertiary nitrates formed in the reaction of β-pinene with nitrate radicals is calculated to be approximately 3-4.5 hr. This is on the same order of magnitude as the hydrolysis lifetime (6 hr) of the proposed tertiary organic nitrates formed from photooxidation of trimethyl benzene in the presence of NO_x (Liu et al., 2012). Results from our study therefore do not suggest that nitrate radical chemistry produces organic nitrates with different hydrolysis rates than what is previously known for primary or tertiary organic nitrates. Instead, this study proposes that the fraction of tertiary organic nitrates produced from nitrate radical chemistry is much lower than SOA produced from photooxidation in the presence of NO_x. While we directly demonstrate this to be true in the case of the β-pinene+NO_3 system, this can also be applied to commonly emitted terpenes, including those with internal double bonds. From the list of terpenes in Guenther et al. (2012), all unsaturated terpenes have at least one double bond with a secondary or primary carbon. For example, α-pinene contains an internal double bond connecting a tertiary carbon to a secondary carbon. The nitrate radical is more likely to attack the less substituted carbon (i.e. the secondary carbon) and form a secondary organic nitrate. As primary/secondary and tertiary organic nitrates have drastically different hydrolysis rates, it is imperative that their relative contribution be accurately represented in models when determining the fate of ambient organic nitrates. A recent study by Browne et al. (2013) modeled the hydrolysis of organic nitrates in a forested region by assuming that 75% of atmospheric organic nitrates formed in the day are composed of tertiary organic nitrates, based on the average fraction of tertiary organic nitrates from the photooxidation of α-pinene and β-pinene in the presence of NO_x. This has implications on not only the organic nitrate fate, but also on the formation of nitric acid, a byproduct of organic nitrate hydrolysis (Sato, 2008). With this, Browne et al. (2013) predicted that hydrolysis of organic nitrates produced in the day time could account for as much as a third to half of all nitric acid production. However, when considering organic nitrates formed both in the day and at

night, the fraction of tertiary organic nitrates in ambient organic nitrates is likely lower than that used by Browne et al. (2013). This is especially true in areas where nitrate radical oxidation is the dominant source of organic nitrates (e.g., NO_x > 75 ppt in forested regions as noted in Browne et al. (2014)). It is recommended that future modeling studies of organic nitrates fates should consider organic nitrates formed both in the day and at night in order to take into account the large contribution of primary organic nitrates (which do not hydrolyze appreciably) formed from nitrate radical oxidation of monoterpenes.

Previous studies suggested that hydrolysis of organic nitrates can be an acid-catalyzed process in both solution (Szmigielski et al., 2010) and directly in the particle phase (Rindelaub et al., 2015). However, it has been found that primary and secondary organic nitrates are stable unless the aerosol is very acidic (pH < 0) (Darer et al., 2011; Hu et al., 2011). We calculate the corresponding change in $(Nitrate:Org)_{norm}$ ratio for the experiments where $(NH_4)_2SO_4$+H_2SO_4 seed is used (data not shown in Fig. 7). We find that for these experiments, the $(Nitrate:Org)_{norm}$ ratio also becomes constant at around 0.9, similar to that of the $(NH_4)_2SO_4$ seed experiments. However, the experiments using $(NH_4)_2SO_4$+H_2SO_4 seed have a more rapid rate of decrease in the $(Nitrate:Org)_{norm}$ ratio. This suggests that while hydrolysis of tertiary nitrates is accelerated under more acidic conditions, primary organic nitrates do not hydrolyze at an observable rate for the pH conditions employed in this study. As the majority of the particulate organic nitrates formed in our experiments are primary nitrates, we infer that particle acidity may not have a significant impact on the hydrolysis of organic nitrates formed in the BVOCs+NO_3 reaction, except in the cases where the double bond on the BVOCs connects two tertiary carbons, such as terpinolene.

4.4) Aerosol Aging in the Dark

While the aging of SOA has been extensively investigated in multiple photooxidation studies and shown to affect aerosol mass (e.g., (Donahue et al., 2012; Henry and Donahue, 2012), little is known regarding aerosol aging by nitrate radicals (Qi et al., 2012). A number of theoretical (Kerdouci et al., 2010, 2014; Rayez et al., 2014) and experimental studies (Atkinson, 1991; Wayne et al., 1991) suggested that hydrogen abstraction by nitrate radicals occurs, especially for

hydrogen atoms attached to aldehyde groups. As shown in Fig. 8, the β-pinene+NO_3 reaction can lead to the formation of compounds with carbonyl groups, allowing for potential nighttime aging of SOA by nitrate radicals. ~~While the CIMS N_2O_5 signals are not quantified, it is clear from our measurements that the N_2O_5 signals are lower (by at least a factor of 2) in the humid "RO_2+HO_2 dominant" and "RO_2+NO_3 dominant" experiments, likely due to their uptake to wet chamber and/or aerosol surfaces (Thornton et al., 2003). Thus, we~~We focus our aerosol aging discussion on the ~~dry~~ "RO_2+NO_3 dominant" experiments, where the oxidant (nitrate radicals) concentrations are higher.

As aerosol ages, first-generation products either functionalize, which decreases volatility, or fragment, which can lead to an overall increase in volatility (Kroll et al., 2009). If fragmentation is the dominant pathway, a decrease in organic mass is expected as products become more volatile and re-partition back to the gas phase. We use the AMS Org:Sulfate ratio as a proxy to examine the effect of aerosol aging on organics mass in our experiments. As wall loss of particles will lead to a decrease in organic loading, normalizing the organic loadings by sulfate allows us to examine the net change in the organics mass over the course of the experiments. The use of Org:sulfate is a good proxy for aerosol aging when the organics only condense onto existing ammonium sulfate particles. A study by (Loza et al., 2012) has demonstrated that in the case of rapid condensation of organic species, the time scale of condensation is less than the time scale of diffusion to existing seed particle. When in this "diffusion-limited growth" regime, the organic mass partially nucleates to form new particles. Since the nucleated particles are smaller than those particles in which ammonium sulfate acted as a seed for condensation, organics contained in these nucleated particles will be lost to the chamber walls more rapidly than the existing seed particles (Fig. S3). This could lead to an overall decrease in the Org:sulfate ratio. In our study, the Org:Sulfate ratio decreases after SOA reaches peak growth (Fig. 6). It is possible that this decrease is caused by wall loss of organic particles formed in the diffusion-limited growth regime. It is also possible that fragmentation of aerosol components is the dominant aging pathway, resulting in a decrease in the Org:Sulfate ratio. ~~Since the Org:Sulfate ratio decreases after SOA reaches peak growth (Fig. 6), it is likely that aerosol fragmentation is the dominant aging pathway of SOA~~. Regardless~~Nevertheless~~, there is still evidence of increased functionalization over the course of the experiments. Rapid loss of organics due to particle wall

loss or fragmentation of SOA ~~Fragmentation of SOA alone~~ would cause all AMS organic families to either decrease or remain constant relative to sulfate. However, Fig. 6 shows that the highly-oxidized fragments (CHOgt1, fragments with greater than 1 oxygen atom) increase slightly relative to sulfate while the non-oxidized fragments (CH) are lost at nearly twice the rate as the slightly oxidized fragments (CHO1). Since non-oxidized fragments are lost more quickly than less-oxidized fragments, it is possible that further particle-phase reactions are leading to the formation of highly oxidized compounds.

For the β-pinene+NO_3 reaction, carboxylic acids can be formed from the abstraction of hydrogen from aldehydes and subsequent oxidation (Fig. 8). The observed ions at *m/z* 356 and *m/z* 372 in CIMS likely correspond~~s~~ to hydroxy carbonyl nitrate and carboxylic acid, respectively. As shown in Fig. 2, *m/z* 356 decreases over the course of the experiment while *m/z* 372 increases. The possible conversion of aldehydes to carboxylic acids is also noticeable in the aerosol chemical composition. The *m/z* 44 (CO_2^+) fragment in the HR-ToF-AMS data likely arise from thermal-decomposition of carboxylic acids (Duplissy et al., 2011) and is commonly used to infer the extent of aerosol aging (Ng et al., 2011). Although the f_{44} (fraction of CO_2^+ ion to total organics) in the typical mass spectrum of β-pinene+NO_3 SOA is low (< 3%), there is a noticeable and continued increase in f_{44} after peak aerosol growth (Fig. 6). Specifically, during the 2.5 hours following peak growth, f_{44} increases by as much as 30% under dry conditions. Under humid conditions, the increase in f_{44} is only 6%. These correspond to a 17% and 6% increase in O:C ratio of the aerosol under dry (O:C ranging from 0.46 to 0.54 for all experiments) and humid conditions (O:C ranging from 0.47 to 0.50), respectively. ~~These observations are consistent with the lower N_2O_5 concentrations in the presence of surface water on chamber walls under humid conditions.~~ The lower degree of aging in humid experiments is consistent with the observation that the CIMS N_2O_5 signals, while not quantified, are clearly lower (by at least a factor of 2) in the humid "RO_2+NO_3 dominant" experiments when compared to dry experiments. This is likely due to the uptake of N_2O_5 to wet chamber and/or aerosol surfaces (Thornton et al., 2003).

It is unlikely that the observed decrease in organic species relative to sulfate and the decrease in gas phase species are due to differences in vapor phase wall loss. Matsunaga and Ziemann (2010) determined that highly-oxidized gaseous organic compounds are lost to the chamber walls

faster than compounds that have a lower degree of oxidation. Additionally, the gas-wall partitioning coefficient for a specific compound has also been shown to increase with decreasing vapor pressure ~~Additionally, the gas-wall partitioning coefficient has also been shown to correlate inversely with the vapor pressure for each compound~~ (Yeh and Ziemann, 2014), with highly oxidized species typically having lower vapor pressures than less oxidized species ~~where highly oxidized species typically have lower vapor pressures~~ (Pankow and Asher, 2008). If vapor-phase wall loss is the driving factor for the decrease of organics in this study, it would be expected that oxidized compounds would be lost to the walls more rapidly. Subsequently, these highly oxidized compounds would re-partition back to the gas phase in order to re-establish particle-gas equilibrium.~~If vapor-phase wall loss is the driving factor for the decrease in organics in this study, it would be expected that oxidized compounds would decrease more rapidly, causing these compounds to re-partition back to the gas phase to re-establish equilibrium.~~ The decrease in organics shown in Fig. 6, however, indicates more rapid losses of non-oxidized fragments compared to oxidized fragments. The less oxidized species measured by CIMS (lower molecular weight) as shown in Fig. 2 also decrease more rapidly than the more oxidized species. Therefore, the change in chemical composition and decrease in vapor phase species is more likely attributable to aerosol aging than to vapor-wall partitioning.

5) Relevance to Ambient Measurements

Results from this study provide the fundamental information to evaluate the extent to which nitrate radical oxidation of monoterpenes contributes to ambient organic aerosol. This reaction provides a direct mechanism for linking anthropogenic and biogenic emissions, and is likely substantial in the southeastern United States, where both types of emissions are high. A recent field campaign, the Southeastern Oxidant and Aerosol Study (SOAS), took place in Centreville, Alabama from June 1st – July 15th, 2013 to investigate the effects of anthropogenic pollution in a region with large natural emissions. Based on positive matrix factorization (PMF) analysis of the HR-ToF-AMS data obtained in SOAS, Xu et al. (2015b) identified an OA subtype termed as less-oxidized oxygenated organic aerosol (LO-OOA), which accounted for 32% of the total OA at Centreville. LO-OOA peaks at night and is well-correlated with particle-phase organic nitrates. These suggest that LO-OOA is produced predominantly from nighttime

monoterpene+NO_3 chemistry, especially from β-pinene+NO_3 as β-pinene has a high nighttime concentration (Xu et al., 2015b). Results from the current laboratory chamber study provide the relevant fundamental data for estimating the amount of aerosol produced from monoterpene+NO_3 in SOAS. The campaign-average loading of non-refractory PM_1 in SOAS is about 8 μg m^{-3} ~~μg/m^3~~ and it has been determined that the aerosol is highly acidic (pH = 0.94±0.59) and contains a large amount of particulate water (5.09±3.76 μg/m^3) (Cerully et al., 2014; Guo et al., 2015~~4~~). At night, the RH can reach up to 90% during the SOAS measuring period (Guo et al., 2015~~4~~). The current chamber study is designed to probe SOA formation from nitrate radical oxidation under atmospherically relevant loadings, under high humidity, and in the presence of seed aerosol of different acidity. The fates of peroxy radicals at night are highly uncertain, which mainly arises from the lack of constraints on the reaction rates of the peroxy radicals with other species, such as RO_2+NO_3 (Brown and Stutz, 2012). In our study, the experiments are conducted under both "RO_2+NO_3 dominant" and "RO_2+HO_2 dominant" regimes to explore the effects of peroxy radial fates on SOA formation. Using a SOA yield of 50% (for a mass loading of 8 μg m^{-3} ~~μg/m^3~~ obtained from the yield curve) in the presence of acidic seed at RH = 70% obtained from "RO_2+HO_2 dominant" experiments, Xu et al. (2015b) estimated that about 50% of nighttime OA could be produced by the reaction of β-pinene with nitrate radicals in SOAS.

It is noted that the LO-OOA factor is also resolved at both rural and urban sites around the greater Atlanta area in all seasons, where HR-ToF-AMS measurements were conducted as part of the Southeastern Center for Air Pollution and Epidemiology study (SCAPE) (Verma et al., 2014; Xu et al., 2015a, b). It is found that LO-OOA made up 18-36% of the total OA in rural and urban areas, suggesting that a fairly large fraction of total OA in the southeastern United States could arise from nitrate radical oxidation of monoterpenes.

Figure 10 shows a comparison of the aerosol mass spectrum from a typical β-pinene+NO_3 experiment from this study and the LO-OOA factor obtained from SOAS data. As LO-OOA could have other sources in addition to monoterpene+NO_3, the two spectra are not in perfect agreement but they do show similar trends above *m/z* 60. Most noticeable of these are *m/z* 67 ($C_5H_7^+$) and *m/z* 91 ($C_7H_7^+$) with a ratio of these two ions ($C_5H_7^+$: $C_7H_7^+$) of about 2.9 (ranging

from 2.5-~~3.5~~ 3.6 in other experiments). The mass spectra for the other SOA-forming systems predicted to be of importance at SOAS, namely, α-pinene ozonolysis (Chhabra et al., 2010), isoprene photooxidation (Chhabra et al., 2010), and nitrate radical initiated isoprene chemistry (Ng et al., 2008), do not show significant intensities at either of these two ions. Therefore, it is likely that high signals at $C_5H_7^+$ and $C_7H_7^+$ in ambient aerosol mass spectrum could be indicative of the presence of β-pinene+NO_3 reaction products. We note that the average NO^+:NO_2^+ ratio for aerosol measured at SOAS is 7.1, consistent with the high NO^+:NO_2^+ ratio from the SOA formed from nitrate radical oxidation of β-pinene in this study.

The gas-phase oxidation products detected by the CIMS in this study can also be used to help interpret ambient data to evaluate the possible contribution of β-pinene+NO_3 reaction. For instance, a significant amount of gas-phase organic nitrate species with MW of 215 amu and 231 amu have been observed during the BEARPEX campaign in Fall 2009 (Beaver et al., 2012). As these species exhibited a nighttime peak, Beaver et al. (2012) suggested that they could arise from nighttime oxidation of α-pinene or β-pinene by nitrate radicals. The proposed mechanism for β-pinene+NO_3 (Fig. 8) show multiple reaction pathways to form species with MW = 215 and MW = 231. Therefore, the oxidation of β-pinene by nitrate radicals represents one possible pathway for the formation of the species detected by Beaver et al. (2012). As the β-pinene+NO_3 reaction has shown to be important at SOAS (Xu et al., 2015b), it is expected that the gas-phase compounds observed in this chamber study could help explain some of the species detected by the multiple CIMS deployed during the SOAS study.

6) Atmospheric Implications

Although photooxidation is expected to be the major oxidation pathway for atmospheric VOCs, nitrate radical oxidation can account for as much as 20% of global BVOCs oxidation and is predicted to lead to an aerosol mass increase by as much as 45% when compared to the modeled case where this chemistry is excluded (Pye et al., 2010). Due to high SOA yields, evaluating the mass of aerosol produced by nitrate radical initiated chemistry is essential to estimate the total organic aerosol burden, both on regional and global scales. Currently, the aerosol yields from nitrate radical oxidation of monoterpenes in most models are assumed to be the same as those

determined from β-pinene+NO_3 reactions in Griffin et al. (1999) (Pye et al., 2010). In this study, we systematically investigate SOA formation from the nitrate radical oxidation of β-pinene under various reaction conditions (dry, humid, differing radical fate) and a wide range of initial hydrocarbon concentrations that are atmospherically relevant. We determine that the SOA yields from the β-pinene+NO_3 systems are consistent with Griffin et al. (1999) for mass loadings > 45 μg m^{-3} ~~μg/m^3~~, but as much as a factor of 4 higher than those reported in Griffin et al. (1999) for lower mass loadings. The lower SOA yields reported in Griffin et al. (1999) could arise from uncertainties in extrapolating data from higher mass loadings to lower mass loadings in that study, as well from slower reaction rates and vapor wall loss effects (Zhang et al., 2014). While it is likely that the SOA yields from the nitrate radical oxidation of various monoterpenes are different (Fry et al., 2014), updating SOA formation from β-pinene+NO_3 with the new yield parameters in future modeling studies would lead to a more accurate prediction of the amount of aerosol formed from this reaction pathway.

Currently, the fate of peroxy radicals (RO_2+HO_2 vs RO_2+NO_3, etc) in the nighttime atmosphere is still highly uncertain (Brown and Stutz, 2012), though recent studies showed that the HO_2 mixing ratio is often on the order of 10 ppt (Mao et al., 2012). Thus, RO_2+HO_2 could be the dominant nighttime fate of peroxy radicals. In this study, we examine the effect of RO_2 fate on aerosol yields for the β-pinene+NO_3 system. Although more ROOH species are produced through the RO_2+HO_2 channel, the SOA yields in the "RO_2+NO_3 dominant" and "RO_2+HO_2 dominant" experiments are comparable ~~and also have similar contributions from organic peroxides (ROOR) (Fig. 9)~~. This indicates that for this system, the overall product chemical composition and volatility distribution may not be very different for the different peroxy radical fates. This is in contrast to results from nitrate radical oxidation of smaller biogenic species, such as isoprene, which have large differences in SOA yields depending on the RO_2 fate (Ng et al., 2008). This suggests that the fates of peroxy radicals in nitrate radical experiments for larger BVOCs (such as monoterpenes and sesquiterpenes) may not be as important as it is for small compounds (such as isoprene) and in photooxidation and ozonolysis experiments (e.g., ~~(~~Presto et al., 2005; Kroll et al., 2006; Ng et al., 2007a; Eddingsaas et al., 2012; Xu et al., 2014). This warrants further studies.

The results from this study provide the first insight for the specific organic nitrate branching ratio on the β-pinene+NO_3 system. We determine that about 90 and 10% of the organic nitrates formed from the β-pinene+NO_3 reaction are primary organic nitrates and tertiary organic nitrates, respectively. As primary and tertiary organic nitrates hydrolyze at drastically different rates, the relative contribution of primary vs. tertiary organic nitrates determined in this work would allow for improved constraints regarding the fates of organic nitrates in the atmosphere. Specifically, we find that the primary organic nitrates do not appear to hydrolyze and the tertiary organic nitrates undergo hydrolysis with a lifetime of 3-4.5 hours. Updating ~~updating~~ the branching ratio (primary vs. tertiary) with organic nitrates formed by the NO_3-initiated oxidation of BVOCs will improve model predictions of hydrolysis of organic nitrates. Hydrolysis of organic nitrates has the potential to create a long term sink for atmospheric nitrogen in the form of nitric acid. Organic nitrates that do not hydrolyze, however, can potentially be photolyzed or oxidized by OH radicals to release NO_x back into the atmosphere (Suarez-Bertoa et al., 2012) or lost by dry or wet deposition.

Results from this chamber study are used to evaluate the contributions from the nitrate radical oxidation of BVOCs to ambient OA in the southeastern United States, where this chemistry is expected to be substantial owing to high natural and anthropogenic emissions in the area. Factor analysis of HR-ToF-AMS data from SOAS and SCAPE field measurements identified an OA subtype (LO-OOA) at these sites which is highly correlated with organic nitrates (Xu et al., 2015a, b). The β-pinene+NO_3 SOA yields obtained under reaction conditions relevant to these field studies are directly utilized to estimate the amount of ambient OA formed from this reaction pathway (Xu et al., 2015b). Specifically, it is estimated that 50% of nighttime OA could be produced by the reaction of β-pinene with nitrate radicals in SOAS (Xu et al., 2015b). Results from this study and Xu et al. (2015b) illustrate the substantial insights one can gain into aerosol formation chemistry and ambient aerosol source apportionment through coordinated fundamental laboratory studies and field measurement studies. Further, multiple gas-phase organic nitrate species are identified in this chamber study, which could be used to help interpret ambient gas-phase composition data obtained from the large suite of gas-phase measurements in SOAS. Owing to difficulties in measuring complex atmospheric processes, laboratory studies are critical in generating fundamental data to understand and predict SOA formation regionally and

globally. In this regard, it is imperative not to view laboratory studies as isolated efforts, but instead to make them essential and integrated parts of research activities in the wider atmospheric chemistry community (e.g., field campaigns).

Acknowledgements

This research was funded by US Environmental Protection Agency STAR grant (Early Career) RD-83540301. L. Xu is in part supported by NSF grant 1242258 and US EPA STAR grant R834799. W._-Y. Tuet is in part supported by the Health Effects Institute under Research Agreement #4943-RFA13-2/14-4. This publication's contents are solely the responsibility of the grantee and do not necessarily represent the official views of the US EPA. Further, US EPA does not endorse the purchase of any commercial products or services mentioned in the publication. M. I. Guzman wishes to acknowledge support from NSF CAREER award (CHE-1255290). The authors would like to thank X. X. Liu, D. X. Chen, D. J. Tanner and H. G. Huey for use and aid with their chemical ionization mass spectrometer, and to E. C. Wood for helpful discussions on the N_2O_5 injection flow tube design.

References

Akagi, S. K., Yokelson, R. J., Burling, I. R., Meinardi, S., Simpson, I., Blake, D. R., McMeeking, G. R., Sullivan, A., Lee, T., Kreidenweis, S., Urbanski, S., Reardon, J., Griffith, D. W. T., Johnson, T. J., and Weise, D. R.: Measurements of reactive trace gases and variable O3 formation rates in some South Carolina biomass burning plumes, Atmos. Chem. Phys., 13, 1141-1165, doi:10.5194/acp-13-1141-2013, 2013.

Arey, J., Aschmann, S. M., Kwok, E. S. C., and Atkinson, R.: Alkyl Nitrate, Hydroxyalkyl Nitrate, and Hydroxycarbonyl Formation from the NOx−Air Photooxidations of C5−C8 n-Alkanes, The Journal of Physical Chemistry A, 105, 1020-1027, doi:10.1021/jp003292z, 2001.

Atkinson, R.: KINETICS AND MECHANISMS OF THE GAS-PHASE REACTIONS OF THE NO3 RADICAL WITH ORGANIC-COMPOUNDS, Journal of Physical and Chemical Reference Data, 20, 459-507, 1991.

Atkinson, R.: Atmospheric Reactions of Alkoxy and β-Hydroxyalkoxy Radicals, Int. J. Chem. Kinet., 29, 99-111, doi:10.1002/(SICI)1097-4601(1997)29:2<99::AID-KIN3>3.0.CO;2-F, 1997.

Atkinson, R., and Arey, J.: Atmospheric degradation of volatile organic compounds, Chemical Reviews, 103, 4605-4638, 2003a.

2174 Atkinson, R., and Arey, J.: Gas-phase Tropospheric Chemistry of Biogenic Volatile Organic
2175 Compounds: A Review, Atmos. Environ., 37, 197-219, 2003b.

2176 Bahreini, R., Keywood, M. D., Ng, N. L., Varutbangkul, V., Gao, S., Flagan, R. C., Seinfeld, J.
2177 H., Worsnop, D. R., and Jimenez, J. L.: Measurements of Secondary Organic Aerosol from
2178 Oxidation of Cycloalkenes, Terpenes, and m-Xylene Using an Aerodyne Aerosol Mass
2179 Spectrometer, Environ. Sci. Technol., 39, 5674-5688, doi:10.1021/es048061a, 2005.

2180 Beaver, M. R., St Clair, J. M., Paulot, F., Spencer, K. M., Crounse, J. D., LaFranchi, B. W., Min,
2181 K. E., Pusede, S. E., Wooldridge, P. J., Schade, G. W., Park, C., Cohen, R. C., and Wennberg, P.
2182 O.: Importance of biogenic precursors to the budget of organic nitrates: observations of
2183 multifunctional organic nitrates by CIMS and TD-LIF during BEARPEX 2009, Atmos. Chem.
2184 Phys., 12, 5773-5785, doi:10.5194/acp-12-5773-2012, 2012.

2185 Berndt, T., and Boge, O.: Gas-phase reaction of NO3 radicals with isoprene: A kinetic and
2186 mechanistic study, International Journal of Chemical Kinetics, 29, 755-765,
2187 doi:10.1002/(sici)1097-4601(1997)29:10<755::aid-kin4>3.0.co;2-l, 1997a.

2188 Berndt, T., and Boge, O.: Products and mechanism of the gas-phase reaction of NO3 radicals
2189 with alpha-pinene, Journal of the Chemical Society-Faraday Transactions, 93, 3021-3027,
2190 doi:10.1039/a702364b, 1997b.

2191 Bonn, B., and Moorgat, G. K.: New particle formation during a- and b-pinene oxidation by O3,
2192 OH and NO3, and the influence of water vapour: particle size distribution studies, Atmos. Chem.
2193 Phys., 2, 183-196, doi:10.5194/acp-2-183-2002, 2002.

2194 Bowman, F. M., Odum, J. R., Seinfeld, J. H., and Pandis, S. N.: Mathematical model for gas-
2195 particle partitioning of secondary organic aerosols, Atmospheric Environment, 31, 3921-3931,
2196 doi:10.1016/s1352-2310(97)00245-8, 1997.

2197 Brown, S. S., deGouw, J. A., Warneke, C., Ryerson, T. B., Dube, W. P., Atlas, E., Weber, R. J.,
2198 Peltier, R. E., Neuman, J. A., Roberts, J. M., Swanson, A., Flocke, F., McKeen, S. A., Brioude,
2199 J., Sommariva, R., Trainer, M., Fehsenfeld, F. C., and Ravishankara, A. R.: Nocturnal isoprene
2200 oxidation over the Northeast United States in summer and its impact on reactive nitrogen
2201 partitioning and secondary organic aerosol, Atmos. Chem. Phys., 9, 3027-3042, 2009.

2202 Brown, S. S., and Stutz, J.: Nighttime radical observations and chemistry, Chemical Society
2203 Reviews, 41, 6405-6447, doi:10.1039/c2cs35181a, 2012.

2204 Brown, S. S., Dube, W. P., Bahreini, R., Middlebrook, A. M., Brock, C. A., Warneke, C., de
2205 Gouw, J. A., Washenfelder, R. A., Atlas, E., Peischl, J., Ryerson, T. B., Holloway, J. S.,
2206 Schwarz, J. P., Spackman, R., Trainer, M., Parrish, D. D., Fehshenfeld, F. C., and Ravishankara,
2207 A. R.: Biogenic VOC oxidation and organic aerosol formation in an urban nocturnal boundary
2208 layer: aircraft vertical profiles in Houston, TX, Atmos. Chem. Phys., 13, 11317-11337,
2209 doi:10.5194/acp-13-11317-2013, 2013.

2210 Browne, E. C., and Cohen, R. C.: Effects of biogenic nitrate chemistry on the NOx lifetime in
2211 remote continental regions, Atmos. Chem. Phys., 12, 11917-11932, doi:10.5194/acp-12-11917-
2212 2012, 2012.

2213 Browne, E. C., Min, K. E., Wooldridge, P. J., Apel, E., Blake, D. R., Brune, W. H., Cantrell, C.
2214 A., Cubison, M. J., Diskin, G. S., Jimenez, J. L., Weinheimer, A. J., Wennberg, P. O., Wisthaler,
2215 A., and Cohen, R. C.: Observations of total RONO2 over the boreal forest: NOx sinks and
2216 HNO3 sources, Atmos. Chem. Phys., 13, 4543-4562, doi:10.5194/acp-13-4543-2013, 2013.

2217 Browne, E. C., Wooldridge, P. J., Min, K. E., and Cohen, R. C.: On the role of monoterpene
2218 chemistry in the remote continental boundary layer, Atmos. Chem. Phys., 14, 1225-1238,
2219 doi:10.5194/acp-14-1225-2014, 2014.

2220 Bruns, E. A., Perraud, V., Zelenyuk, A., Ezell, M. J., Johnson, S. N., Yu, Y., Imre, D.,
2221 Finlayson-Pitts, B. J., and Alexander, M. L.: Comparison of FTIR and Particle Mass
2222 Spectrometry for the Measurement of Particulate Organic Nitrates, Environ. Sci. Technol., 44,
2223 1056-1061, doi:10.1021/es9029864, 2010.

2224 Canagaratna, M. R., Jimenez, J. L., Kroll, J. H., Chen, Q., Kessler, S. H., Massoli, P.,
2225 Hildebrandt Ruiz, L., Fortner, E., Williams, L. R., Wilson, K. R., Surratt, J. D., Donahue, N. M.,
2226 Jayne, J. T., and Worsnop, D. R.: Elemental ratio measurements of organic compounds using
2227 aerosol mass spectrometry: characterization, improved calibration, and implications, Atmos.
2228 Chem. Phys., 15, 253-272, doi:10.5194/acp-15-253-2015, 2015.

2229 Carter, W. P. L., Darnall, K. R., Lloyd, A. C., Winer, A. M., and Pitts Jr, J. N.: Evidence for
2230 Alkoxy Radical Isomerization in Photooxidations of C_4-C_6 Alkanes under Simulated
2231 Atmospheric Conditions, Chem. Phys. Lett., 42, 22-27, doi:http://dx.doi.org/10.1016/0009-
2232 2614(76)80543-X, 1976.

2233 Cerully, K. M., Bougiatioti, A., Hite, J. R., Guo, H., Xu, L., Ng, N. L., Weber, R. J., and Nenes,
2234 A.: On the Link Between Hygroscopicity, Volatility, and Oxidation State of Ambient and Water-
2235 Soluble Aerosol in the Southeastern United Sates., Atmos. Chem. Phys. Discuss., 14, 30835-
2236 30877, doi:doi:10.5194/acpd-14-30835-2014, 2014.

2237 Chen, Q., Farmer, D. K., Rizzo, L. V., Pauliquevis, T., Kuwata, M., Karl, T. G., Guenther, A.,
2238 Allan, J. D., Coe, H., Andreae, M. O., Pöschl, U., Jimenez, J. L., Artaxo, P., and Martin, S. T.:
2239 Submicron particle mass concentrations and sources in the Amazonian wet season (AMAZE-08),
2240 Atmos. Chem. Phys., 15, 3687-3701, doi:10.5194/acp-15-3687-2015, 2015.

2241 Chen, X., Hulbert, D., and Shepson, P. B.: Measurement of the organic nitrate yield from OH
2242 reaction with isoprene, Journal of Geophysical Research: Atmospheres, 103, 25563-25568,
2243 doi:10.1029/98JD01483, 1998.

2244 Chhabra, P. S., Flagan, R. C., and Seinfeld, J. H.: Elemental analysis of chamber organic aerosol
2245 using an aerodyne high-resolution aerosol mass spectrometer, Atmos. Chem. Phys., 10, 4111-
2246 4131, doi:10.5194/acp-10-4111-2010, 2010.

2247 Chung, S. H., and Seinfeld, J. H.: Global distribution and climate forcing of carbonaceous
2248 aerosols, Journal of Geophysical Research: Atmospheres, 107, 4407,
2249 doi:10.1029/2001JD001397, 2002.

2250 Darer, A. I., Cole-Filipiak, N. C., O'Connor, A. E., and Elrod, M. J.: Formation and Stability of
2251 Atmospherically Relevant Isoprene-Derived Organosulfates and Organonitrates, Environ. Sci.
2252 Technol., 45, 1895-1902, doi:10.1021/es103797z, 2011.

2253 Day, D. A., Liu, S., Russell, L. M., and Ziemann, P. J.: Organonitrate group concentrations in
2254 submicron particles with high nitrate and organic fractions in coastal southern California,
2255 Atmospheric Environment, 44, 1970-1979, doi:10.1016/j.atmosenv.2010.02.045, 2010.

2256 de Gouw, J. A., Middlebrook, A. M., Warneke, C., Goldan, P. D., Kuster, W. C., Roberts, J. M.,
2257 Fehsenfeld, F. C., Worsnop, D. R., Canagaratna, M. R., Pszenny, A. A. P., Keene, W. C.,
2258 Marchewka, M., Bertman, S. B., and Bates, T. S.: Budget of organic carbon in a polluted
2259 atmosphere: Results from the New England Air Quality Study in 2002, Journal of Geophysical
2260 Research-Atmospheres, 110, D16305, doi:16310.11029/12004JD005623, 2005.

2261 DeCarlo, P. F., Kimmel, J. R., Trimborn, A., Northway, M. J., Jayne, J. T., Aiken, A. C., Gonin,
2262 M., Fuhrer, K., Horvath, T., Docherty, K. S., Worsnop, D. R., and Jimenez, J. L.: Field-
2263 deployable, high-resolution, time-of-flight aerosol mass spectrometer, Analytical Chemistry, 78,
2264 8281-8289, doi:10.1021/ac061249n, 2006.

2265 Dibble, T. S.: Reactions of the alkoxy radicals formed following OH-addition to alpha-pinene
2266 and beta-pinene. C-C bond scission reactions, Journal of the American Chemical Society, 123,
2267 4228-4234, doi:10.1021/ja003553i, 2001.

2268 Dillon, T. J., and Crowley, J. N.: Direct detection of OH formation in the reactions of HO(2)
2269 with CH(3)C(O)O(2) and other substituted peroxy radicals, Atmos. Chem. Phys., 8, 4877-4889,
2270 2008.

2271 Donahue, N. M., Robinson, A. L., Stanier, C. O., and Pandis, S. N.: Coupled partitioning,
2272 dilution, and chemical aging of semivolatile organics, Environ. Sci. Technol., 40, 2635-2643,
2273 doi:10.1021/es052297c, 2006.

2274 Donahue, N. M., Henry, K. M., Mentel, T. F., Kiendler-Scharr, A., Spindler, C., Bohn, B.,
2275 Brauers, T., Dorn, H. P., Fuchs, H., Tillmann, R., Wahner, A., Saathoff, H., Naumann, K.-H.,
2276 Moehler, O., Leisner, T., Mueller, L., Reinnig, M.-C., Hoffmann, T., Salo, K., Hallquist, M.,
2277 Frosch, M., Bilde, M., Tritscher, T., Barmet, P., Praplan, A. P., DeCarlo, P. F., Dommen, J.,
2278 Prevot, A. S. H., and Baltensperger, U.: Aging of biogenic secondary organic aerosol via gas-
2279 phase OH radical reactions, Proceedings of the National Academy of Sciences of the United
2280 States of America, 109, 13503-13508, doi:10.1073/pnas.1115186109, 2012.

2281 Duplissy, J., DeCarlo, P. F., Dommen, J., Alfarra, M. R., Metzger, A., Barmpadimos, I., Prevot,
2282 A. S. H., Weingartner, E., Tritscher, T., Gysel, M., Aiken, A. C., Jimenez, J. L., Canagaratna, M.
2283 R., Worsnop, D. R., Collins, D. R., Tomlinson, J., and Baltensperger, U.: Relating
2284 hygroscopicity and composition of organic aerosol particulate matter, Atmos. Chem. Phys., 11,
2285 1155-1165, doi:10.5194/acp-11-1155-2011, 2011.

2286 Eberhard, J., Muller, C., Stocker, D. W., and Kerr, J. A.: Isomerization of Alkoxy Radicals under
2287 Atmospheric Conditions, Environ. Sci. Technol., 29, 232-241, doi:10.1021/es00001a600, 1995.

2288 Eddingsaas, N. C., Loza, C. L., Yee, L. D., Seinfeld, J. H., and Wennberg, P. O.: alpha-pinene
2289 photooxidation under controlled chemical conditions - Part 1: Gas-phase composition in low-
2290 and high-NOx environments, Atmos. Chem. Phys., 12, 6489-6504, doi:10.5194/acp-12-6489-
2291 2012, 2012.

2292 Ervens, B., Turpin, B. J., and Weber, R. J.: Secondary organic aerosol formation in cloud
2293 droplets and aqueous particles (aqSOA): a review of laboratory, field and model studies, Atmos.
2294 Chem. Phys., 11, 11069-11102, doi:10.5194/acp-11-11069-2011, 2011.

2295 Farmer, D. K., Matsunaga, A., Docherty, K. S., Surratt, J. D., Seinfeld, J. H., Ziemann, P. J., and
2296 Jimenez, J. L.: Response of an aerosol mass spectrometer to organonitrates and organosulfates
2297 and implications for atmospheric chemistry, Proceedings of the National Academy of Sciences
2298 of the United States of America, 107, 6670-6675, doi:10.1073/pnas.0912340107, 2010.

2299 Farmer, E. H., Koch, H. P., and Sutton, D. A.: The Course of Autoxidation Reactions in
2300 Polyisoprenes and Allied Compounds. Part VII. Rearrangement of Double Bonds During
2301 Autoxidation, J. Chem. Soc., 541-547, doi:10.1039/JR9430000541, 1943.

2302 Fry, J. L., Kiendler-Scharr, A., Rollins, A. W., Wooldridge, P. J., Brown, S. S., Fuchs, H., Dubé,
2303 W., Mensah, A., dal Maso, M., Tillmann, R., Dorn, H. P., Brauers, T., and Cohen, R. C.: Organic
2304 nitrate and secondary organic aerosol yield from NO3 oxidation of β-pinene evaluated using a
2305 gas-phase kinetics/aerosol partitioning model, Atmos. Chem. Phys., 9, 1431-1449,
2306 doi:10.5194/acp-9-1431-2009, 2009.

2307 Fry, J. L., Kiendler-Scharr, A., Rollins, A. W., Brauers, T., Brown, S. S., Dorn, H. P., Dubé, W.
2308 P., Fuchs, H., Mensah, A., Rohrer, F., Tillmann, R., Wahner, A., Wooldridge, P. J., and Cohen,
2309 R. C.: SOA from limonene: role of NO3 in its generation and degradation, Atmos. Chem. Phys.,
2310 11, 3879-3894, doi:10.5194/acp-11-3879-2011, 2011.

2311 Fry, J. L., Draper, D. C., Zarzana, K. J., Campuzano-Jost, P., Day, D. A., Jimenez, J. L., Brown,
2312 S. S., Cohen, R. C., Kaser, L., Hansel, A., Cappellin, L., Karl, T., Roux, A. H., Turnipseed, A.,
2313 Cantrell, C., Lefer, B. L., and Grossberg, N.: Observations of gas- and aerosol-phase organic
2314 nitrates at BEACHON-RoMBAS 2011, Atmos. Chem. Phys., 13, 8585-8605, doi:10.5194/acp-
2315 13-8585-2013, 2013.

2316 Fry, J. L., Draper, D. C., Barsanti, K. C., Smith, J. N., Ortega, J., Winkler, P. M., Lawler, M. J.,
2317 Brown, S. S., Edwards, P. M., Cohen, R. C., and Lee, L.: Secondary Organic Aerosol Formation
2318 and Organic Nitrate Yield from NO3 Oxidation of Biogenic Hydrocarbons, Environ. Sci.
2319 Technol., 48, 11944-11953, doi:10.1021/es502204x, 2014.

2320 Fuentes, J., Wang, D., Bowling, D., Potosnak, M., Monson, R., Goliff, W., and Stockwell, W.:
2321 Biogenic Hydrocarbon Chemistry within and Above a Mixed Deciduous Forest, Journal of
2322 Atmospheric Chemistry, 56, 165-185, doi:10.1007/s10874-006-9048-4, 2007.

2323 Fuentes, J. D., Lerdau, M., Atkinson, R., Baldocchi, D., Bottenheim, J. W., Ciccioli, P., Lamb,
2324 B., Geron, C., Gu, L., Guenther, A., Sharkey, T. D., and Stockwell, W.: Biogenic hydrocarbons
2325 in the atmospheric boundary layer: A review, Bull. Amer. Meteorol. Soc., 81, 1537-1575,
2326 doi:10.1175/1520-0477(2000)081<1537:bhitab>2.3.co;2, 2000.

2327 Gao, S., Ng, N. L., Keywood, M., Varutbangkul, V., Bahreini, R., Nenes, A., He, J., Yoo, K. Y.,
2328 Beauchamp, J. L., Hodyss, R. P., Flagan, R. C., and Seinfeld, J. H.: Particle Phase Acidity and
2329 Oligomer Formation in Secondary Organic Aerosol, Environ. Sci. Technol., 38, 6582-6589,
2330 doi:10.1021/es049125k, 2004.

2331 Gaston, C. J., Thornton, J. A., and Ng, N. L.: Reactive uptake of N2O5 to internally mixed
2332 inorganic and organic particles: the role of organic carbon oxidation state and inferred organic
2333 phase separations, Atmos. Chem. Phys., 14, 5693-5707, doi:10.5194/acp-14-5693-2014, 2014.

2334 Griffin, R. J., Cocker, D. R., Flagan, R. C., and Seinfeld, J. H.: Organic aerosol formation from
2335 the oxidation of biogenic hydrocarbons, Journal of Geophysical Research-Atmospheres, 104,
2336 3555-3567, doi:10.1029/1998jd100049, 1999.

2337 Guenther, A. B., Jiang, X., Heald, C. L., Sakulyanontvittaya, T., Duhl, T., Emmons, L. K., and
2338 Wang, X.: The Model of Emissions of Gases and Aerosols from Nature version 2.1
2339 (MEGAN2.1): an extended and updated framework for modeling biogenic emissions,
2340 Geoscientific Model Development, 5, 1471-1492, doi:10.5194/gmd-5-1471-2012, 2012.

2341 Guo, H., Xu, L., Bougiatioti, A., Cerully, K. M., Capps, S. L., Hite Jr, J. R., Carlton, A. G., Lee,
2342 S. H., Bergin, M. H., Ng, N. L., Nenes, A., and Weber, R. J.: Fine-particle water and pH in the
2343 southeastern United States, Atmos. Chem. Phys., 15, 5211-5228, doi:10.5194/acp-15-5211-2015,
2344 2015.

2345 Hallquist, M., Wangberg, I., Ljungstrom, E., Barnes, I., and Becker, K. H.: Aerosol and product
2346 yields from NO3 radical-initiated oxidation of selected monoterpenes, Environ. Sci. Technol.,
2347 33, 553-559, doi:10.1021/es980292s, 1999.

2348 Hasson, A. S., Tyndall, G. S., Orlando, J. J., Singh, S., Hernandez, S. Q., Campbell, S., and
2349 Ibarra, Y.: Branching Ratios for the Reaction of Selected Carbonyl-Containing Peroxy Radicals
2350 with Hydroperoxy Radicals, The Journal of Physical Chemistry A, 116, 6264-6281,
2351 doi:10.1021/jp211799c, 2012.

2352 Hatch, L. E., Luo, W., Pankow, J. F., Yokelson, R. J., Stockwell, C. E., and Barsanti, K. C.:
2353 Identification and quantification of gaseous organic compounds emitted from biomass burning
2354 using two-dimensional gas chromatography-time-of-flight mass spectrometry, Atmos. Chem.
2355 Phys., 15, 1865-1899, doi:10.5194/acp-15-1865-2015, 2015.

2356 Henry, K. M., and Donahue, N. M.: Photochemical Aging of α-Pinene Secondary Organic
2357 Aerosol: Effects of OH Radical Sources and Photolysis, The Journal of Physical Chemistry A,
2358 116, 5932-5940, doi:10.1021/jp210288s, 2012.

2359 Hoyle, C. R., Berntsen, T., Myhre, G., and Isaksen, I. S. A.: Secondary organic aerosol in the
2360 global aerosol – chemical transport model Oslo CTM2, Atmos. Chem. Phys., 7, 5675-
2361 5694, doi:10.5194/acp-7-5675-2007, 2007.

2362 Hu, K. S., Darer, A. I., and Elrod, M. J.: Thermodynamics and kinetics of the hydrolysis of
2363 atmospherically relevant organonitrates and organosulfates, Atmos. Chem. Phys., 11, 8307-8320,
2364 doi:10.5194/acp-11-8307-2011, 2011.

2365 Huey, L. G.: Measurement of trace atmospheric species by chemical ionization mass
2366 spectrometry: Speciation of reactive nitrogen and future directions, Mass Spectrom. Rev., 26,
2367 166-184, doi:10.1002/mas.20118, 2007.

2368 Iinuma, Y., Muller, C., Berndt, T., Boge, O., Claeys, M., and Herrmann, H.: Evidence for the
2369 existence of organosulfates from beta-pinene ozonolysis in ambient secondary organic aerosol,
2370 Environ. Sci. Technol., 41, 6678-6683, doi:10.1021/es070938t, 2007.

2371 Jacobs, M. I., Burke, W. J., and Elrod, M. J.: Kinetics of the reactions of isoprene-derived
2372 hydroxynitrates: gas phase epoxide formation and solution phase hydrolysis, Atmos. Chem.
2373 Phys., 14, 8933-8946, doi:10.5194/acp-14-8933-2014, 2014.

2374 Jaoui, M., Kleindienst, T. E., Docherty, K. S., Lewandowski, M., and Offenberg, J. H.:
2375 Secondary organic aerosol formation from the oxidation of a series of sesquiterpenes: alpha-
2376 cedrene, beta-caryophyllene, alpha-humulene and alpha-farnesene with O-3, OH and NO3
2377 radicals, Environmental Chemistry, 10, 178-193, doi:10.1071/en13025, 2013.

2378 Jenkin, M. E., Hurley, M. D., and Wallington, T. J.: Investigation of the radical product channel
2379 of the CH3C(O)O2 + HO2 reaction in the gas phase, Physical Chemistry Chemical Physics, 9,
2380 3149-3162, doi:10.1039/B702757E, 2007.

2381 Kanakidou, M., Seinfeld, J. H., Pandis, S. N., Barnes, I., Dentener, F. J., Facchini, M. C., Van
2382 Dingenen, R., Ervens, B., Nenes, A., Nielsen, C. J., Swietlicki, E., Putaud, J. P., Balkanski, Y.,
2383 Fuzzi, S., Horth, J., Moortgat, G. K., Winterhalter, R., Myhre, C. E. L., Tsigaridis, K., Vignati,
2384 E., Stephanou, E. G., and Wilson, J.: Organic aerosol and global climate modelling: a review,
2385 Atmos. Chem. Phys., 5, 1053-1123, 2005.

2386 Kerdouci, J., Picquet-Varrault, B., and Doussin, J. F.: Prediction of Rate Constants for Gas-Phase
2387 Reactions of Nitrate Radical with Organic Compounds: A New Structure-Activity Relationship,
2388 ChemPhysChem, 11, 3909-3920, doi:10.1002/cphc.201000673, 2010.

2389 Kerdouci, J., Picquet-Varrault, B., and Doussin, J. F.: Structure-activity relationship for the gas-
2390 phase reactions of NO3 radical with organic compounds: Update and extension to aldehydes,
2391 Atmospheric Environment, 84, 363-372, doi:10.1016/j.atmosenv.2013.11.024, 2014.

2392 Keywood, M. D., Varutbangkul, V., Bahreini, R., Flagan, R. C., and Seinfeld, J. H.: Secondary
2393 organic aerosol formation from the ozonolysis of cycloalkenes and related compounds, Environ.
2394 Sci. Technol., 38, 4157-4164, doi:10.1021/es035363o, 2004.

2395 Kirchner, F., and Stockwell, W. R.: Effect of peroxy radical reactions on the predicted
2396 concentrations of ozone, nitrogenous compounds, and radicals, Journal of Geophysical Research:
2397 Atmospheres, 101, 21007-21022, doi:10.1029/96JD01519, 1996.

2398 Kroll, J. H., Ng, N. L., Murphy, S. M., Flagan, R. C., and Seinfeld, J. H.: Secondary Organic
2399 Aerosol Formation from Isoprene Photooxidation, Environ. Sci. Technol., 40, 1869-1877,
2400 doi:10.1021/es0524301, 2006.

2401 Kroll, J. H., and Seinfeld, J. H.: Chemistry of secondary organic aerosol: Formation and
2402 evolution of low-volatility organics in the atmosphere, Atmospheric Environment, 42, 3593-
2403 3624, doi:10.1016/j.atmosenv.2008.01.003, 2008.

2404 Kroll, J. H., Smith, J. D., Che, D. L., Kessler, S. H., Worsnop, D. R., and Wilson, K. R.:
2405 Measurement of fragmentation and functionalization pathways in the heterogeneous oxidation of
2406 oxidized organic aerosol, Physical Chemistry Chemical Physics, 11, 8005-8014,
2407 doi:10.1039/b905289e, 2009.

2408 Kwan, A. J., Chan, A. W. H., Ng, N. L., Kjaergaard, H. G., Seinfeld, J. H., and Wennberg, P. O.:
2409 Peroxy radical chemistry and OH radical production during the NO3-initiated oxidation of
2410 isoprene, Atmos. Chem. Phys., 12, 7499-7515, doi:10.5194/acp-12-7499-2012, 2012.

2411 Lewis, C. W., Klouda, G. A., and Ellenson, W. D.: Radiocarbon measurement of the biogenic
2412 contribution to summertime PM-2.5 ambient aerosol in Nashville, TN, Atmospheric
2413 Environment, 38, 6053-6061, doi:http://dx.doi.org/10.1016/j.atmosenv.2004.06.011, 2004.

2414 Li, Y., Chen, Q., Guzman, M., Chan, C., and Martin, S.: Second-generation products contribute
2415 substantially to the particle-phase organic material produced by β-caryophyllene ozonolysis,
2416 Atmos. Chem. Phys., 11, 121-132, 2011.

2417 Liu, S., Shilling, J. E., Song, C., Hiranuma, N., Zaveri, R. A., and Russell, L. M.: Hydrolysis of
2418 Organonitrate Functional Groups in Aerosol Particles, Aerosol Sci. Technol., 46, 1359-1369,
2419 doi:10.1080/02786826.2012.716175, 2012.

2420 Loza, C. L., Chan, A. W. H., Galloway, M. M., Keutsch, F. N., Flagan, R. C., and Seinfeld, J. H.:
2421 Characterization of Vapor Wall Loss in Laboratory Chambers, Environ. Sci. Technol., 44, 5074-
2422 5078, doi:10.1021/es100727v, 2010.

2423 Loza, C. L., Chhabra, P. S., Yee, L. D., Craven, J. S., Flagan, R. C., and Seinfeld, J. H.:
2424 Chemical aging of m-xylene secondary organic aerosol: laboratory chamber study, Atmos.
2425 Chem. Phys., 12, 151-167, doi:10.5194/acp-12-151-2012, 2012.

2426 Mao, J., Ren, X., Zhang, L., Van Duin, D. M., Cohen, R. C., Park, J. H., Goldstein, A. H.,
2427 Paulot, F., Beaver, M. R., Crounse, J. D., Wennberg, P. O., DiGangi, J. P., Henry, S. B.,
2428 Keutsch, F. N., Park, C., Schade, G. W., Wolfe, G. M., Thornton, J. A., and Brune, W. H.:
2429 Insights into hydroxyl measurements and atmospheric oxidation in a California forest, Atmos.
2430 Chem. Phys., 12, 8009-8020, doi:10.5194/acp-12-8009-2012, 2012.

Marley, N. A., Gaffney, J. S., Tackett, M., Sturchio, N. C., Heraty, L., Martinez, N., Hardy, K. D., Marchany-Rivera, A., Guilderson, T., MacMillan, A., and Steelman, K.: The impact of biogenic carbon sources on aerosol absorption in Mexico City, Atmospheric Chemistry and Physics, 9, 1537-1549, 2009.

Matsunaga, A., and Ziemann, P. J.: Yields of beta-hydroxynitrates, dihydroxynitrates, and trihydroxynitrates formed from OH radical-initiated reactions of 2-methyl-1-alkenes, Proceedings of the National Academy of Sciences of the United States of America, 107, 6664-6669, doi:10.1073/pnas.0910585107, 2010.

McLaren, R., Salmon, R. A., Liggio, J., Hayden, K. L., Anlauf, K. G., and Leaitch, W. R.: Nighttime chemistry at a rural site in the Lower Fraser Valley, Atmospheric Environment, 38, 5837-5848, doi:10.1016/j.atmosenv.2004.03.074, 2004.

McNeill, V. F., Wolfe, G. M., and Thornton, J. A.: The Oxidation of Oleate in Submicron Aqueous Salt Aerosols: Evidence of a Surface Process, The Journal of Physical Chemistry A, 111, 1073-1083, doi:10.1021/jp066233f, 2007.

Miller, B.: Advanced Organic Chemistry: Reactions and Mechanisms, Journal of Chemical Education, 76, p. 320, doi:10.1021/ed076p320.2, 1999.

Miller, B.: Advanced Organic Chemistry: Reactions and Mechanisms, 2nd ed., Pearson/Prentice Hall, Lebanon, IN, 2003.

Ng, N. L., Chhabra, P. S., Chan, A. W. H., Surratt, J. D., Kroll, J. H., Kwan, A. J., McCabe, D. C., Wennberg, P. O., Sorooshian, A., Murphy, S. M., Dalleska, N. F., Flagan, R. C., and Seinfeld, J. H.: Effect of NOx level on secondary organic aerosol (SOA) formation from the photooxidation of terpenes, Atmos. Chem. Phys., 7, 5159-5174, 2007a.

Ng, N. L., Kroll, J. H., Chan, A. W. H., Chhabra, P. S., Flagan, R. C., and Seinfeld, J. H.: Secondary organic aerosol formation from m-xylene, toluene, and benzene, Atmos. Chem. Phys., 7, 3909-3922, doi:10.5194/acp-7-3909-2007, 2007b.

Ng, N. L., Kwan, A. J., Surratt, J. D., Chan, A. W. H., Chhabra, P. S., Sorooshian, A., Pye, H. O. T., Crounse, J. D., Wennberg, P. O., Flagan, R. C., and Seinfeld, J. H.: Secondary organic aerosol (SOA) formation from reaction of isoprene with nitrate radicals (NO3), Atmos. Chem. Phys., 8, 4117-4140, 2008.

Ng, N. L., Canagaratna, M. R., Jimenez, J. L., Chhabra, P. S., Seinfeld, J. H., and Worsnop, D. R.: Changes in organic aerosol composition with aging inferred from aerosol mass spectra, Atmos. Chem. Phys., 11, 6465-6474, doi:10.5194/acp-11-6465-2011, 2011.

Nguyen, T. B., Roach, P. J., Laskin, J., Laskin, A., and Nizkorodov, S. A.: Effect of humidity on the composition of isoprene photooxidation secondary organic aerosol, Atmos. Chem. Phys., 11, 6931-6944, doi:DOI 10.5194/acp-11-6931-2011, 2011.

Nguyen, T. B., Crounse, J. D., Schwantes, R. H., Teng, A. P., Bates, K. H., Zhang, X., St. Clair, J. M., Brune, W. H., Tyndall, G. S., Keutsch, F. N., Seinfeld, J. H., and Wennberg, P. O.:

Overview of the Focused Isoprene eXperiment at the California Institute of Technology (FIXCIT): mechanistic chamber studies on the oxidation of biogenic compounds, Atmos. Chem. Phys., 14, 13531-13549, doi:10.5194/acp-14-13531-2014, 2014.

Odum, J. R., Hoffmann, T., Bowman, F., Collins, D., Flagan, R. C., and Seinfeld, J. H.: Gas/Particle Partitioning and Secondary Organic Aerosol Yields, Environ. Sci. Technol., 30, 2580-2585, doi:10.1021/es950943+, 1996.

Odum, J. R., Jungkamp, T. P. W., Griffin, R. J., Forstner, H. J. L., Flagan, R. C., and Seinfeld, J. H.: Aromatics, reformulated gasoline, and atmospheric organic aerosol formation, Environ. Sci. Technol., 31, 1890-1897, doi:10.1021/es960535l, 1997a.

Odum, J. R., Jungkamp, T. P. W., Griffin, R. J., Flagan, R. C., and Seinfeld, J. H.: The atmospheric aerosol-forming potential of whole gasoline vapor, Science, 276, 96-99, doi:10.1126/science.276.5309.96, 1997b.

Orlando, J. J., and Tyndall, G. S.: Laboratory studies of organic peroxy radical chemistry: an overview with emphasis on recent issues of atmospheric significance, Chemical Society Reviews, 41, 6294-6317, doi:10.1039/C2CS35166H, 2012.

Ouchi, A., Liu, C., Kaneda, M., and Hyugano, T.: Photochemical C–C Bond Formation between Alcohols and Olefins by an Environmentally Benign Radical Reaction, Eur. J. Org. Chem., 2013, 3807-3816, doi:10.1002/ejoc.201300115, 2013.

Pankow, J. F., and Asher, W. E.: SIMPOL.1: a simple group contribution method for predicting vapor pressures and enthalpies of vaporization of multifunctional organic compounds, Atmos. Chem. Phys., 8, 2773-2796, 2008.

Pavia, D., Lampman, G., Kriz, G., and Vyvyan, J.: Introduction to spectroscopy, Cengage Learning, 2008.

Perraud, V., Bruns, E. A., Ezell, M. J., Johnson, S. N., Greaves, J., and Finlayson-Pitts, B. J.: Identification of Organic Nitrates in the NO3 Radical Initiated Oxidation of α-Pinene by Atmospheric Pressure Chemical Ionization Mass Spectrometry, Environ. Sci. Technol., 44, 5887-5893, doi:10.1021/es1005658, 2010.

Perring, A. E., Wisthaler, A., Graus, M., Wooldridge, P. J., Lockwood, A. L., Mielke, L. H., Shepson, P. B., Hansel, A., and Cohen, R. C.: A product study of the isoprene+NO3 reaction, Atmos. Chem. Phys., 9, 4945-4956, doi:10.5194/acp-9-4945-2009, 2009.

Presto, A. A., Huff Hartz, K. E., and Donahue, N. M.: Secondary Organic Aerosol Production from Terpene Ozonolysis. 2. Effect of NOx Concentration, Environ. Sci. Technol., 39, 7046-7054, doi:10.1021/es050400s, 2005.

Presto, A. A., and Donahue, N. M.: Investigation of alpha-pinene plus ozone secondary organic aerosol formation at low total aerosol mass, Environ. Sci. Technol., 40, 3536-3543, doi:10.1021/es052203z, 2006.

Pye, H. O. T., Chan, A. W. H., Barkley, M. P., and Seinfeld, J. H.: Global modeling of organic aerosol: the importance of reactive nitrogen (NOx and NO3), Atmos. Chem. Phys., 10, 11261-11276, doi:10.5194/acp-10-11261-2010, 2010.

Qi, L., Nakao, S., and Cocker, D. R., III: Aging of secondary organic aerosol from alpha-pinene ozonolysis: Roles of hydroxyl and nitrate radicals, Journal of the Air & Waste Management Association, 62, 1359-1369, doi:10.1080/10962247.2012.712082, 2012.

Rastogi, N., Zhang, X. L., Edgerton, E. S., Ingall, E., and Weber, R. J.: Filterable water-soluble organic nitrogen in fine particles over the southeastern USA during summer, Atmospheric Environment, 45, 6040-6047, doi:10.1016/j.atmosenv.2011.07.045, 2011.

Rayez, M.-T., Rayez, J.-C., Kerdouci, J., and Picquet-Varrault, B.: Theoretical Study of the Gas-Phase Reactions of NO3 Radical with a Series of trans-2-Unsaturated Aldehydes: From Acrolein to trans-2-Octenal, The Journal of Physical Chemistry A, 118, 5149-5155, doi:10.1021/jp503619d, 2014.

Rindelaub, J. D., McAvey, K. M., and Shepson, P. B.: The photochemical production of organic nitrates from α-pinene and loss via acid-dependent particle phase hydrolysis, Atmospheric Environment, 100, 193-201, doi:http://dx.doi.org/10.1016/j.atmosenv.2014.11.010, 2015.

Rollins, A. W., Kiendler-Scharr, A., Fry, J. L., Brauers, T., Brown, S. S., Dorn, H. P., Dube, W. P., Fuchs, H., Mensah, A., Mentel, T. F., Rohrer, F., Tillmann, R., Wegener, R., Wooldridge, P. J., and Cohen, R. C.: Isoprene oxidation by nitrate radical: alkyl nitrate and secondary organic aerosol yields, Atmos. Chem. Phys., 9, 6685-6703, 2009.

Rollins, A. W., Browne, E. C., Min, K. E., Pusede, S. E., Wooldridge, P. J., Gentner, D. R., Goldstein, A. H., Liu, S., Day, D. A., Russell, L. M., and Cohen, R. C.: Evidence for NOx Control over Nighttime SOA Formation, Science, 337, 1210-1212, doi:10.1126/science.1221520, 2012.

Rollins, A. W., Pusede, S., Wooldridge, P., Min, K. E., Gentner, D. R., Goldstein, A. H., Liu, S., Day, D. A., Russell, L. M., Rubitschun, C. L., Surratt, J. D., and Cohen, R. C.: Gas/particle partitioning of total alkyl nitrates observed with TD-LIF in Bakersfield, Journal of Geophysical Research-Atmospheres, 118, 6651-6662, doi:10.1002/jgrd.50522, 2013.

Russell, G. A.: Deuterium-isotope Effects in the Autoxidation of Aralkyl Hydrocarbons. Mechanism of the Interaction of Peroxy Radicals, J. Am. Cgem. Soc., 79, 3871-3877, doi:10.1021/ja01571a068, 1957.

Russell, M., and Allen, D. T.: Predicting secondary organic aerosol formation rates in southeast Texas, Journal of Geophysical Research: Atmospheres, 110, D07S17, doi:10.1029/2004JD004722, 2005.

Sato, K.: Detection of nitrooxypolyols in secondary organic aerosol formed from the photooxidation of conjugated dienes under high-NOx conditions, Atmospheric Environment, 42, 6851-6861, doi:10.1016/j.atmosenv.2008.05.010, 2008.

2541 Saunders, S. M., Jenkin, M. E., Derwent, R. G., and Pilling, M. J.: Protocol for the development
2542 of the Master Chemical Mechanism, MCM v3 (Part A): tropospheric degradation of non-
2543 aromatic volatile organic compounds, Atmos. Chem. Phys., 3, 161-180, 2003.

2544 Schichtel, B. A., Malm, W. C., Bench, G., Fallon, S., McDade, C. E., Chow, J. C., and Watson,
2545 J. G.: Fossil and contemporary fine particulate carbon fractions at 12 rural and urban sites in the
2546 United States, Journal of Geophysical Research: Atmospheres, 113, D02311,
2547 doi:10.1029/2007JD008605, 2008.

2548 Schröder, K., Junge, K., Spannenberg, A., and Beller, M.: Design of a bio-inspired imidazole-
2549 based iron catalyst for epoxidation of olefins: Mechanistic insights, Catalysis Today, 157, 364-
2550 370, doi:10.1016/j.cattod.2010.04.034, 2010.

2551 Slusher, D. L., Huey, L. G., Tanner, D. J., Flocke, F. M., and Roberts, J. M.: A thermal
2552 dissociation–chemical ionization mass spectrometry (TD-CIMS) technique for the simultaneous
2553 measurement of peroxyacyl nitrates and dinitrogen pentoxide, Journal of Geophysical Research:
2554 Atmospheres, 109, D19315, doi:10.1029/2004JD004670, 2004.

2555 Spittler, M., Barnes, I., Bejan, I., Brockmann, K. J., Benter, T., and Wirtz, K.: Reactions of NO3
2556 radicals with limonene and alpha-pinene: Product and SOA formation, Atmospheric
2557 Environment, 40, S116-S127, doi:10.1016/j.atmosenv.2005.09.093, 2006.

2558 Stockwell, C. E., Veres, P. R., Williams, J., and Yokelson, R. J.: Characterization of biomass
2559 burning emissions from cooking fires, peat, crop residue, and other fuels with high-resolution
2560 proton-transfer-reaction time-of-flight mass spectrometry, Atmos. Chem. Phys., 15, 845-865,
2561 doi:10.5194/acp-15-845-2015, 2015.

2562 Stolle, A., Ondruschka, B., and Hopf, H.: Thermal Rearrangements of Monoterpenes and
2563 Monoterpenoids, Helvetica Chimica Acta, 92, 1673-1719, doi:10.1002/hlca.200900041, 2009.

2564 Suarez-Bertoa, R., Picquet-Varrault, B., Tamas, W., Pangui, E., and Doussin, J. F.: Atmospheric
2565 Fate of a Series of Carbonyl Nitrates: Photolysis Frequencies and OH-Oxidation Rate Constants,
2566 Environ. Sci. Technol., 46, 12502-12509, doi:10.1021/es302613x, 2012.

2567 Surratt, J. D., Lewandowski, M., Offenberg, J. H., Jaoui, M., Kleindienst, T. E., Edney, E. O.,
2568 and Seinfeld, J. H.: Effect of Acidity on Secondary Organic Aerosol Formation from Isoprene,
2569 Environ. Sci. Technol., 41, 5363-5369, doi:10.1021/es0704176, 2007.

2570 Szmigielski, R., Vermeylen, R., Dommen, J., Metzger, A., Maenhaut, W., Baltensperger, U., and
2571 Claeys, M.: The acid effect in the formation of 2-methyltetrols from the photooxidation of
2572 isoprene in the presence of NOx, Atmospheric Research, 98, 183-189,
2573 doi:http://dx.doi.org/10.1016/j.atmosres.2010.02.012, 2010.

2574 Thornton, J. A., Braban, C. F., and Abbatt, J. P. D.: N2O5 hydrolysis on sub-micron organic
2575 aerosols: the effect of relative humidity, particle phase, and particle size, Physical Chemistry
2576 Chemical Physics, 5, 4593-4603, doi:10.1039/B307498F, 2003.

Turrà, N., Neuenschwander, U., Baiker, A., Peeters, J., and Hermans, I.: Mechanism of the Catalytic Deperoxidation of tert-Butylhydroperoxide with Cobalt(II) Acetylacetonate, Chem.-Eur. J., 16, 13226-13235, doi:10.1002/chem.201000489, 2010.

Vereecken, L., and Peeters, J.: Nontraditional (Per)oxy Ring-Closure Paths in the Atmospheric Oxidation of Isoprene and Monoterpenes, J. Phys. Chem. A, 108, 5197-5204, doi:10.1021/jp049219g, 2004.

Vereecken, L., and Peeters, J.: A Theoretical Study of the OH-initiated Gas-phase Oxidation Mechanism of β-pinene ($C_{10}H_{16}$): First Generation Products, Phys. Chem. Chem. Phys., 14, 3802-3815, doi:10.1039/C2CP23711C, 2012.

Verma, V., Fang, T., Guo, H., King, L., Bates, J. T., Peltier, R. E., Edgerton, E., Russell, A. G., and Weber, R. J.: Reactive oxygen species associated with water-soluble PM2.5 in the southeastern United States: spatiotemporal trends and source apportionment, Atmos. Chem. Phys., 14, 12915-12930, doi:10.5194/acp-14-12915-2014, 2014.

Wängberg, I., Barnes, I., and Becker, K. H.: Product and Mechanistic Study of the Reaction of NO3 Radicals with α-Pinene, Environ. Sci. Technol., 31, 2130-2135, doi:10.1021/es960958n, 1997.

Wayne, R. P., Barnes, I., Biggs, P., Burrows, J. P., Canosamas, C. E., Hjorth, J., Lebras, G., Moortgat, G. K., Perner, D., Poulet, G., Restelli, G., and Sidebottom, H.: THE NITRATE RADICAL - PHYSICS, CHEMISTRY, AND THE ATMOSPHERE, Atmospheric Environment Part a-General Topics, 25, 1-203, doi:10.1016/0960-1686(91)90192-a, 1991.

Weber, R. J., Sullivan, A. P., Peltier, R. E., Russell, A., Yan, B., Zheng, M., de Gouw, J., Warneke, C., Brock, C., Holloway, J. S., Atlas, E. L., and Edgerton, E.: A study of secondary organic aerosol formation in the anthropogenic-influenced southeastern United States, J. Geophys. Res.-Atmos., 112, D13302, doi:13310.11029/12007JD008408, 2007.

Xu, H., Wentworth, P. J., Howell, N. W., and Joens, J. A.: Temperature Dependent Near-UV Molar Absorptivities of Aliphatic Aldehydes and Ketones in Aqueous Solution, Spectrochim. Acta A, 49, 1171-1178, doi:http://dx.doi.org/10.1016/0584-8539(93)80076-M, 1993.

Xu, L., Kollman, M. S., Song, C., Shilling, J. E., and Ng, N. L.: Effects of NOx on the Volatility of Secondary Organic Aerosol from Isoprene Photooxidation, Environ. Sci. Technol., 48, 2253-2262, doi:10.1021/es404842g, 2014.

Xu, L., Suresh, S., Guo, H., Weber, R. J., and Ng, N. L.: Aerosol characterization over the southeastern United States using high resolution aerosol mass spectrometry: spatial and seasonal variation of aerosol composition, sources, and organic nitrates, Atmos. Chem. Phys. Discuss., 15, 10479-10552, doi:10.5194/acpd-15-10479-2015, 2015a.

Xu, L., Guo, H., Boyd, C. M., Klein, M., Bougiatioti, A., Cerully, K. M., Hite, J. R., Isaacman-VanWertz, G., Kreisberg, N. M., Knote, C., Olson, K., Koss, A., Goldstein, A. H., Hering, S. V., de Gouw, J., Baumann, K., Lee, S.-H., Nenes, A., Weber, R. J., and Ng, N. L.: Effects of anthropogenic emissions on aerosol formation from isoprene and monoterpenes in the

2615 southeastern United States, Proceedings of the National Academy of Sciences of the United
2616 States of America, 112, 37-42, doi:10.1073/pnas.1417609112, 2015b.

2617 Yeh, G. K., and Ziemann, P. J.: Alkyl Nitrate Formation from the Reactions of C8–C14 n-
2618 Alkanes with OH Radicals in the Presence of NOx: Measured Yields with Essential Corrections
2619 for Gas–Wall Partitioning, The Journal of Physical Chemistry A, 118, 8147-8157,
2620 doi:10.1021/jp500631v, 2014.

2621 Yu, Y., Ezell, M. J., Zelenyuk, A., Imre, D., Alexander, L., Ortega, J., D'Anna, B., Harmon, C.
2622 W., Johnson, S. N., and Finlayson-Pitts, B. J.: Photooxidation of alpha-pinene at high relative
2623 humidity in the presence of increasing concentrations of NOx, Atmospheric Environment, 42,
2624 5044-5060, doi:10.1016/j.atmosenv.2008.02.026, 2008.

2625 Zaveri, R. A., Berkowitz, C. M., Brechtel, F. J., Gilles, M. K., Hubbe, J. M., Jayne, J. T.,
2626 Kleinman, L. I., Laskin, A., Madronich, S., Onasch, T. B., Pekour, M. S., Springston, S. R.,
2627 Thornton, J. A., Tivanski, A. V., and Worsnop, D. R.: Nighttime chemical evolution of aerosol
2628 and trace gases in a power plant plume: Implications for secondary organic nitrate and
2629 organosulfate aerosol formation, NO3 radical chemistry, and N2O5 heterogeneous hydrolysis,
2630 Journal of Geophysical Research-Atmospheres, 115, D12304, doi:10.1029/2009jd013250, 2010.

2631 Zhang, X., Cappa, C. D., Jathar, S. H., McVay, R. C., Ensberg, J. J., Kleeman, M. J., and
2632 Seinfeld, J. H.: Influence of vapor wall loss in laboratory chambers on yields of secondary
2633 organic aerosol, Proceedings of the National Academy of Sciences of the United States of
2634 America, 111, 5802-5807, doi:10.1073/pnas.1404727111, 2014.

2635 Zhang, X., Schwantes, R. H., McVay, R. C., Lignell, H., Coggon, M. M., Flagan, R. C., and
2636 Seinfeld, J. H.: Vapor wall deposition in Teflon chambers, Atmos. Chem. Phys., 15, 4197-4214,
2637 doi:10.5194/acp-15-4197-2015, 2015.

2638 Zhao, R., Lee, A. K. Y., and Abbatt, J. P. D.: Investigation of Aqueous-Phase Photooxidation of
2639 Glyoxal and Methylglyoxal by Aerosol Chemical Ionization Mass Spectrometry: Observation of
2640 Hydroxyhydroperoxide Formation, J. Phys. Chem. A, 116, 6253-6263, doi:10.1021/jp211528d,
2641 2012.

2642 Zheng, W., Flocke, F. M., Tyndall, G. S., Swanson, A., Orlando, J. J., Roberts, J. M., Huey, L.
2643 G., and Tanner, D. J.: Characterization of a thermal decomposition chemical ionization mass
2644 spectrometer for the measurement of peroxy acyl nitrates (PANs) in the atmosphere, Atmos.
2645 Chem. Phys., 11, 6529-6547, doi:10.5194/acp-11-6529-2011, 2011.

2646 Ziemann, P. J., and Atkinson, R.: Kinetics, products, and mechanisms of secondary organic
2647 aerosol formation, Chemical Society Reviews, 41, 6582-6605, doi:10.1039/c2cs35122f, 2012.

Figure Captions

Figure1: Schematic of the Georgia Tech Environmental Chamber facility (GTEC).

Figure 2: Time series of the gas-phase organic nitrate species measured by the CIMS and the corresponding aerosol formation measured by HR-ToF-AMS (organics mass) and SMPS (aerosol volume) (Experiment 30 in Table 1). The gas-phase species at *m/z* 356 decreases over the course of the experiment while the species at *m/z* 372 increases steadily.

Figure 3: Aerosol mass yield as a function of organic mass loading for the β-pinene+NO_3 reaction under "RO_2+NO_3 dominant" conditions. The aerosol mass yields obtained in this study are compared to those measured in previous chamber studies by Griffin et al. (1999) and Fry et al. (2009). The aerosol mass yields obtained in this study are fitted using the two-product model proposed previously by Odum et al. (1996). The yield parameters obtained in this study and those from Griffin et al. (1999) are shown in Table 2. In order to better compare the aerosol mass yields obtained in this study to that by Griffin et al. (1999), ~~an aerosol density of 1.41 g/cm^3 is applied to the~~ measurements by Griffin et al. (1999) are adjusted to a temperature of 298K and density of 1.41 g cm^{-3}. The x-axis error bars represent one standard deviation of volume measured by SMPS at peak growth. The y-axis error bars represent uncertainty in yield calculated by an 8% uncertainty in chamber volume, 5% uncertainty in hydrocarbon injection, and one standard deviation of the aerosol volume measured by SMPS at peak growth.

Figure 4: Aerosol mass yield as a function of organic mass loading for the β-pinene+NO_3 reaction under "RO_2+HO_2 dominant" conditions. These aerosol mass yields are compared to the yield curve (solid line) for the NO_3+β-pinene under "RO_2+NO_3 dominant" conditions. The x-axis error bars represent one standard deviation of volume measured by SMPS at peak growth. The y-axis error bars represent uncertainty in yield calculated by an 8% uncertainty in chamber volume, 5% uncertainty in hydrocarbon injection, and one standard deviation of the aerosol volume measured by SMPS at peak growth.

Figure 5: High-resolution aerosol mass spectrum of the SOA formed from the β-pinene+NO_3 reaction under dry, ammonium sulfate seed, and "RO_2+NO_3 dominant" conditions (Experiment 5 in Table 1). The mass spectrum is colored by the ion type to indicate the contribution of each ion type to the mass spectrum. Only ions up to *m/z* 160 are shown as the signals beyond *m/z* 160 are minimal. Ions that contribute significantly to the total signal are also labeled.

Figure 6: Time series of mass concentrations of the major organic families (normalized to the sulfate mass concentration) as measured by the HR-ToF-AMS at RH < 2% under "RO_2+NO_3 dominant" conditions (Experiment 5 in Table 1). The least oxidized organic species (i.e. Family CH) decreases rapidly at the start of the experiment, and has the largest decrease among the three major organic families.

Figure 7: The AMS Nitrate:Org ratio of humid (RH = 50%) experiments normalized to the corresponding dry experiments with same initial β-pinene mixing ratio, five-minute averaged, for "RO_2+NO_3 dominant" experiments. This ratio is referred to as $(Nitrate:Org)_{norm}$ in the main text. For comparison purposes, all data are normalized to the highest $(Nitrate:Org)_{norm}$ ratio.

Figure 8: Generation of gas-phase species with molecular weights (MW) of 215, 229, and 231 amu detected by CIMS (red font), aerosol species with MW = 245 amu in filters analyzed by UHPLC-MS (blue font). Reaction numbers are given in green font and reaction with generic radical **Q**$^{\bullet}$ (e.g., NO_3, RO_2, etc.) is used to symbolize any species abstracting hydrogen atoms. Reactions which can be accomplished by any of the radicals present (RO_2, HO_2, NO_3 etc.) are symbolized by reaction with generic radical **L**$^{\bullet}$. Reactions enhanced in the RO_2+HO_2 dominant pathway are highlighted in purple.

Figure 9: Ratio of the total areas integrated under UV-visible chromatograms collected at 235 nm (gray bars, ROOR and ROOH) ~~235 nm~~ and 270 nm (teal bars, -C=O and -ONO_2) ~~270 nm~~ relative to 205 nm for experiments dominated by (left-hand side panel) RO_2+NO_3 reaction and (right-hand side panel) RO_2+HO_2 reaction under both humid and dry conditions.

Figure 10: A comparison of mass spectra obtained from this work and the LO-OOA factor identified from PMF analysis of the HR-ToF-AMS data from the SOAS field campaign. (a) Mass spectrum of the SOA formed from the β-pinene+NO_3 reaction at RH = 70 % under "RO_2+HO_2 dominant" conditions and $(NH_4)_2SO_4$+H_2SO_4 seed (Experiment 34 in Table 1). (b) Mass spectrum for the LO-OOA factor identified from PMF analysis of the SOAS HR-ToF-AMS data (Xu et al., 2015b). The mass spectra are colored by the ion type to indicate their contribution to the mass spectra. Ions $C_5H_7^+$ (*m/z* 67) and $C_7H_7^+$ (*m/z* 91) are distinctive for the β-pinene mass spectrum (Section 5 of main text). To facilitate comparison, *m/z* > 50 have been multiplied by a factor of 3 in the LO-OOA spectrum.

Figure 1:

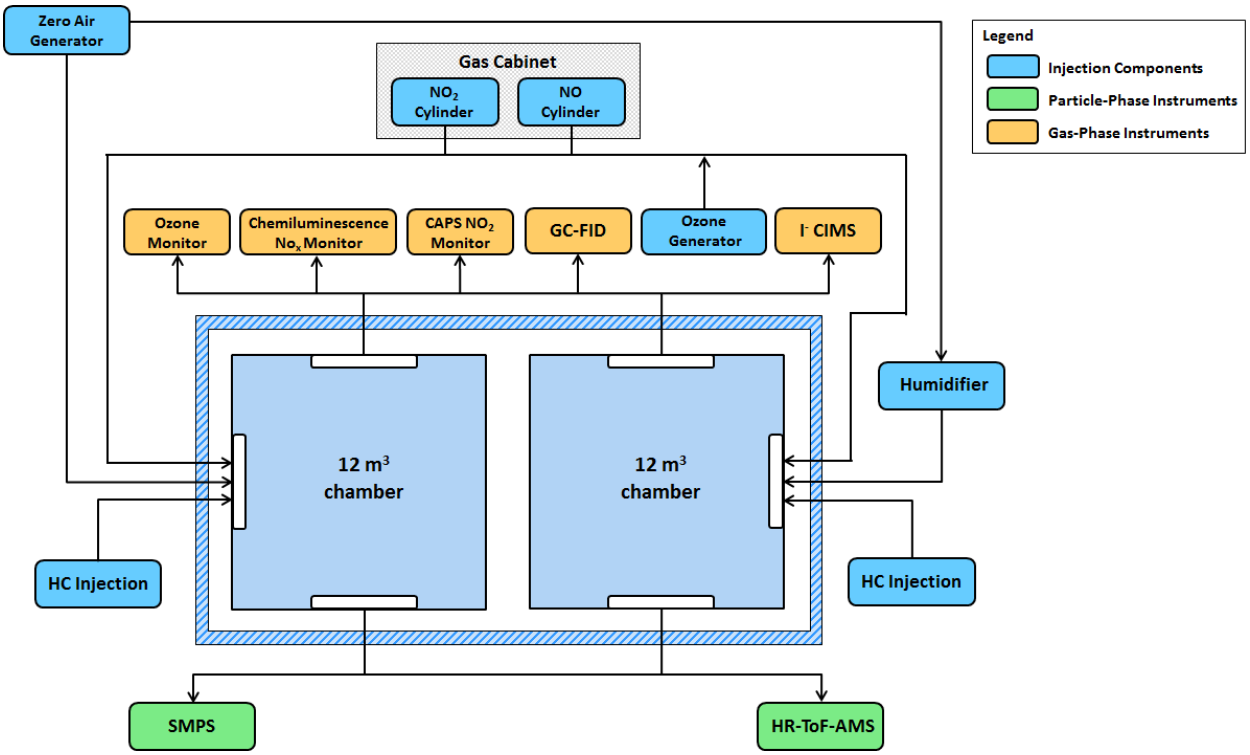
Zero Air Generator
Gas Cabinet
NO2 Cylinder
NO Cylinder
Legend
Injection Components
Particle-Phase Instruments
Gas-Phase Instruments
Ozone Monitor
Chemiluminescence NOx Monitor
CAPS NO2 Monitor
GC-FID
Ozone Generator
I- CIMS
Humidifier
12 m3 chamber
12 m3 chamber
HC Injection
HC Injection
SMPS
HR-ToF-AMS

Figure 2:

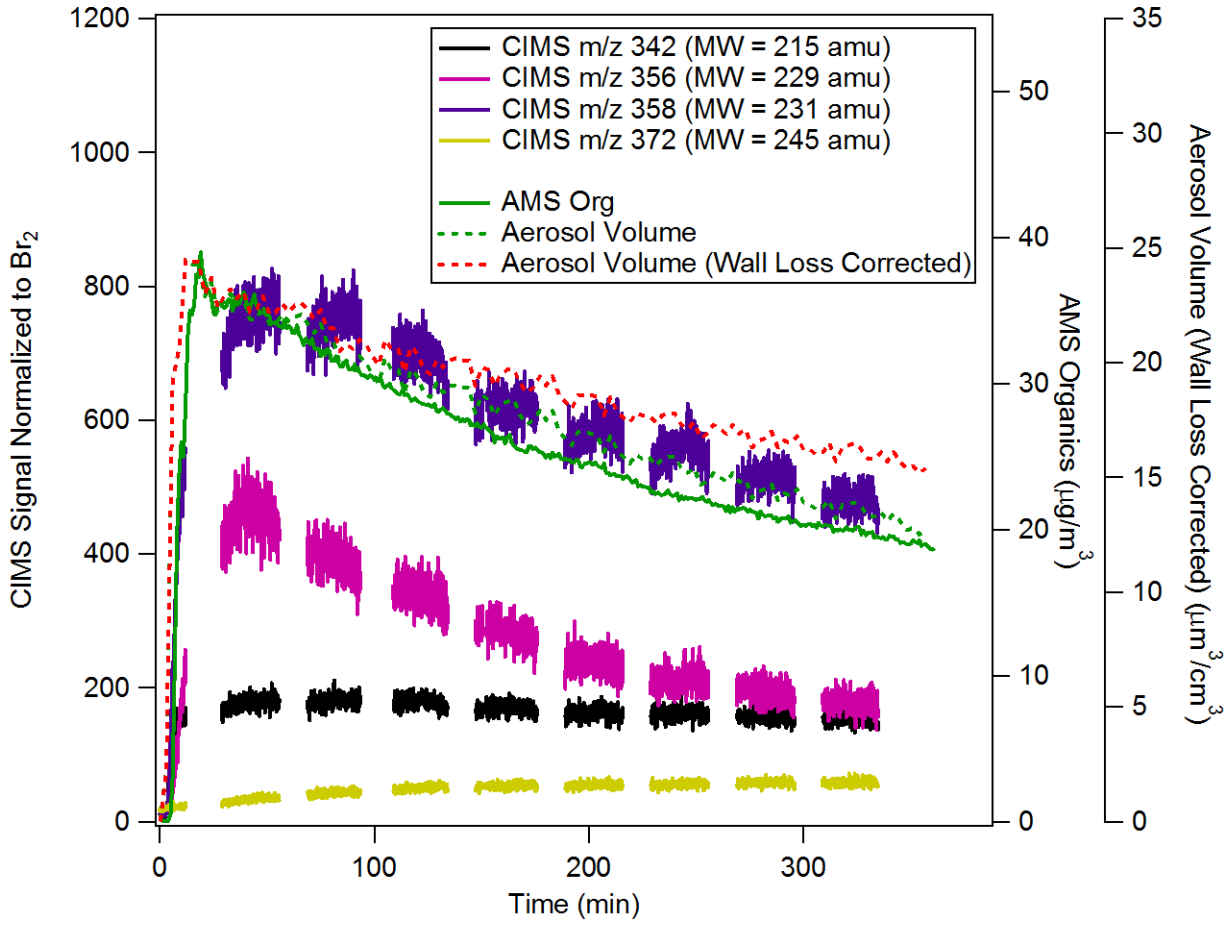
CIMS m/z 342 (MW = 215 amu)
CIMS m/z 356 (MW = 229 amu)
CIMS m/z 358 (MW = 231 amu)
CIMS m/z 372 (MW = 245 amu)
AMS Org
Aerosol Volume
Aerosol Volume (Wall Loss Corrected)
CIMS Signal Normalized to Br2
AMS Organics (μg/m3)
Aerosol Volume (Wall Loss Corrected) (μm3/cm3)
Time (min)
0
200
400
600
800
1000
1200
0
10
20
30
40
50
0
5
10
15
20
25
30
35
0
100
200
300

2771 Figure 3:

2772

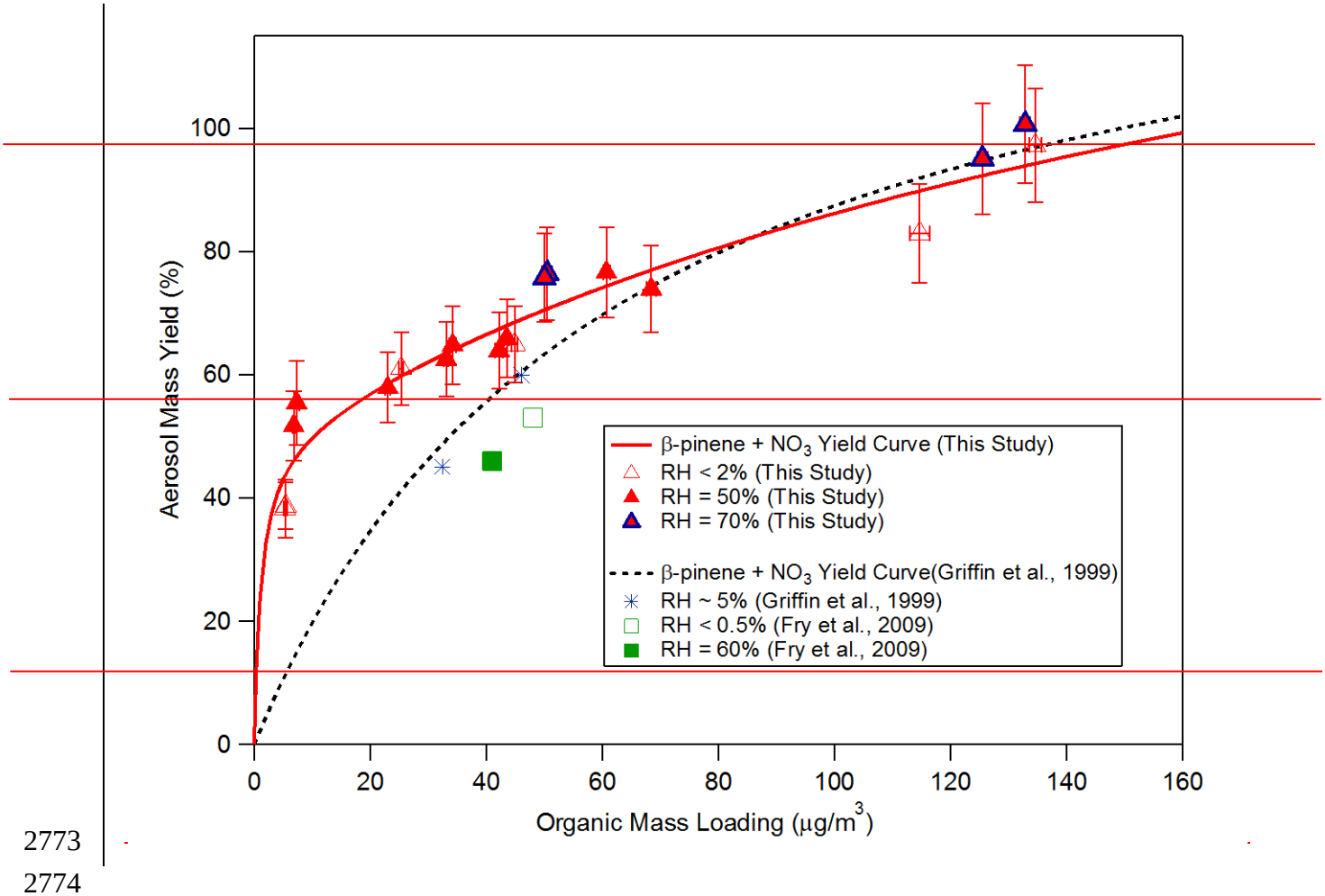

2773

2774

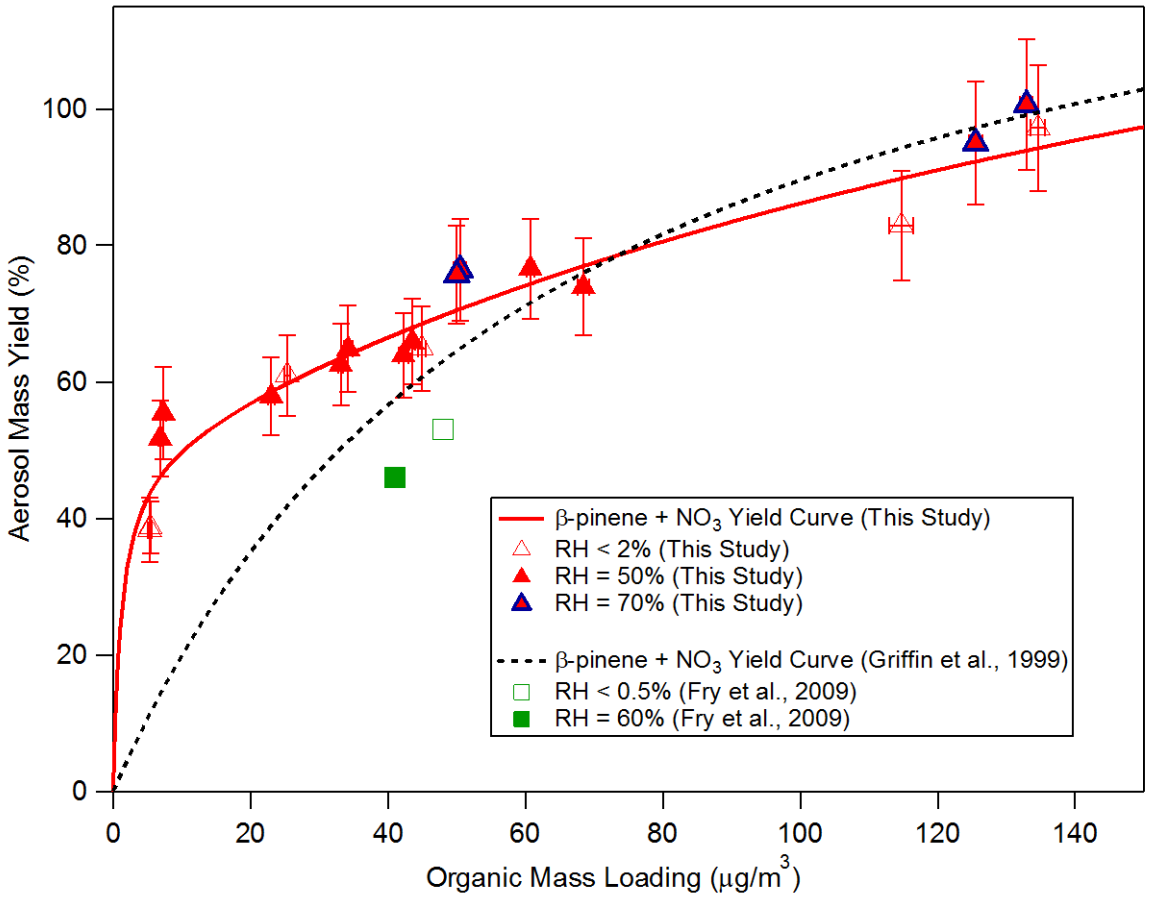
Aerosol Mass Yield (%)
Organic Mass Loading (μg/m3)
0
20
40
60
80
100
120
140
β-pinene + NO3 Yield Curve (This Study)
RH < 2% (This Study)
RH = 50% (This Study)
RH = 70% (This Study)
β-pinene + NO3 Yield Curve (Griffin et al., 1999)
RH < 0.5% (Fry et al., 2009)
RH = 60% (Fry et al., 2009)

Figure 4:

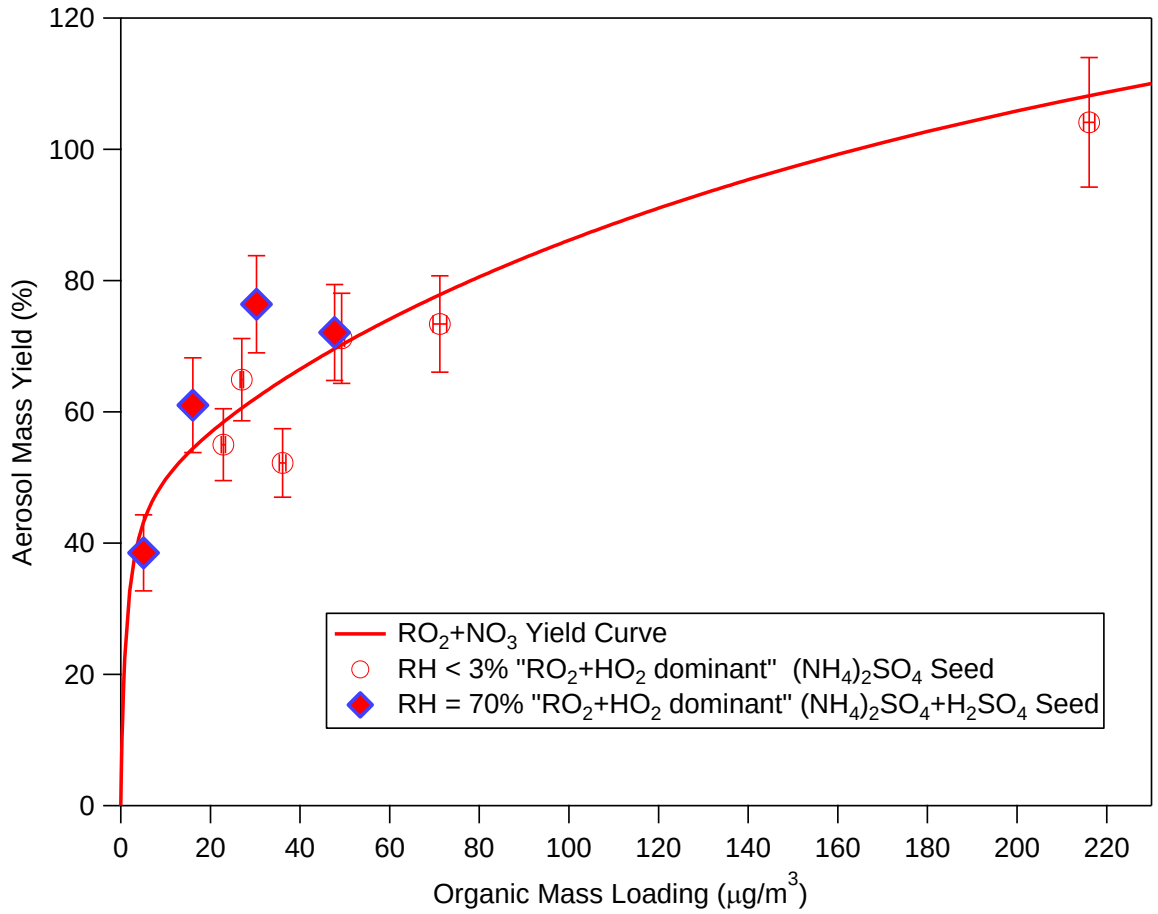
Aerosol Mass Yield (%)
Organic Mass Loading (μg/m3)
RO2+NO3 Yield Curve
RH < 3% "RO2+HO2 dominant" (NH4)2SO4 Seed
RH = 70% "RO2+HO2 dominant" (NH4)2SO4+H2SO4 Seed

Figure 5:

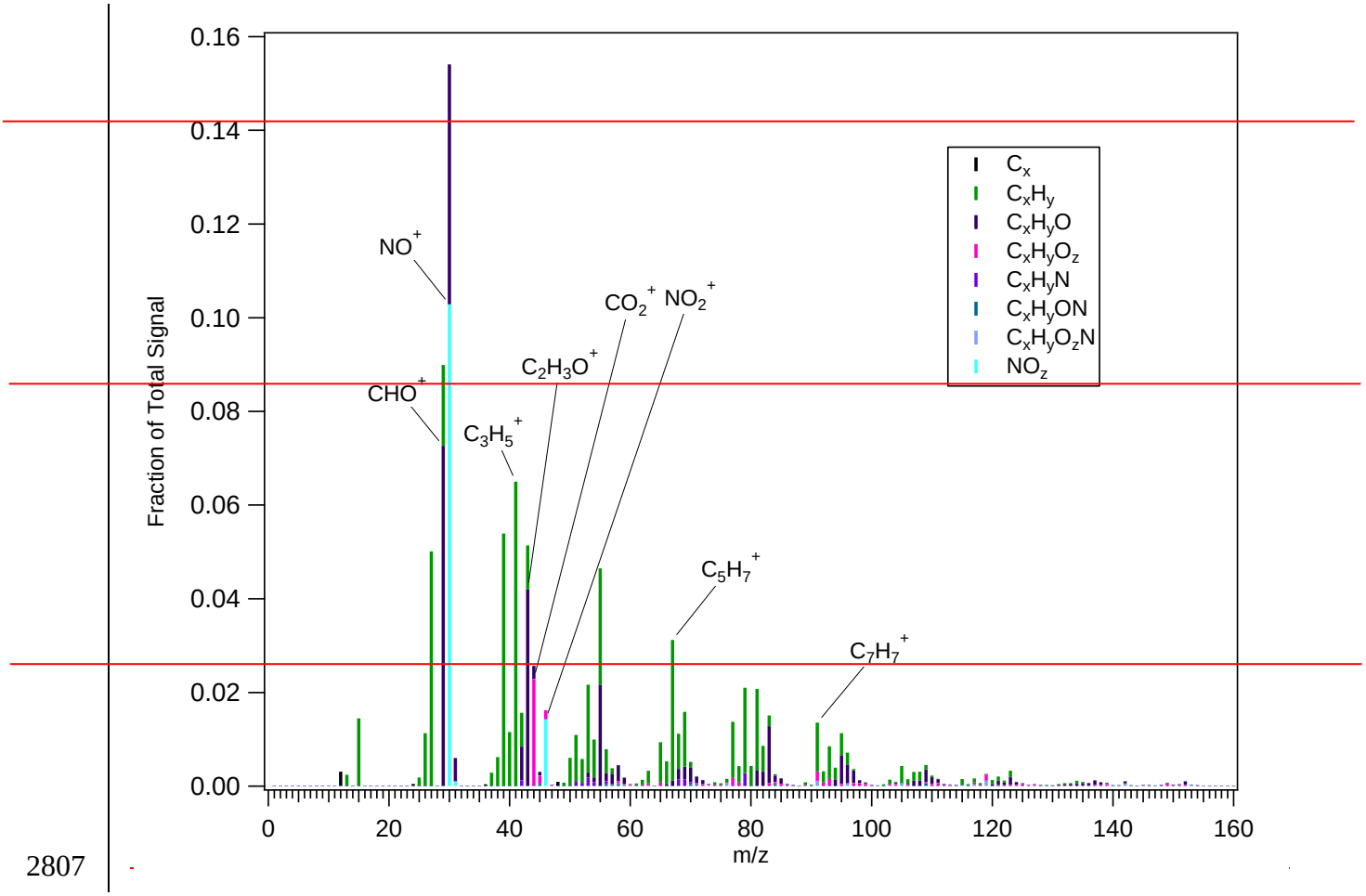
Fraction of Total Signal
0.16
0.14
0.12
0.10
0.08
0.06
0.04
0.02
0.00
0
20
40
60
80
100
120
140
160
m/z
NO+
CHO+
C3H5+
C2H3O+
CO2+
NO2+
C5H7+
C7H7+
Cx
CxHy
CxHyO
CxHyOz
CxHyN
CxHyON
CxHyOzN
NOz

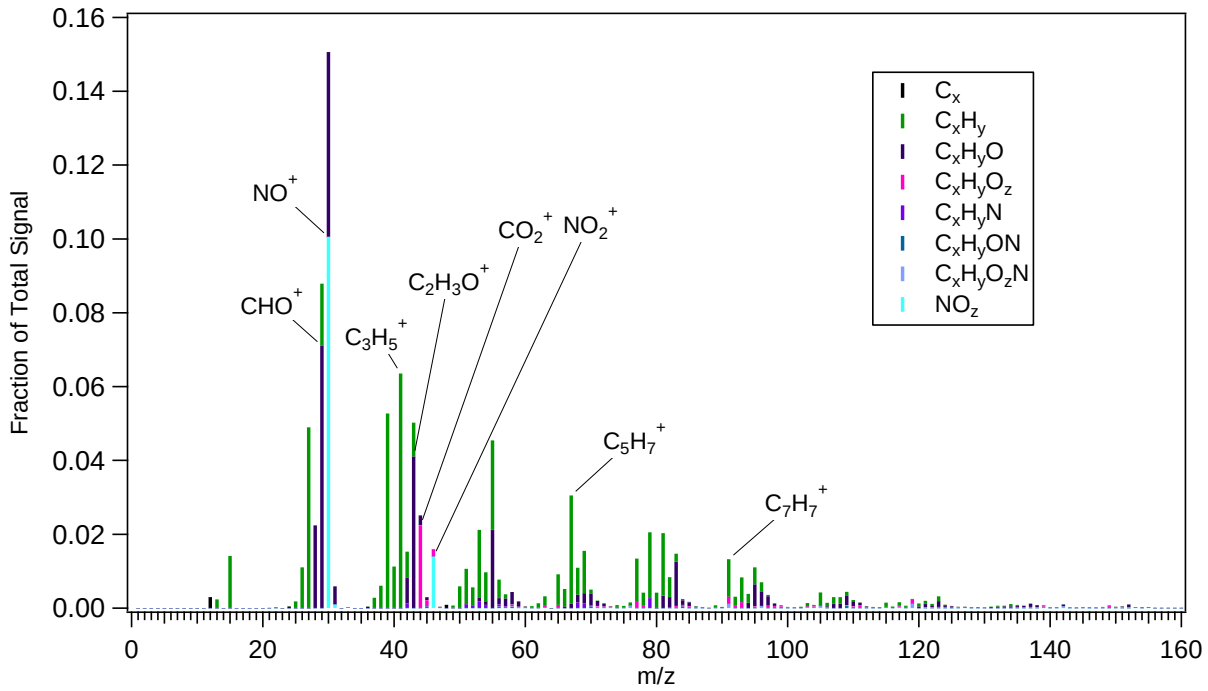
Fraction of Total Signal
0.16
0.14
0.12
0.10
0.08
0.06
0.04
0.02
0.00
0
20
40
60
80
100
120
140
160
m/z
NO+
CHO+
C3H5+
C2H3O+
CO2+
NO2+
C5H7+
C7H7+
Cx
CxHy
CxHyO
CxHyOz
CxHyN
CxHyON
CxHyOzN
NOz

Figure 6:

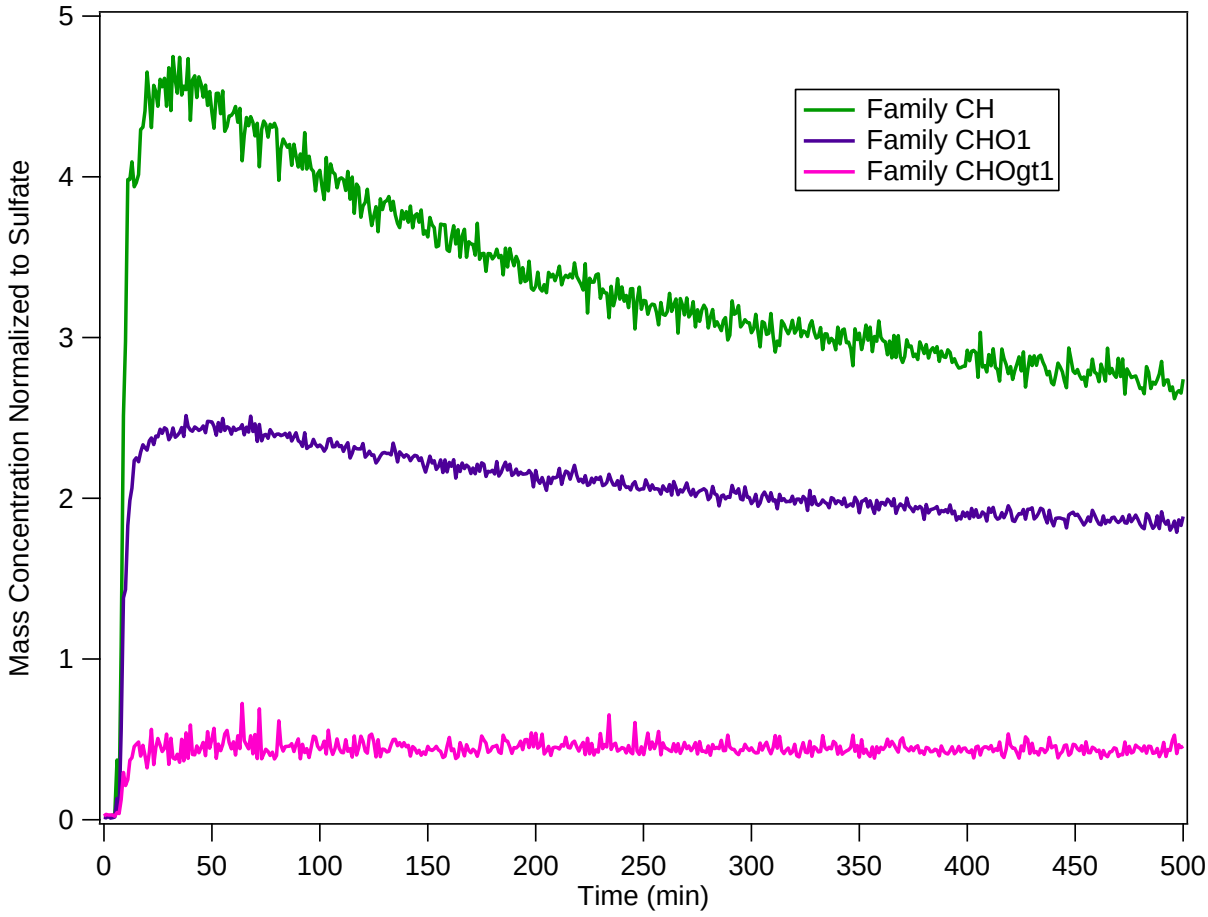
Family CH
Family CHO1
Family CHOgt1
Mass Concentration Normalized to Sulfate
Time (min)
0
1
2
3
4
5
0
50
100
150
200
250
300
350
400
450
500

2843

2844 Figure 7:

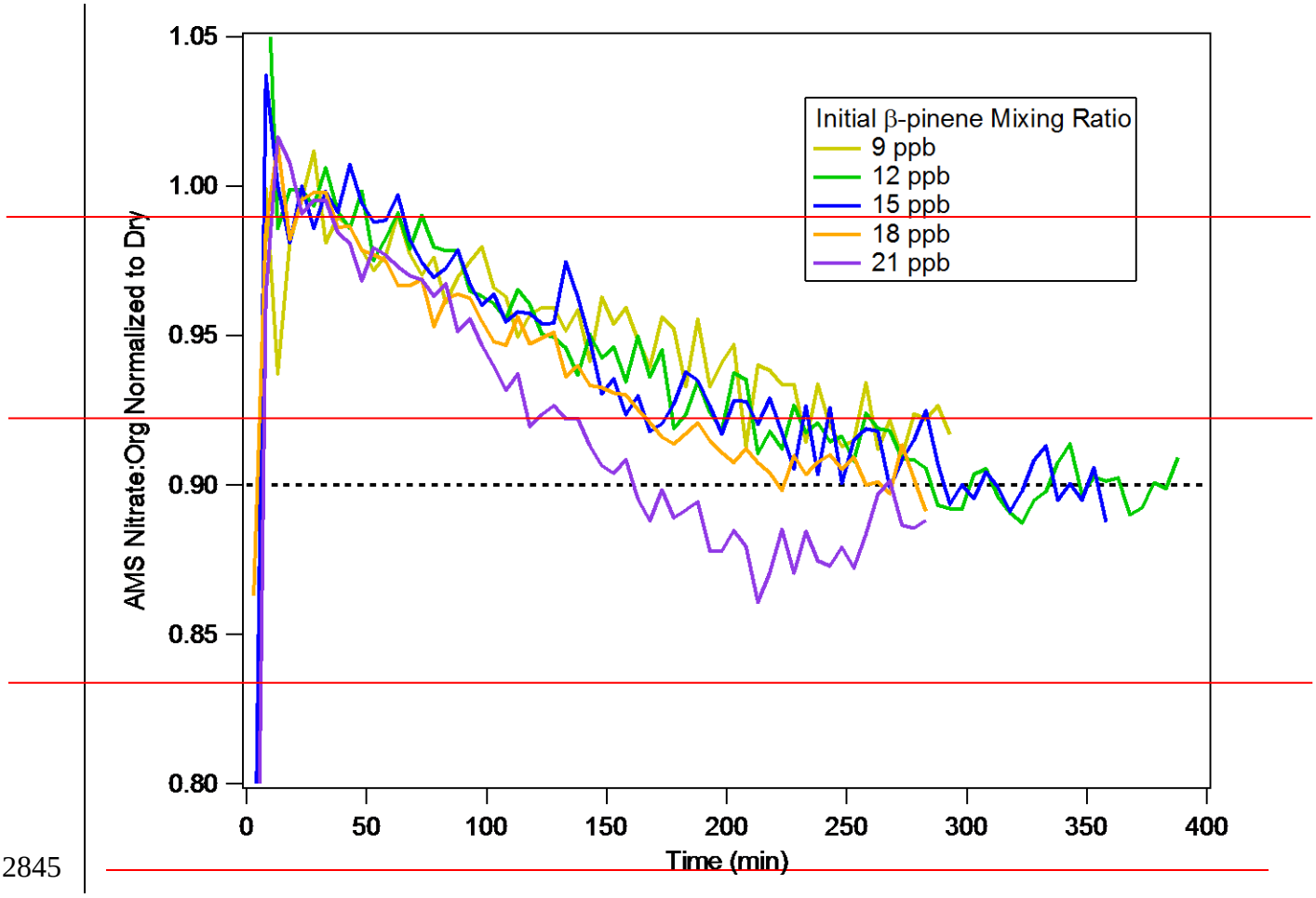

2845

2846

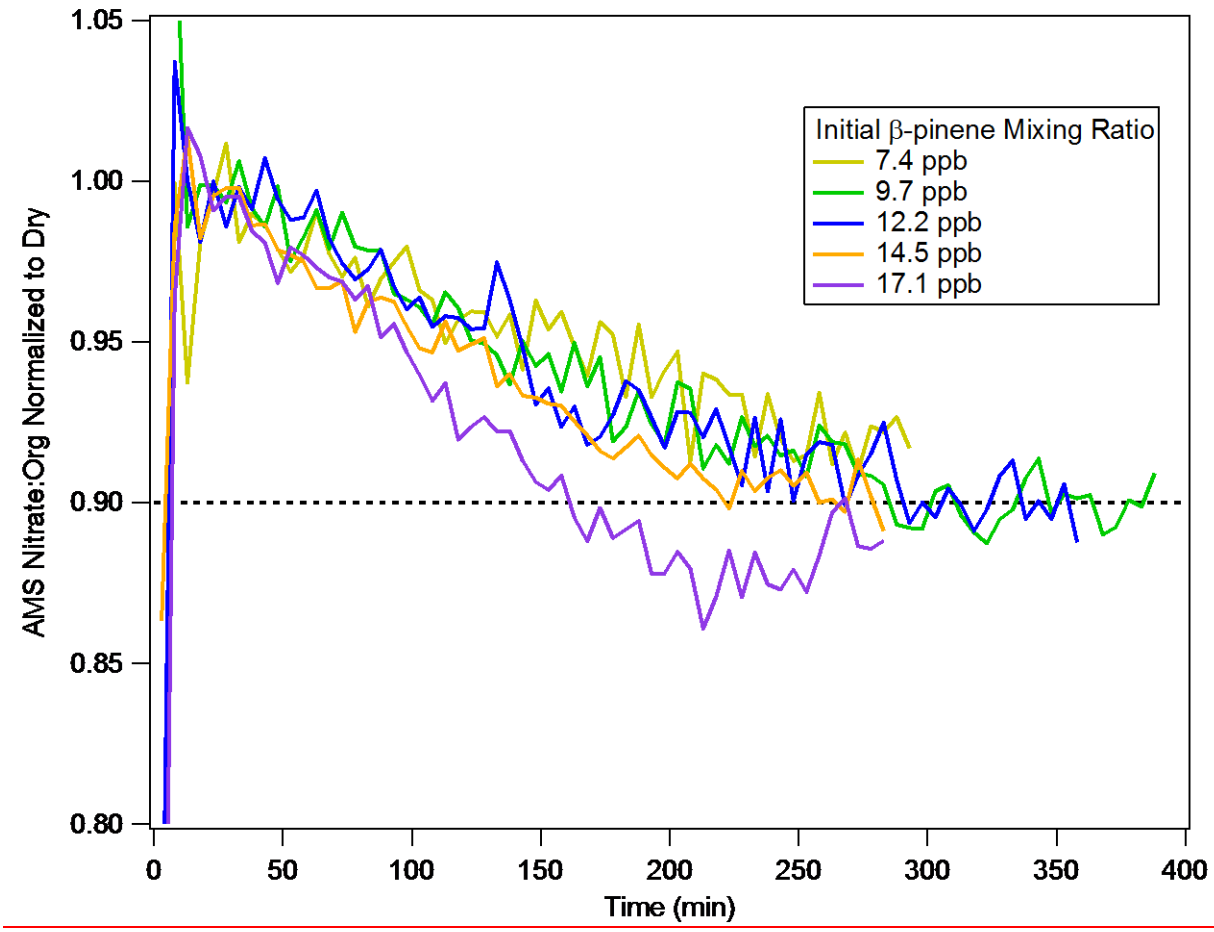
1.05
1.00
0.95
0.90
0.85
0.80
AMS Nitrate:Org Normalized to Dry
0
50
100
150
200
250
300
350
400
Time (min)
Initial β-pinene Mixing Ratio
7.4 ppb
9.7 ppb
12.2 ppb
14.5 ppb
17.1 ppb

2868 Figure 8:

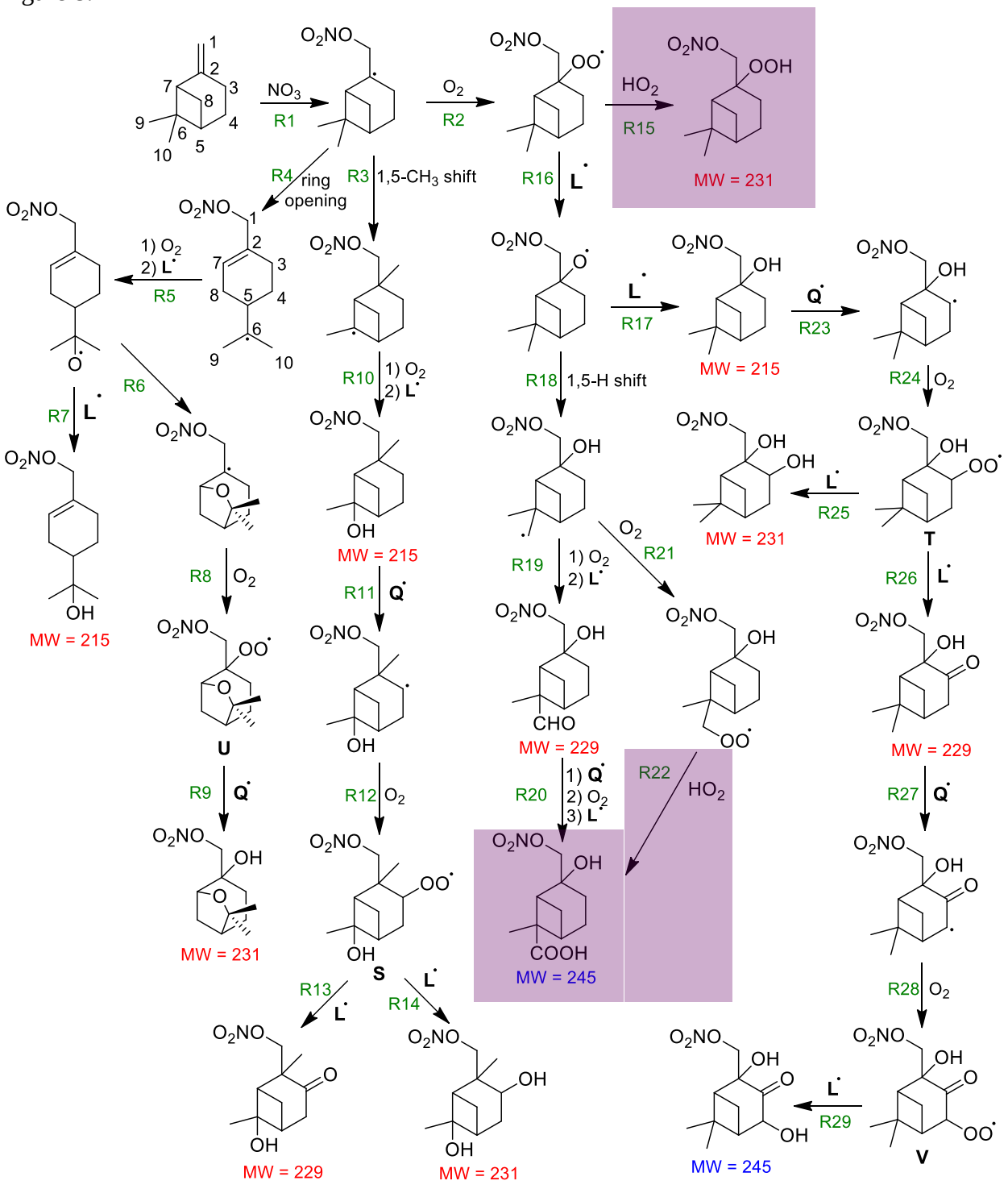

2869

2870

2871

2872

2873

Figure 9:

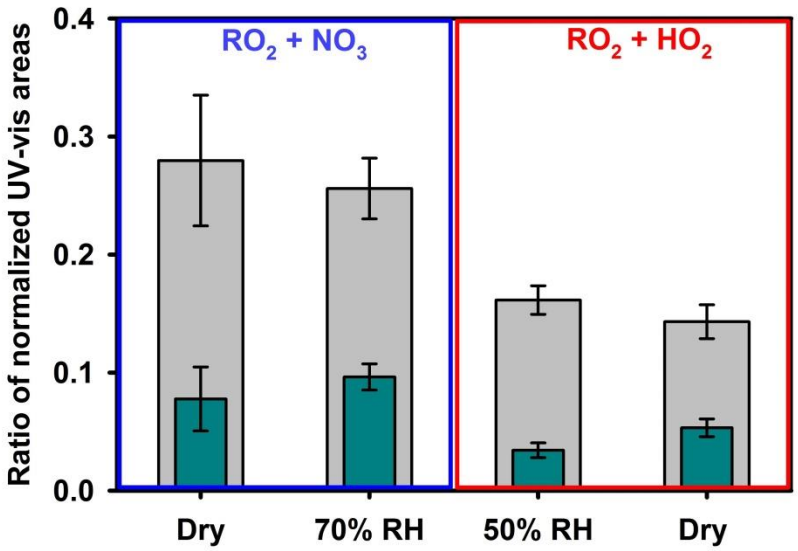
Ratio of normalized UV-vis areas
0.4
0.3
0.2
0.1
0.0
RO2 + NO3
RO2 + HO2
Dry
70% RH
50% RH
Dry

2886 Figure 10:

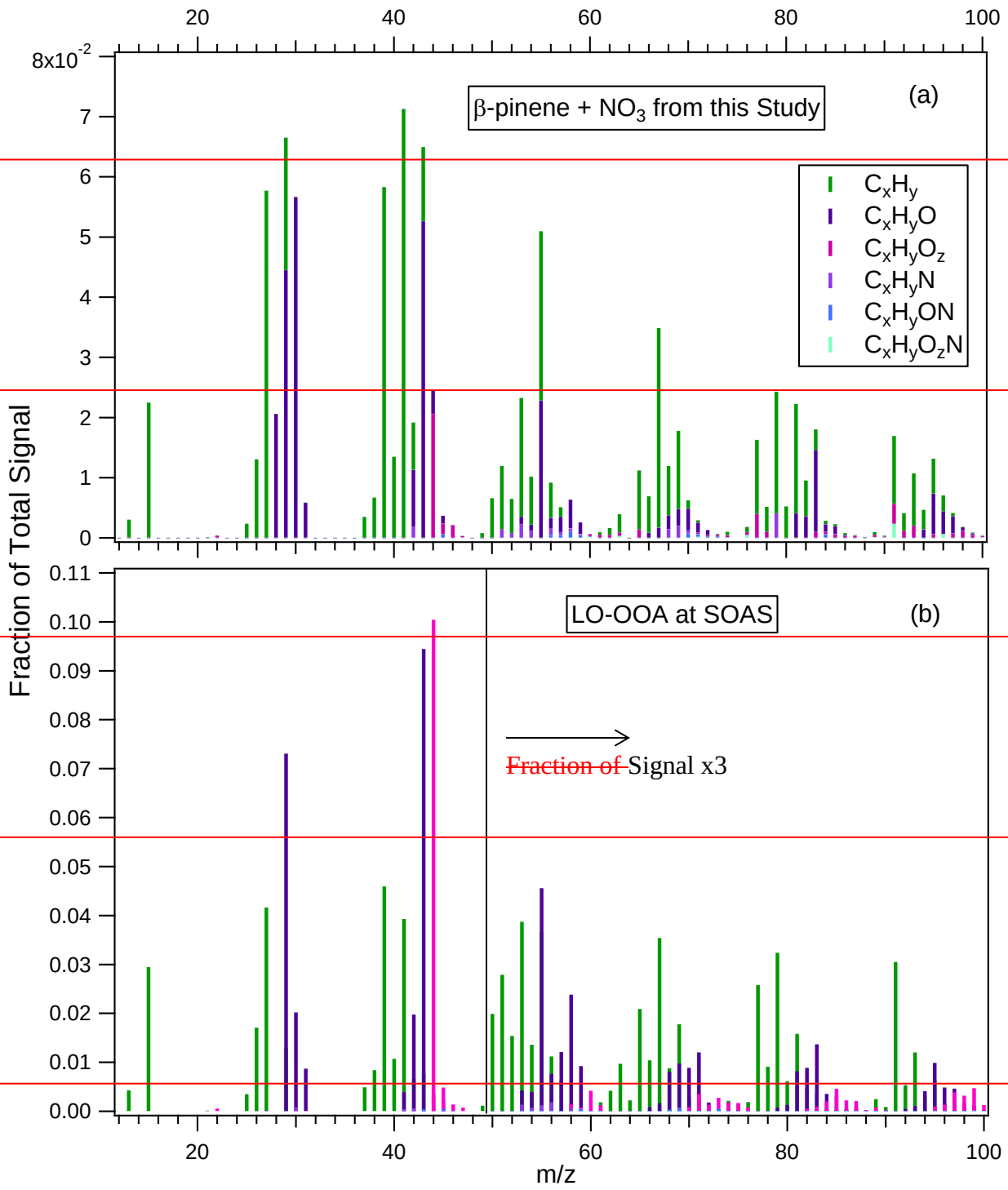

2887

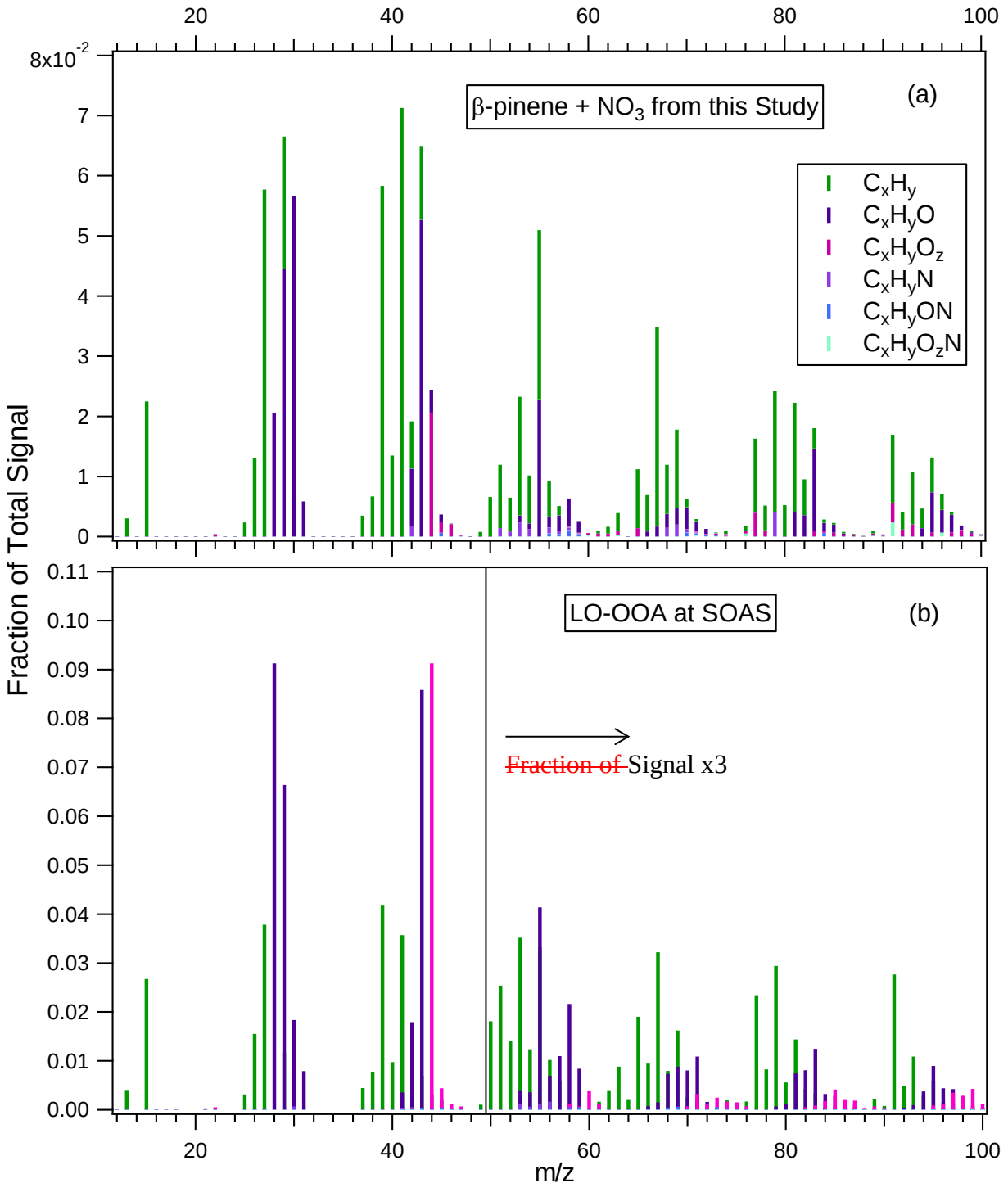

2888

2889

2890

Table 1: Experimental conditions and aerosol mass yields for all experiments

Experiment	RH (%)	Condition	Seed	ΔHC^c (ppb)	ΔHC^c ($\mu g/m^3$)	$\Delta M_o{}^d$ ($\mu g/m^3$)	Mass Yield (%)
1	< 2	RO_2+NO_3	AS[a]	2.5±0.2	13.8±1.3	5.3±0.41	38.3±5.5
2	< 2	RO_2+NO_3	AS	2.5±0.2	13.8±1.3	5.4±0.15	38.7±4.0
3	< 2	RO_2+NO_3	AS	7.4±0.7	41.5±3.9	25.3±0.54	61.0±6.0
4	< 2	RO_2+NO_3	AS	9.9±0.9	55.4±5.2	--[e]	--
5	< 2	RO_2+NO_3	AS	12.4±1.2	69.2±6.5	--	--
6	< 2	RO_2+NO_3	AS	12.4±1.2	69.2±6.5	44.9±0.73	64.9±6.3
7	< 2	RO_2+NO_3	AS	14.9±1.4	83.0±7.8	--	--
8	< 2	RO_2+NO_3	AS	17.4±1.6	96.9±9.1	--	--
9	< 2	RO_2+NO_3	AS	24.8±2.4	138.4±13.1	134.6±1.51	97.2±9.3
10	< 2	RO_2+NO_3	AS	24.8±2.4	138.4±13.1	114.7±2.51	82.9±8.2
11	51	RO_2+NO_3	AS	2.4±0.2	13.2±1.2	7.3±0.57	55.4±8.2
12	50	RO_2+NO_3	AS	2.4±0.2	13.2±1.2	6.8±0.36	51.7±6.3
13	49	RO_2+NO_3	AS	7.1±0.7	39.6±3.7	23.0±0.65	57.9±6.0
14	49	RO_2+NO_3	AS	9.5±0.9	52.8±5.0	34.2±0.89	64.8±6.6
15	51	RO_2+NO_3	AS	9.5±0.9	52.8±5.0	33.1±0.56	62.5±6.1
16	50	RO_2+NO_3	AS	11.9±1.1	66.1±6.2	43.5±0.60	65.9±6.4
17	50	RO_2+NO_3	AS	11.9±1.1	66.1±6.2	42.2±0.98	63.9±6.4
18	51	RO_2+NO_3	AS	14.2±1.3	79.3±7.5	60.7±0.83	76.6±7.4
19	51	RO_2+NO_3	AS	16.6±1.6	92.5±8.7	68.4±1.26	73.9±7.2
20	71	RO_2+NO_3	AS	11.9±1.1	66.1±6.2	50.5±1.32	76.4±7.8
21	70	RO_2+NO_3	AS	11.9±1.1	66.1±6.2	50.0±0.44	75.7±7.2
22	72	RO_2+NO_3	AS	23.7±2.2	132.1±12.5	125.5±1.35	95.0±9.0
23	68	RO_2+NO_3	AS	23.7±2.2	132.1±12.5	132.9±1.33	100.6±9.5
24	51	RO_2+NO_3	AS+SA[b]	7.1±0.7	39.6±3.7	25.5±0.69	64.4±6.6
25	50	RO_2+NO_3	AS+SA	11.9±1.1	66.1±6.2	46.4±1.10	70.4±6.8
26	51	RO_2+NO_3	AS+SA	16.6±1.6	92.5±8.7	74.4±1.23	80.5±7.7
27	< 3	RO_2+HO_2	AS	7.4±0.7	41.5±3.9	27.0 ±0.54	64.9±6.4
28	< 3	RO_2+HO_2	AS	7.4±0.7	41.5±3.9	22.9±0.71	55.0±5.8
29	< 3	RO_2+HO_2	AS	12.4±1.2	69.2±6.5	49.3±0.97	71.2±7.1
30	< 3	RO_2+HO_2	AS	12.4±1.2	69.2±6.5	36.1±1.17	52.2±5.6
31	< 2	RO_2+HO_2	AS	17.4±1.6	96.9±9.1	71.2±2.32	73.4±7.8
32	< 3	RO_2+HO_2	AS	37.3±3.5	207.6±19.6	216.1±1.96	104.1±9.9
33	49	RO_2+HO_2	AS	35.6±3.4	198.2±18.7	147.8±1.42	74.6±7.1
34	69	RO_2+HO_2	AS+SA	2.4±0.2	13.2±1.2	5.1±0.59	38.5±8.1
35	69	RO_2+HO_2	AS+SA	4.7±0.4	26.4±2.5	16.1±1.14	61.0±9.0
36	66	RO_2+HO_2	AS+SA	7.1±0.7	39.6±3.7	30.3±0.71	76.4±7.8
37	66	RO_2+HO_2	AS+SA	11.9±1.1	66.1±6.2	47.7±1.77	72.1±8.1
38	< 1	RO_2+NO_3	None	12.4±1.2	69.2±6.5	42.3±0.46	61.1±5.8
39	50	RO_2+NO_3	None	11.9±1.1	66.1±6.2	44.3±0.34	67.0±6.4
40	<2	RO_2+HO_2	None	12.4±1.2	69.2±6.5	18.7±0.51	27.0±2.8
41	66	RO_2+HO_2	None	11.9±1.1	66.1±6.2	28.5±0.60	43.1±4.2

42	50	RO_2+HO_2	None	11.9±1.1	66.1±6.2	18.4±0.34	27.8±2.7
43	<2	RO_2+HO_2	AS*	12.4±1.2	69.2±6.5	33.6±0.79	48.5±4.9
4544	68	RO_2+HO_2	AS+SA*	11.9±1.1	66.1±6.2	46.6±0.86	70.6±7.0
4645	66	RO_2+HO_2	AS+SA*	11.9±1.1	66.1±6.2	44.5±0.87	67.3±6.7

*Experiments with seed concentrations greater than the typical seed concentrations for investigating vapor wall loss effects

[a]$(NH_4)_2SO_4$ Seed

[b]$(NH_4)_2SO_4+H_2SO_4$ Seed

[c]Uncertainties in hydrocarbon concentration are calculated from an 8% uncertainty in chamber volume and 5% uncertainty in hydrocarbon mass

[d]Uncertainties in aerosol mass loading are calculated from one standard deviation of aerosol volume as measured by the SMPS

[e]"--" denotes experiments where there is no SMPS data

Table 2: Fit parameters for two-product model proposed by Odum et al. (1996)

	α_1	K_1	α_2	K_2
β-pinene+NO_3 (this study)	1.187	0.004546	0.496	0.880
Griffin et al. (1999)	1.464	0.01630158		

Table 3: Coefficients for the Volatility Basis Set Proposed by Donahue et al. (2006)

	Saturation Vapor Pressure, C* (μg/m^3)			
	0.11	110	10100	1001000
β-pinene+NO_3 (this study)	0.3730.272	0.0330.000	0.0000.437	0.9410.291
Griffin et al. (1999)	0.0000.000	0.0000.117	0.3010.785	1.2040